SSI-DT46215037

Doctor Thesis

Analysis of high-frequency electromagnetic devices based on equivalent circuit and homogenization method

Qiao Liu

A dissertation submitted in partial fulfillment
Of the requirements for the degree of
Doctor of Engineering

Division of System Science and Informatics
Graduate School of Information Science and Technology
Hokkaido University

Doctor Thesis
Submitted to Graduate School of Information Science and Technology
Hokkaido University
In partial fulfillment of the requirements for the degree of
Doctor of Engineering

Qiao Liu

Thesis Committee:	**Professor**	**Hajime IGARASHI (Chief examiner)**
	Professor	**So NOGUCHI**
	Professor	**Hiroyuki KITA**
	Associate Professor	

SSI-DT46215037

Analysis of high-frequency electromagnetic devices based on equivalent circuit and homogenization method

Qiao Liu

Abstract

For the reduction of device size, the driving frequency of power electronics circuits has been increased. The impedance of magnetic devices such as inductors and wireless power transfer (WPT) working at high frequency would be frequency dependent owing to the eddy current effect and displacement current effect. Although the devices can be analyzed using Finite Element Method (FEM), it needs large computing cost at high frequencies because they must be discretized into elements much smaller than skin depth. It is more prominent in the time domain simulation.

Therefore, alternative methods are required to accelerate the calculations, and the equivalent circuit is one choice. Recently Cauer circuit, equivalent circuit with displacement current and homogenized method are usually applied to solve problems shown below.

- When the working frequency is high, due to the proximity effect and skin effect the resistance of the device will increase and the inductance will decrease, it is time-consuming if we use FEM to do the simulation especially in time domain with complex input and applied in power system.
- For the winding in motor, because of the high-frequency harmonic in input Pulse-Width Modulation (PWM) wave, magnet in the rotor and the saturation of core, the copper loss of windings is of large consumption to calculate.
- Due to the stray capacitance, a high frequency inductor or coils in WPT has self-resonant points. When the inductor works at frequency higher than the first self-resonant frequency,

it becomes capacitive, and the resistance and reactance increase sharply around the resonant point. Such analysis can hardly be performed only using magneto-quasistatic FEM unless the Darwin approximation is introduced.

In this paper, based on the conventional FEM, homogenization method and other algorithms, the equivalent circuits are built to accelerate the simulation process of magnetic devices working at high frequency considering the eddy current and displacement current effect.

In Chapter 2, the basic construction of Cauer circuit and the AVM to calculate the parameters of Cauer circuit are introduced. The method to get the input impedance for building Cauer circuit, containing formula calculation and FEM calculation are shown. The Cauer circuit is used to represent the WPT and inductor. The nonlinearity and displacement of WPT are considered in the Cauer circuit. The result in frequency domain and time domain are shown in this chapter.

In Chapter 3, the basic theory of homogenization method is introduced and compared with Dowell's method. The impedance is calculated using homogenized method and Cauer circuit is built on the impedance. The results of Cauer circuit containing nonlinearity in time and frequency domain are shown. To consider windings influenced by external magnetic field, another type of Cauer circuit is built based on the complex permeability. The copper loss of windings considering the external influence is calculated using the homogenized Cauer circuit.

In Chapter 4, the equivalent circuit with displacement current is introduced to represent the magnetic devices and describe how to calculate the parameters of the equivalent circuit with displacement current using complex mutual inductance. The model is applied to analyze the inductor and wireless power transfer. The resonant point and the power factor are simulated using the equivalent circuit. The result in time domain simulation will also be shown in the chapter.

List of Contents

List of Figures

List of Tables

Chapter 1 Introduction

In this chapter, the background, purposes of the research, and the outline of this thesis will be described.

1.1 Background

With the ongoing trend of reducing device size in power electronics circuits, there has been a significant increase in the driving frequency of these circuits. However, this shift presents challenges, particularly in the impedance behavior of magnetic devices such as inductors and wireless power transfer (WPT) systems operating at high frequencies. These challenges arise due to the frequency-dependent nature of impedance caused by the eddy current effect and displacement effect [1]-[2]. While Finite Element Method (FEM) can be employed to analyze these devices, it becomes computationally expensive, especially at high frequencies. This computational burden arises from the necessity to discretize the devices into elements much smaller than the skin depth. This issue becomes even more pronounced in time domain simulations, where the complexity of the analysis further escalates. Therefore, equivalent circuit and homogenization method are applied to accelerate the simulation of high-frequency magnetic devices in both frequency and time domain [3]-[6].

When there is no need to consider the displacement current, the magneto-quasistatic FEM is applied. Skin effect and displacement current still have to be taken into consideration. Cauer circuit is an applicable surrogate model to represent the magnetic device in high frequency. It has been shown that the response of magneto-quasistatic systems can be represented by a Cauer equivalent circuit, which is synthesized by the model order reduction of the FE equations [7]-[8].

Their responses can be analyzed effectively using a Cauer circuit in both frequency and time domains. Moreover, the Cauer circuit can also be synthesized by curve fitting to the input impedance of a magneto-quasistatic system, either computed or measured [3], [9], without using an elaborate procedure based on model-order reduction as in [7]-[8]. However, it remains unclear whether this fitting based Cauer circuit is valid for magnetic devices with (i) magnetic saturation, (ii) a PWM input, or (iii) geometric or material parameters that can be changed.

Some research has been completed orient to the displacement current between the coils caused by the parallel capacitance [10]. Due to the stray capacitance, a high frequency inductor has self-resonant points. When the inductor works at frequency larger than the first self-resonant frequency, it becomes capacitive, and the resistance and reactance increase sharply around the resonant point [11]. Such analysis can hardly be performed only using finite element method (FEM) unless the Darwin approximation is introduced, which is currently under basic studies for a commercial use. For spiral shape inductor, a mixed-potential volume integral-equation approach has been introduced in [12]. Moreover, an analytical method to compute the capacitance between windings has been introduced in [13]. These methods can derive the impedance of a winding coil while the eddy current effect is not considered. The equivalent circuit method to consider the inductance and capacitance among the coils has been proposed in [14]-[15]. This method has been extended to consider the AC resistance owing to the eddy currents in [16], in which its value is determined by repeating the eddy current analysis based on FEM and circuit analysis.

1.2 Purposes and methods

- When we don’t have to consider the displacement current in magnetic device, we use the Cauer circuit to consider the eddy current and nonlinearity. The parameters of Cauer circuit are calculated using adjoint variable method (AVM) based on the input impedance of magnetic devices. The Cauer circuit is embedded into the power system using LTSpice to do the time domain simulation [17].

- When the device is influenced by the external magnetic field, the conventional Cauer circuit cannot work that a new type of Cauer circuit derived from formula is applied to solve this problem. Decomposing the complex permeability into fractions that has the same construction with Cauer circuit. Based on this type of Cauer circuit, the copper loss of windings in motor and inductor with external influence considering eddy current can be simulated directly. The external magnetic field is simulated using FEM software.
- For the inductor and WPT working at very high frequency that the displacement current must be considered, the equivalent circuit with displacement current is applied. The complex mutual inductance is used in the surrogate model to consider the proximity effect and all the parameters are simulated from quasi-static magnetic field FEM. To solve the circuit, I used Python to analyze the circuit. The equivalent circuit with displacement current using complex mutual inductance can consider the eddy current and displacement current at same time without several iterations [18].

1.3 Thesis Outline

Chapter 1: Introduction

Describe the research background and purposes of this thesis.

Chapter 2: Cauer equivalent circuit based on the input data

The basic construction of Cauer circuit and the AVM to calculate the parameters of Cauer circuit are introduced. The method to get the input impedance for building Cauer circuit, containing formula calculation and FEM calculation are shown. The Cauer circuit is used to represent the WPT and inductor. The nonlinearity and displacement of WPT are considered in the Cauer circuit. The result in frequency domain and time domain are shown in this chapter.

Chapter 3: Cauer circuit based on the homogenized method

The basic theory of homogenization method is introduced. The impedance is calculated using homogenized method and Cauer circuit is built on the impedance. The results of Cauer circuit containing nonlinearity in time and frequency domain are shown. To consider windings influenced by external magnetic field from the rotor magnet, another type of Cauer circuit is built based on the complex permeability. The copper loss of windings considering the external influence is calculated using the Cauer circuit and compared with conventional FEM.

Chapter 4: Equivalent circuit with displacement current of inductor considering eddy currents and resonance

The equivalent circuit with displacement current is introduced to represent the magnetic devices. The detail of how to calculate the parameters of the equivalent circuit with displacement current using complex mutual inductance are described. The model is applied to analyze the inductor and WPT. The resonant point and the power factor are simulated using the surrogate model. The result in time domain simulation will also be shown in the chapter.

Chapter 5: Conclusion

Give a summary of the research and forecast the future research direction.

Chapter 2 Cauer equivalent circuit based on the input data

In this chapter, the research background and basic theory of Cauer circuit will be introduced in detail firstly, following by that of magneto-quasistatic FEM to calculate the input data. Then, the proposed works are going to be introduced in turn.

2.1 Cauer circuit

To downsize the electric devices, such as transformers, electric motors, and inductors, the driving frequency has been increased, which has led to an increase in eddy current losses due to the skin and proximity effects shown in Fig. 2-1.

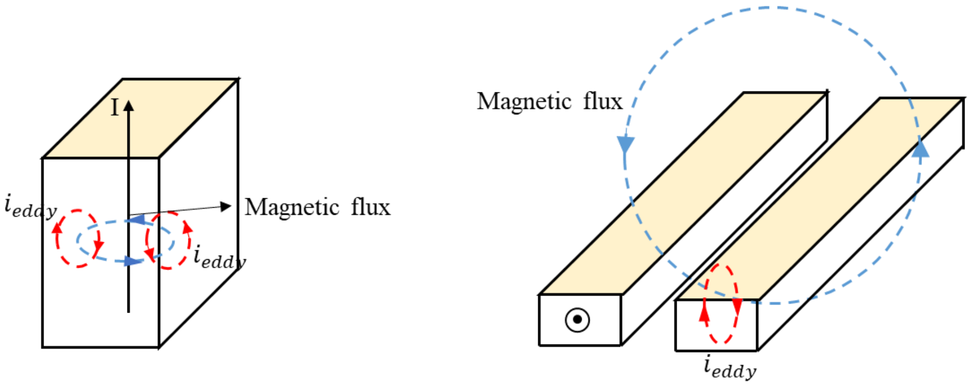

(a) Skin effect (b) Proximity effect

Fig. 2-1 Eddy current effect

The magneto-quasistatic can compute the eddy currents effectively, although its computational cost can be large because the device model has to be discretized into sufficient elements that are smaller than the skin depth. In particular, repeated FE analysis in a design process can be unacceptably time consuming. Cauer circuit is an optional surrogate model to accelerate the simulation considering eddy current in both frequency and time domain [19]-[20]. In previous research, the Cauer equivalent circuit of a steel sheet is derived from the analytical solution to the quasi-static Maxwell's equations [19]-[21]. Moreover, Cauer circuit can also be derived from 2-D and 3-D magneto-quasistatic Maxwell's equation [22]-[23]. It concludes that Cauer circuit can be applied in a wide range of magnetic devices such as induction motor, permanent magnet synchronous motors (PMSM) and WPT [8], [17].

The identification method can also be applied to determine the circuit parameters of Cauer circuit based on curve fitting. The parameters are determined so that the error between the input impedance of the equivalent circuit and that of the electric device of interest is minimized. The identification of equivalent circuit parameters using genetic algorithm (GA) has been adopted because of their high search ability and versatility [24]-[28]. GA would fail to determine the circuit parameters uniquely because of its stochastic attributes [29]. It also has a relatively high computational cost.

Sensitivity analysis based on the adjoint technique is a deterministic approach, that has been applied for circuit design [30]-[37]. Tellegen's approach uses an adjoint network and is widely used for circuit design [30]-[32]. It is also possible to compute the sensitivity of circuit equations directly based on the adjoint variable method (AVM) [33]-[37]. Particularly, the complex AVM has been proposed for analyzing complex systems, such as *RL* circuits [36]-[37]. Deterministic approaches are much simpler and have a smaller computational cost compared with GA. AVM is applied on identification of the Cauer circuit parameters that has the above-mentioned engineering importance. Based on the Cauer circuit derived from AVM, electric devices containing nonlinear material are represented [38].

With these approaches, the synthesized Cauer equivalent circuit can be embedded into circuit simulators and the time-domain analysis can be readily performed [17].

2.1.1 Construction of Cauer circuit

The construction of Cauer circuit used to represent the magnetic device is shown in Fig. 2-2.

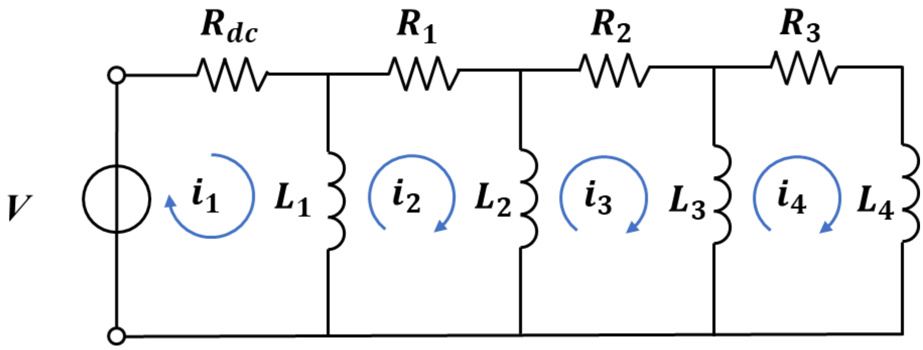

Fig. 2-2 Construction of a 4-stage Cauer circuit

Based on the basic circuit theory, the impedance of the Cauer circuit can be derived as (2.1). All the parameters in formula are shown in Fig. 2-2. Obviously, the impedance of the Cauer circuit is frequency based.

$$Z(\omega) = R_{dc} + \cfrac{1}{\cfrac{1}{j\omega L_1} + \cfrac{1}{R_1 + \cfrac{1}{\cfrac{1}{j\omega L_2} + \cdots}}} \tag{2.1}$$

A physical interpretation can be applied to the Cauer equivalent circuit, where R_{dc} and $L_1(\varphi)$ denote the DC resistance and inductance of the device, respectively. Nonlinearity can be introduced into $L_1(\varphi)$ to account for magnetic saturation in the core. At sufficiently low frequency, most of the current flows through R_{dc} and L_1 because $j\omega L_1$ is much smaller than the impedance of higher stages. As the frequency increases, the eddy current and the demagnetizing effect of the eddy current begin to make an impact. These are represented by R_1, R_2 ... *and* L_2, L_3 ... etc.

Based on the physical meaning of the Cauer circuit, it can be applied to represent the magnetic device in high frequency domain. The impedance of the Cauer circuit should fit with the device at every frequency. Moreover, to advance the process, magneto-quasistatic analysis is necessary.

2.2 Magneto-quasistatic FEM

Magneto-quasistatic FEM in frequency domain is necessary to build the Cauer circuit, either we use the adjoint variable method or the model order reduction method. It is applied to calculate the impedance or get the admittance function of magnetic device working in high frequency, while the displacement current is ignored.

In electromagnetism, the magneto-quasistatic Maxwell's equations are a set of equations that describe the behavior of electric and magnetic fields in situations where the electric field changes relatively slowly compared to the magnetic field. These equations are derived from the full set of Maxwell's equations under the assumption of quasi-static conditions, where electromagnetic waves are negligible, and electric fields vary slowly with time.

The full set of Maxwell integral equation shown as

$$\nabla \cdot \boldsymbol{E} = \frac{\rho}{\varepsilon_0} \tag{2.2}$$

$$\nabla \cdot \boldsymbol{B} = 0 \tag{2.3}$$

$$\nabla \times \boldsymbol{E} = -\frac{d\boldsymbol{B}}{dt} \tag{2.4}$$

$$\nabla \times \boldsymbol{B} = \mu_0 \boldsymbol{J} + \mu_0 \varepsilon_0 \frac{d\boldsymbol{E}}{dt} \tag{2.5}$$

Where $\boldsymbol{B}$, $\boldsymbol{E}$ represent the electric field strength and magnetic flux density at the point. μ_0 and ε_0 denote the permeability of free space and the permittivity of free space. $\boldsymbol{J}$ denotes the current density at the point.

As the electric field changes slowly and the change caused by the electric field can be ignored, the formula (2.5) is rewritten into

$$\nabla \times \boldsymbol{B} = \mu_0 \boldsymbol{J} \tag{2.6}$$

Under quasi-static conditions, the displacement current term $\mu_0 \varepsilon_0 \frac{dE}{dt}$ is typically neglected since it becomes negligible compared to the current density in most practical scenarios. This equation relates the circulation of the magnetic field around a closed path to the electric current passing through the surface enclosed by that path.

Following the magneto-quasistatic Maxwell's equations, FEM is applied to solve the magnetic and electric field of the magnetic device. For convenience we introduce the vector potential as the variable calculated in FEM program. The relationship between vector potential $\boldsymbol{A}$ and magnetic flux density is shown as

$$\nabla \times \boldsymbol{A} = \boldsymbol{B} \tag{2.7}$$

The magneto-quasistatic Maxwell's equation in frequency domain considering the eddy current caused by changing magnetic field can be written as

$$\nabla \times v(\nabla \times \boldsymbol{A}) + \boldsymbol{j}\omega\sigma(\boldsymbol{A} + \nabla\varphi) = \boldsymbol{J_0} \tag{2.8}$$

$$\nabla \cdot \{\boldsymbol{j}\omega\sigma(\boldsymbol{A} + \nabla\varphi)\} = 0 \tag{2.9}$$

Where v, ω, σ, φ and $\boldsymbol{J_0}$ denotes magnetic reluctivity, operating frequency, conductivity, scalar potential and input current density. The second part on the left-hand side of formula (2.8) represents the eddy current. Formula (2.9) indicates that there are no magnetic monopoles (isolated magnetic charges). The magnetic field lines always form closed loops.

Firstly, the model and air region are divided into small elements. Consequently, by applying the Galerkin method with the weighted residue method to (2.8) and (2.9), we obtain

$$\sum_j \boldsymbol{A}_j \left[\int_\Omega \nabla \times \boldsymbol{N}_i \cdot v \nabla \times \boldsymbol{N}_j d\Omega + j\omega\sigma \int_\Omega \boldsymbol{N}_i \times \boldsymbol{N}_j \, d\Omega\right] + j\omega\sigma \sum_k \varphi_k \int_\Omega \boldsymbol{N}_i \cdot \nabla N_k d\Omega$$
$$= I \int_\Omega \boldsymbol{N}_i \cdot J_0 d\Omega \tag{2.10}$$

$$j\omega\sigma \sum_j \boldsymbol{A}_j \int_\Omega \boldsymbol{N}_j \cdot \nabla N_u d\Omega + j\omega\sigma \sum_k \varphi_k \int_\Omega \nabla N_k \cdot \nabla N_u d\Omega = 0 \tag{2.11}$$

Where $\boldsymbol{N}_i$, N_i, I and J_0 denote the vector and scalar interpolation function, current, and unit current density, respectively. Incomplete Cholesky Conjugate Gradient method(ICCG) can be applied to solve the matrix and the distribution of $\boldsymbol{A}$, $\boldsymbol{B}$, current density and stored energy in model everywhere will be calculated. The result of self-made 2D axisymmetric magneto-quasistatic

FEM program is shown in Fig. 2-3. The vector potential of a 6-turn inductor whose operating frequency is 1MHz is calculated.

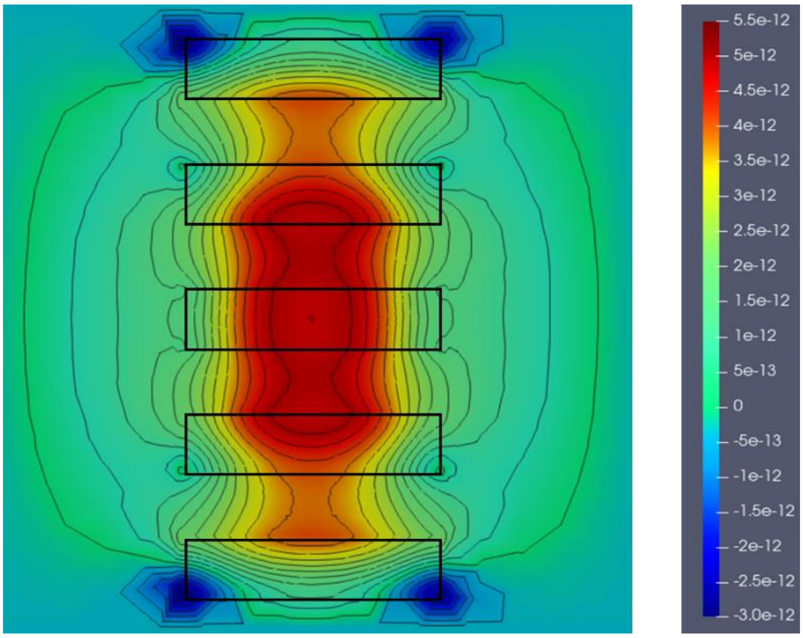

Fig. 2-3 Vector potential calculated from self-made FEM program

2.3 Methods to calculate the parameters of Cauer circuit

2.3.1 Model order reduction method

In this section, the model order reduction method will be introduced shortly. Based on the magneto-quasistatic FEM introduced in section 2.2 and the Padé via Lanczos (PVL) approximation [7], [22], the transfer function that corresponds to the admittance function of Cauer circuit, denoted here by $Y(\omega)$ can derived. Consequently, $Y(\omega)$ is represented by a rational function of the formula.

$$Y(\omega) = \frac{\beta_0 + \beta_1(j\omega) + \beta_2(j\omega)^2 + \cdots}{\alpha_0 + \alpha_1(j\omega) + \alpha_2(j\omega)^2 + \cdots} \tag{2.12}$$

By applying Euclid algorithm to formula (2.12), we can get a continued fraction in the form of (2.1). It corresponds to the input impedance of Cauer circuit in Fig. 2-2.

2.3.2 Identification method

The Cauer circuit can also be synthesized by curve fitting to the input impedance of a magneto-quasistatic system, either computed or measured [3], [17], without using the procedure based on model-order reduction as in [3] and [7]. Moreover, it's the method used in this thesis.

To calculate the parameters of Cauer circuit, genetic algorithm is an optional method [29]. However, based on the basic circuit theory, AVM can be applied and being more efficient and precise [3]. The purpose of the identification method is to minimize the error between the impedance of Cauer circuit and input impedance.

The optimization object is the parameters $\boldsymbol{x} = [R_1,\ R_2, \dots\ R_{p-1},\ X_1,\ X_2, \dots\ X_p]$ of p-stage Cauer circuit. In [3] the objective function is set as

$$min\, F(\boldsymbol{x}) \quad F(\boldsymbol{x}) = \sum_{q=1}^{N_s} \left| Z\left(\boldsymbol{x}, R_{DC}, \omega_q\right) - Z_s\left(\omega_q\right) \right|^2 \tag{2.13}$$

where N_s, ω_q, $Z\left(\boldsymbol{x},\ R_{DC},\ \omega_q\right)$, and $Z_s(\omega_q)$ denote the number of sampling points, qth angular frequency, impedance of the Cauer circuit, and measured (or computed) impedance, respectively.

However, for the inductive devices operating in high frequency, the reactance of the device is much larger than its resistance and the impedance at high frequency is much larger than it in low frequency. The objective function (2.13) may cause the error in the result of resistance and impedance in low frequency. Thus, regularization method is applied, and the optimization problem is adjusted into (2.14) to minimize the error [17].

$$F(\boldsymbol{x}) = \sum_{q=1}^{N_s} \frac{\left| R\left(\boldsymbol{x},\ R_{DC}, \omega_q\right) - R_s\left(\omega_q\right) \right|^2}{\left| R_s\left(\omega_q\right) \right|^2} + \frac{\left| X\left(\boldsymbol{x},\ R_{DC}, \omega_q\right) - X_s\left(\omega_q\right) \right|^2}{\left| X_s\left(\omega_q\right) \right|^2} \tag{2.14}$$

As it is difficult to calculate the sensitivity $\frac{dF(x)}{dx_n}$, the AVM is adopted based on the basic circuit equation in Cauer circuit. Here we consider the circuit equation of 4-stage Cauer circuit in Fig. 2-2 and is expressed as

$$\boldsymbol{Z}_{kl}(\omega_s)\boldsymbol{i} = \boldsymbol{v} \tag{2.15}$$

$$\boldsymbol{Z}_{kl}(\omega_s) = \begin{cases} -j\dfrac{\omega}{\omega_0}X_{l-1} & (k = l-1) \\ R_{l-1} + j\dfrac{\omega}{\omega_0}(X_{l-1} + X_l) & (k = l) \\ -j\dfrac{\omega}{\omega_0}X_l & (k = l+1) \end{cases} \tag{2.16}$$

$$\boldsymbol{i} = [i_1, i_2, i_3, i_4]^{\boldsymbol{t}} \tag{2.17}$$

$$\boldsymbol{v} = [V, 0,\ 0,\ 0]^{\boldsymbol{t}} \tag{2.18}$$

Where $\boldsymbol{v}$ denotes the input voltage, and $R_{l-1} = R_{dc}$ when $k = l = 1$. In addition, the reactance $X_k = \omega_0 L_k$ is defined with the maximum sampling frequency ω_0.

The argument objective function is combined with the adjoint variable as

$$\min \bar{F}(\boldsymbol{x}) \qquad \bar{F}(\boldsymbol{x}) = F(\boldsymbol{x}) + \sum_{q=1}^{N_s} \boldsymbol{\phi}_q^t\left(\boldsymbol{Z_{kl}}(\omega_q)\boldsymbol{i}_q - \boldsymbol{v}\right) \tag{2.19}$$

$$s.t. R_k \geq 0, L_k \geq 0 \ \ (k = 1,2..p)$$

where $\boldsymbol{\phi}_q^t$ denotes the adjoint variable, which corresponds to the Lagrange multiplier in the context of nonlinear programming. As $\boldsymbol{i}_q$ is the solution of (2.15), $F(\boldsymbol{x}) \approx \bar{F}(\boldsymbol{x})$. The derivation of $\bar{F}(\boldsymbol{x})$ with respect to the n_{th} variable in Cauer circuit x_n can be given as

$$\frac{\partial \bar{F}(\boldsymbol{x})}{\partial x_n} = \sum_{q=1}^{N_s}[\boldsymbol{\phi}_q^t \frac{\partial \boldsymbol{Z_{kl}}(\omega_q)}{\partial x_n}\boldsymbol{i}_q + \left\{\boldsymbol{Z_{kl}}(\omega_q)\boldsymbol{\phi}_q + \frac{\partial F(\boldsymbol{x})}{\partial \boldsymbol{i}_q}\right\}^t \frac{\partial \boldsymbol{i}_q}{\partial x_n}] \tag{2.20}$$

$\boldsymbol{i}_q$ is assumed that is the implicit function of x_n. It is still difficult to calculate the sensitivity of $\boldsymbol{i}_q$ with respect to x_n, thus we try to eliminate the secondary part in (2.20) under the condition of

$$\boldsymbol{Z_{kl}}(\omega_q)\boldsymbol{\phi}_q + \frac{\partial F(\boldsymbol{x})}{\partial \boldsymbol{i}_q} = 0 \tag{2.21}$$

We solve the adjoint function based on (2.21) to obtain the value of $\boldsymbol{\phi}_q$. Here, the right-hand side in (2.21) is not guaranteed that $F(\boldsymbol{x})$ is a holomorphic function that satisfies the Cauchy–Riemann equations. For this reason, the complex AVM is applied [36]-[37], and the formula is modified to

$$\boldsymbol{Z_{kl}}(\omega_q)\boldsymbol{\phi}_q = \frac{\partial F(\boldsymbol{x})}{\partial \boldsymbol{i}_q^r} - j\frac{\partial F(\boldsymbol{x})}{\partial \boldsymbol{i}_q^i} \tag{2.22}$$

where the superscripts r and i denote the real and imaginary parts, respectively. The right hand of (2.22) only relates to the first stage of $\boldsymbol{i}_q$, as the impedance of Cauer circuit $Z(\boldsymbol{x},\ R_{DC},\ \omega_q)$ is calculated by $V/\boldsymbol{i}_{q1}$.

Consequently, by substituting $\boldsymbol{\phi}_q$ back to (2.20) the sensitivity with respect to x_n is derived as [37]

$$\frac{\partial \bar{F}(\boldsymbol{x})}{\partial x_n} = -Re\left(\sum_{q=1}^{N_s} \boldsymbol{i}_q^t \frac{\partial \boldsymbol{Z_{kl}}(\omega_q)}{\partial x_n}\boldsymbol{\phi}_q\right) \tag{2.23}$$

Although the parameters of Cauer circuit can be calculated by the formula, we still must add a constraint that all the parameters should be larger than zero. To do so, constraint functions $g_k(\boldsymbol{x})$ are introduced and the optimized problem is changed into

$$\min \bar{F}(\boldsymbol{x})$$

$$s.t. \quad g_i(x) \geq 0 \quad i = 1,2 \dots 2p-1$$

$$g_i(x) = \boldsymbol{x}_{i_{th}} \tag{2.24}$$

After introducing the slack variable y_i^2, the optimized problem is modified to

$$\min \bar{F}(\boldsymbol{x})$$

$$s.t. \quad g_i(x) - y_i^2 = 0 \tag{2.25}$$

Next, we introduce an extended Lagrangian variable $\boldsymbol{\lambda}$ and a penalty *r* to add the limitation [39]. Thus, the new objective function is derived as

$$L(x,y,\lambda) = \bar{F}(\boldsymbol{x}) + \sum_{0}^{2p-1} \lambda_i\{g_i(x) - y_i^2\} + \frac{1}{2}r\sum_{0}^{2p-1}\{g_i(x) - y_i^2\}^2 \tag{2.26}$$

To get the extreme value of $L(x,y,\lambda)$, the minimization of y_i is performed as

$$\frac{\partial L(x,y,\lambda)}{\partial y_i} = 2\lambda_i y_i + 2r\{g_i(x) - y_i^2\}y_i = 0 \tag{2.27}$$

The requirement for y_i is

$$g_i(x) - y_i^2 = \min\left(g_i(x),\ -\frac{\lambda_i}{r}\right) \tag{2.28}$$

By substituting (2.28) back to (2.26), the final objective function is changed into

$$\min M(\boldsymbol{x},\boldsymbol{\lambda},r) = F(\boldsymbol{x})$$

$$+\sum_{q=1}^{N_s}\boldsymbol{\phi}_q^t\left(\boldsymbol{Z_{kl}}(\omega_q)\boldsymbol{i}_q - \boldsymbol{v}\right) + \frac{1}{2r}\sum_k[\{\min(0, rg_k(\boldsymbol{x}) + \lambda_k)\}^2 - \lambda_k{}^2] \tag{2.29}$$

The derivative of $M(\boldsymbol{x})$ with respect to $\boldsymbol{x}$ is

$$\frac{\partial M(\boldsymbol{x})}{\partial x_n} = \sum_{q=1}^{N_s}\left[\boldsymbol{\phi}_q^t\frac{\partial \boldsymbol{Z_{kl}}(\omega_q)}{\partial x_n}\boldsymbol{i}_q + \left\{\boldsymbol{Z_{kl}}(\omega_q)\boldsymbol{\phi}_q + \frac{\partial F(\boldsymbol{x})}{\partial \boldsymbol{i}_q}\right\}^t\frac{\partial \boldsymbol{i}_q}{\partial x_n}\right]$$

$$+\frac{1}{r}\sum_k[\min(0, rg_k(\boldsymbol{x}) + \lambda_k)\frac{\partial \min(0, rg_k(\boldsymbol{x}) + \lambda_k)}{\partial x_n}] \tag{2.30}$$

To update the parameters, we employ the quasi-Newton method based on the Broyden–Fletcher–Goldfarb–Shanno algorithm. The rule of updating the $\boldsymbol{\lambda}$ is expressed as

$$\lambda_i{}^{k+1} = \lambda_i{}^k + t^k[g_i(x^k) - (y_i{}^k)^2] = \min\left(0, \lambda_i{}^k + r^k g_i(x^k)\right) \tag{2.31}$$

For all samplings, if

$$\left|\min\left\{\min\left(g_i(x^k),\ -\frac{\lambda_i{}^k}{t^k}\right)\right\}\right| > \beta\left|\min\left\{\min\left(g_i(x^{k-1}),\ -\frac{\lambda_i{}^{k-1}}{t^{k-1}}\right)\right\}\right| \tag{2.32}$$

r will be updated following

$$t^{k+1} = \alpha t^k \tag{2.33}$$

where $1 < \alpha \le 10$ and $0 < \beta < 1$.

To sum up the flowchart of the AVM is shown in Fig. 2-4.

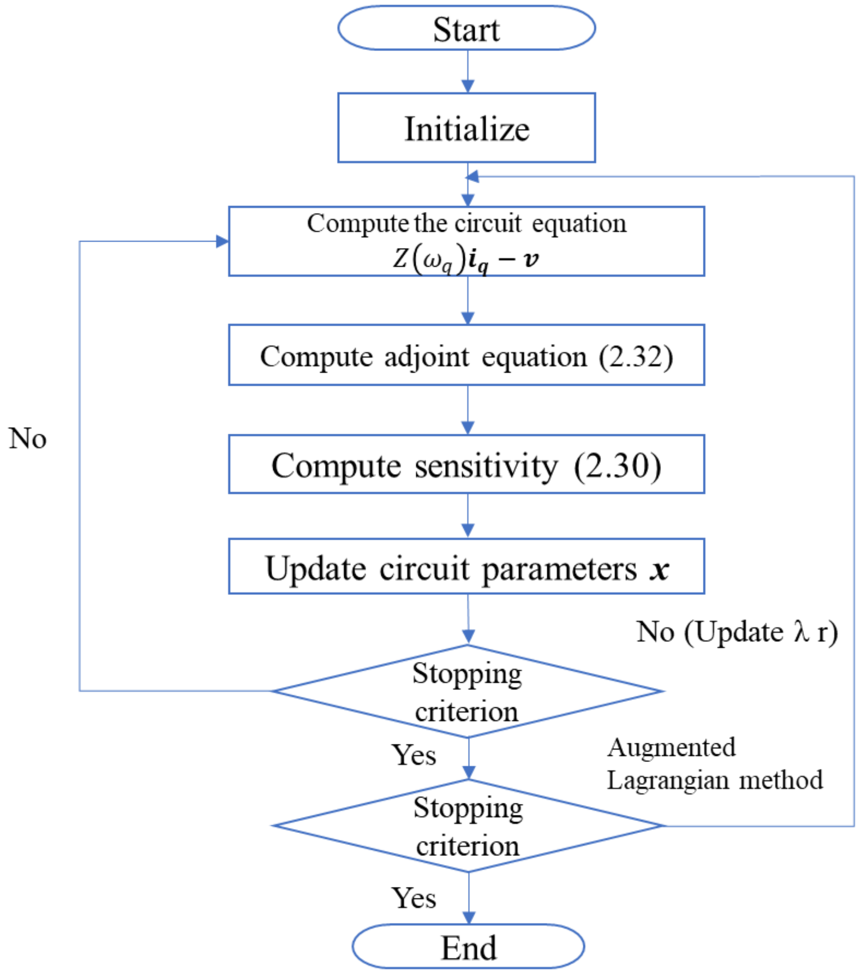

Fig. 2-4 Flowchart of AVM

The optimization parameters for AVM are shown in Table. 1.

Table. 1 Parameters in algorithm

Initial circuit parameters $\boldsymbol{x}^0$	**1.0Ω**	Initial multiplier value $\boldsymbol{\lambda}^0$	**0.0**
Initial penalty parameter $\boldsymbol{r}^0$	10	Stopping criterion of Quasi-Newton method	$\left\lvert\frac{\partial M(\boldsymbol{x},\boldsymbol{\lambda},r)}{\partial \boldsymbol{x}}\right\rvert < 10^{-8}$
Stopping criterion of augmented Lagrangian method	$\lvert\min\{\boldsymbol{g}(\boldsymbol{x}), -\boldsymbol{\lambda}/2r\}\rvert < 10^{-6}$	Updating parameters α, β	2, 0.5

The procedure of the algorithm is described as follows

(a) Set the initial program parameters as shown in Table. 1.

The parameters can be modified by the experience to accelerate the calculation, especially the initial parameters $\boldsymbol{x^0}$.

(b) Solve the circuit

Solve the circuit by computing the circuit equation. In this step we will get the impedance matrix $\boldsymbol{Z_{kl}}(\omega_q)$ and current vector $\boldsymbol{I}$.

(c) Compute the adjoint variable

The adjoint variable is calculated from the equation (2.22), the $\frac{\partial \boldsymbol{Z_{kl}}(\omega_q)}{\partial x_n}$ in the equation can be calculated based on the equation (2,16). The right-hand item can be calculated directly based on $V/\boldsymbol{i}_{q1}$.

(d) Compute the sensitivity

Substitute the value of adjoint variable back to the equation (2.30).

(e) Update the parameters x^n to x^{n+1}

Based on the quasi-Newton method, the parameters are updated. After this step, the stopping criterion of iteration will be checked. If the stopping criterion is not satisfied, the program will go back to step (b). Otherwise, the program will go on to next step.

(f) Check the stopping criterion of argument Lagrangian method

The $\boldsymbol{x}^n$ will be checked if the stopping criterion of argument Lagrangian method is satisfied to avoid the negative value. If the stopping criterion is not satisfied, the parameters r and λ^0 will be updated. Otherwise, the program will end and the $\boldsymbol{x}^n$ is the final result.

2.4 Transformer represented by Cauer circuit

In this section, we build the math model of second side short transformer. The resistance and leakage inductance are calculated using the formula. Consequently, Cauer circuit is built using the calculated impedance based on the AVM to simulate the inrush current.

2.4.1 Leakage inductance

We consider the leakage flux in the transformer shown in Fig. 2-5. Let us assume that the secondary side is short. In this situation, the main flux is canceled out so that the leakage flux is dominant. We also assume that the permeability of the core is infinite, and the magnetic field is negligible. Although the permeability of the steel sheet would be reduced as frequency increases, it is still much larger than the air. Moreover, we assume that the winding is sufficiently long in y and z directions so that the magnetic and electric fields are represented by $\boldsymbol{H} = H(x)\boldsymbol{z}$ and $\boldsymbol{E} = E(x)\boldsymbol{y}$, respectively.

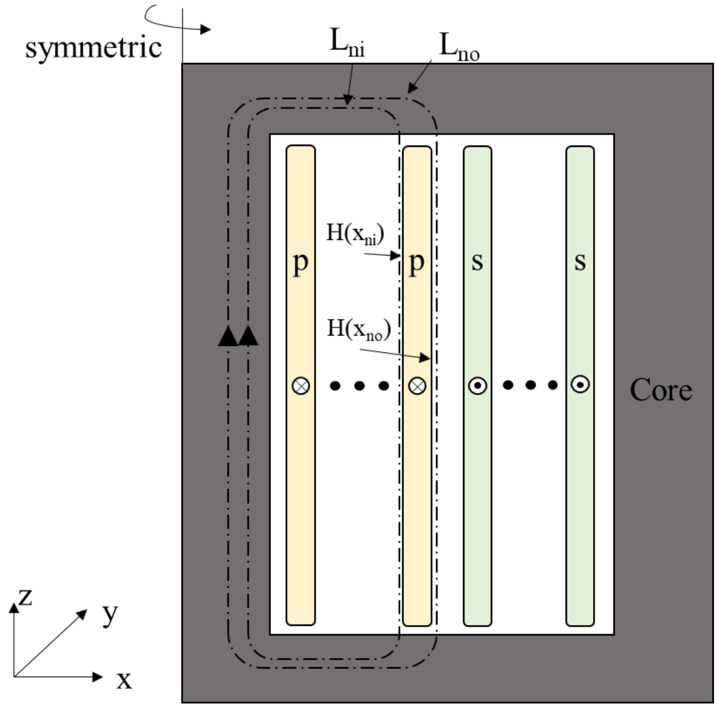

Fig. 2-5 The schematic diagram of transformer

By solving the one-dimensional magnetic diffusion equation derived from the Maxwell equations under the quasi-static approximation.

$$\frac{d^2H}{dx^2} - \gamma^2 H = 0 \tag{2.34}$$

Where $\gamma = \sqrt{j\omega\mu_0\sigma}$, we obtain

$$H(x) = H_1 e^{\gamma x} + H_2 e^{-\gamma x} \tag{2.35}$$

Based on the boundary condition and invoking Ampere's law for the L_n and L_{n-1}, the distribution of magnetic field strength in nth layer is expressed as [40]-[41]

$$H(x) = H_0 \frac{nsinh(\gamma x) + (n-1)\sinh(\gamma t - \gamma x)}{\sinh(\gamma t)} \tag{2.36}$$

Where n and t are the layer number and is layer thickness, and x begins from the inner side of each layer. The magnetic field in the air gap and insulation layer, which are constant, can also be obtained. The distribution of ***H*** in secondary side can also be calculated in the same way. Magnetomotive force (MMF) in primary layer, insulation layer and secondary layer is shown in Fig. 2-6.

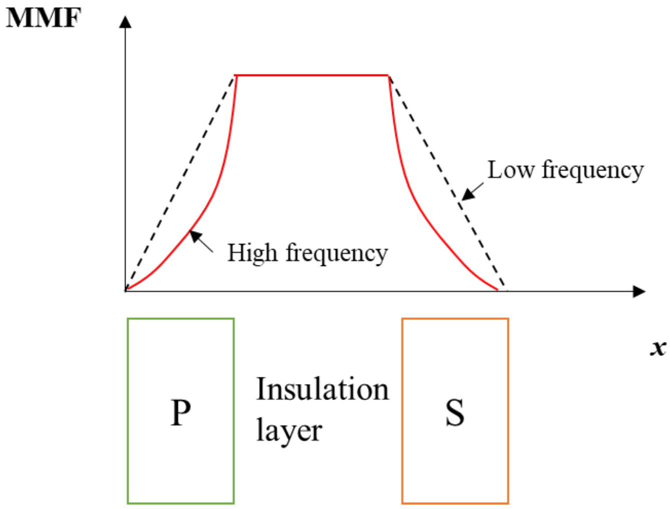

Fig. 2-6 MMF between the layers

The stored energy in layer reduces in high frequency and from the stored magnetic energy in the winding and insulation layers, we find that the inductance is represented by

$$L_{lk} = \frac{2}{2I^2}\int \mu H H^* \, dV = \frac{\mu_0 l_w n_p}{6h_w}$$
$$\left(\frac{2{n_p}^2(k_1+2k_2)(p+1)}{a\,(\cosh(2at)-\cos(2at))} + \frac{(p+1)(k_1-4k_2)}{pa\,(\cosh(2at)-\cos(2at))}\right.$$
$$\left. + \left(2{n_p}^2 + 2p{n_p}^2 + \frac{1}{p} + 1\right) t_i\right) \tag{2.37}$$

$$k_1 = \sinh(2at) - \sin(2at) \quad k_2 = \sin(at)\cosh(at) - \cos(at)\sinh(at) \quad a = \sqrt{\frac{wu_0\sigma}{2}}$$

where $l_w, h_w, n_p,\ p,\ t_i$ denote the length and height of the windings, the number of turns of the primary winding, the ratio of the primary and secondary number of turns and thickness of the insulation layer.

2.4.2 AC resistance

We also can evaluate the AC resistance of the transformer from the stored energy in electric field.

$$R_{ac}I^2 = \int \sigma E E^* \, dV \tag{2.38}$$

The electric field strength could be calculated from the distribution of $\boldsymbol{H}$ and we have

$$E_y = -\frac{dH_z}{\sigma dx} = -H_0 \frac{n\gamma \cosh(\gamma x) - (n-1)\gamma \cosh(\gamma t - \gamma x)}{\sigma \sinh(\gamma t)} \tag{2.39}$$

The electric field strength in insulation layers is assumed as 0. By submitting (2.39) to (2.38), we obtain [42]

$$R_{ac} = \frac{l_w a n_p}{3\sigma h_w(\cosh(2at) - \cos(2at))}\left(2{n_p}^2(k_3 - 2k_4)(p+1) + \frac{(p+1)(k_3+4k_4)}{p}\right) \tag{2.40}$$

where $k_3 = \sinh(2at) + \sin(2at)$, $k_4 = \sin(at)\cosh(at) + \cos(at)\sinh(at)$.

2.4.3 Simulation result of Cauer circuit

The impedance of secondary side short transformer is calculated based on the formula and FEM software JMAG^{TM}. The parameters of the transformer are shown in Table. 2

Table. 2 Transformer parameters

μ_r	h_w	l_w	n_p/n_s	t/t_i
2200	26mm	62.8mm	6/6	0.2/0.25mm

Based on the impedance calculated from formula, the 4-stage Cauer circuit is built based on AVM method and the impedance is compared with FEM and formula. The operating frequency is from 1Hz to 2MHz. The convergency progress is shown in Fig. 2-7. The parameters of Cauer circuit are shown in Table. 3. It costs less than 1 minute to get the result.

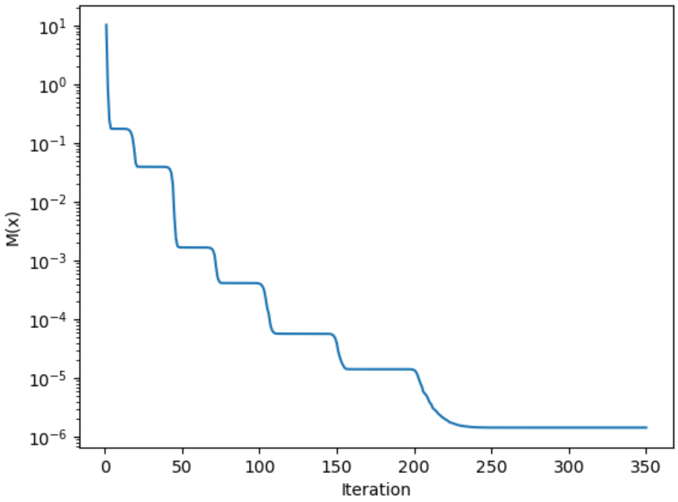

Fig. 2-7 The progress of convergency

Table. 3 Parameters of Cauer circuit

	R_{DC}, L_1	R_2, L_2	R_3, L_3	R_4, L_4
$R(\Omega)$	2.08E-03	1.79E+00	5.51E+01	1.82E+02
L(H)	1.98E-07	3.43E-07	1.70E-06	4.93E-07

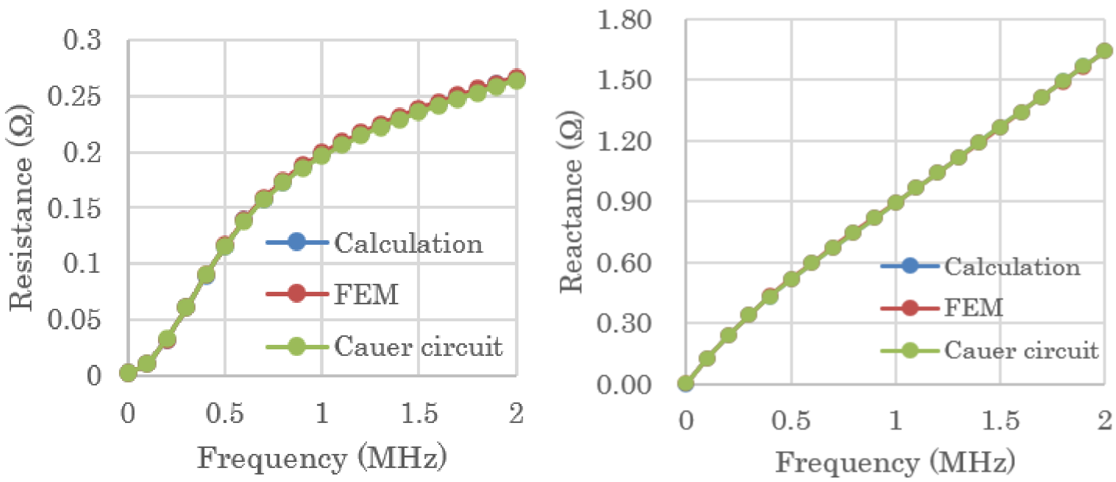

(a) Resistance (b) Reactance

Fig. 2-8 The AC resistance and leakage inductance

We find that the three impedances all fit well with each other in Fig. 2-8. It is concluded that the Cauer circuit can perform well in frequency domain.

Following that, the performance of Cauer circuit in time domain will also be validated with time domain FEM for simulating the inrush current of the transformer. We also carry out the time-domain analysis of the *R-L* circuit which has the frequency characteristics derived from formula using circuit simulation software LTSpice.

The result of inrush current is given in Fig. 2-9. The input is 10MHz voltage source.

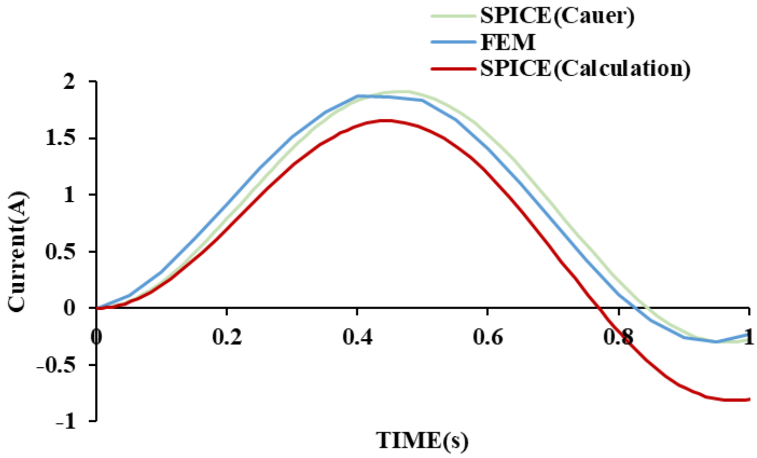

Fig. 2-9 Inrush current at 1MHz

It is seen that the results are consistent. The error in Spice(Calculation), computed from the formulas, is due to the fact that only the fundamental mode is considered. The results computed by the Cauer circuit in Spice(Cauer) agree well with those computed by FEM. Moreover, Cauer circuit based on the input impedance calculated from formula is less time-consuming than FEM especially in time domain simulation.

2.5 Inductor represented by Cauer circuit

In this section, we do the validation of the following items. (i) magnetic saturation, (ii) PWM input. We consider the inductor shown in Fig. 2-10 to compute the impedance in frequency domain. The inductor core is made of soft magnetic composite.

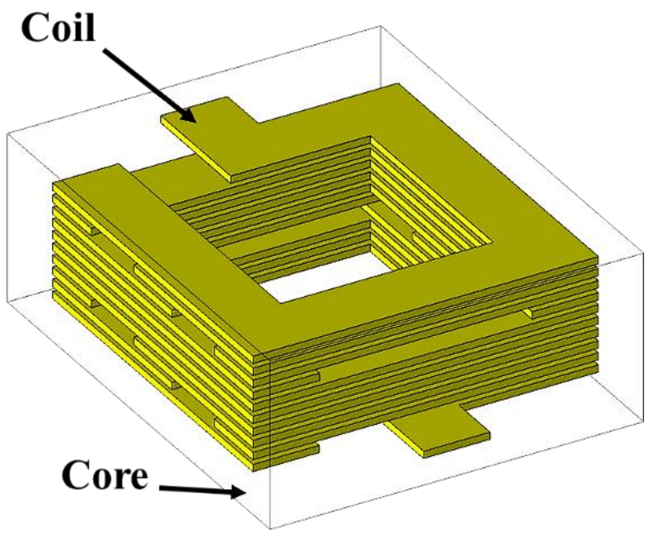

Fig. 2-10 Inductor model

Firstly, we consider the Cauer circuit in frequency domain without the nonlinearity of the core. While calculating in the FEM software JMAG™, the input current is set as a small value that is far from the saturation of the core. Based on the operating frequency that 5-stage Cauer circuit is chosen to represent the model. The parameters of Cauer circuit are shown in Table. 4.

Table. 4 Parameters of Cauer circuit of inductor

	R_{DC}, L_1	R_2, L_2	R_3, L_3	R_4, L_4	R_5, L_5
R(Ω)	0.059	1.77E+02	2.06E+03	1.04E+04	3.16E+10
L(H)	8.54E-07	5.01E-05	1.25E-04	1.02E-04	1.52E-06

The impedance of Cauer circuit is compared with the result of FEM as shown in Fig. 2-11.

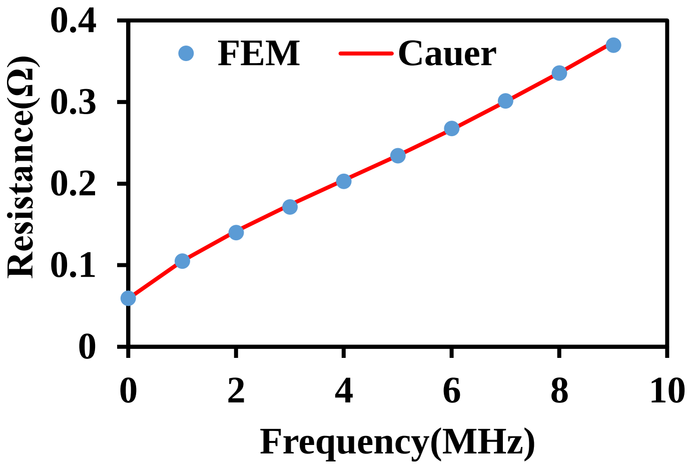

(a) Resistance of the inductor

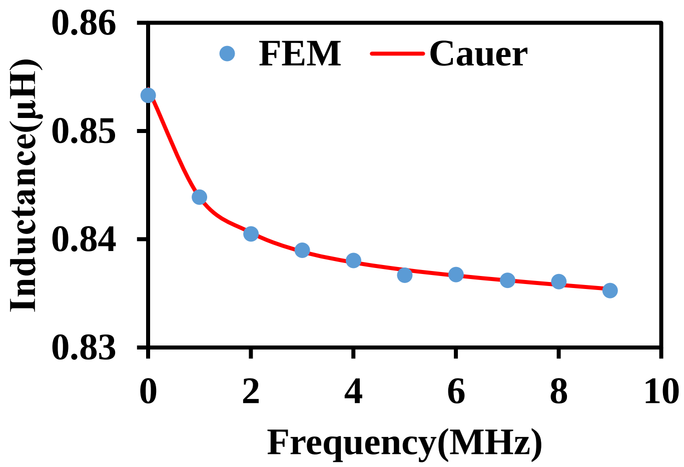

(b) Resistance of the inductor

Fig. 2-11 Impedance of inductor

The parameters of the Cauer circuit in Table. 4 were assumed to be linear during the identification process. To account for magnetic saturation in the magnetic core, nonlinearity was introduced to the primal inductance such that $L_1 = \Phi(I)/I$ in Fig. 2-2 [38], which is obtained from magnetostatic FE analysis.

This method assumes that the induced eddy currents are represented in the higher stages of the Cauer circuit and are so weak that they do not influence the magnetic saturation. Under this condition, we only introduce the nonlinearity into the primal inductance.

The current response and copper loss in the transient process are plotted in Fig. 2-12 and Fig. 2-13 respectively, where the circuit is excited by a singular wave of 10 V at 1 MHz. In these figures, nonlinear Cauer and Cauer represent the results computed from the Cauer circuits with and without nonlinearity in L_1. It can be concluded from Fig. 2-12 and Fig. 2-13 that the results computed from the Cauer circuit with nonlinearity agree better than those computed from the Cauer circuit without nonlinearity. Specifically, the loss computed from the Cauer circuit without nonlinearity significantly differs from those obtained by the other two approaches.

Notably, the Cauer circuit requires only several seconds for time-domain simulation based on the circuit simulation software LTSpice, whereas the FEM requires one hour for one period using a device with an Intel(R) Core(TM) i7-9700 CPU @ 3.00 GHz, which has also been used for other computations presented here.

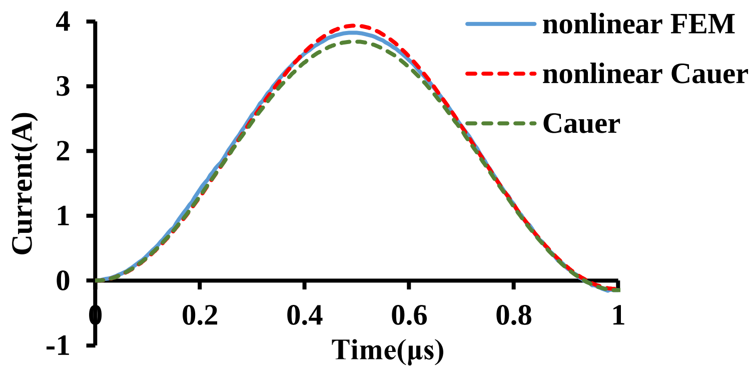

Fig. 2-12 Current response of inductor

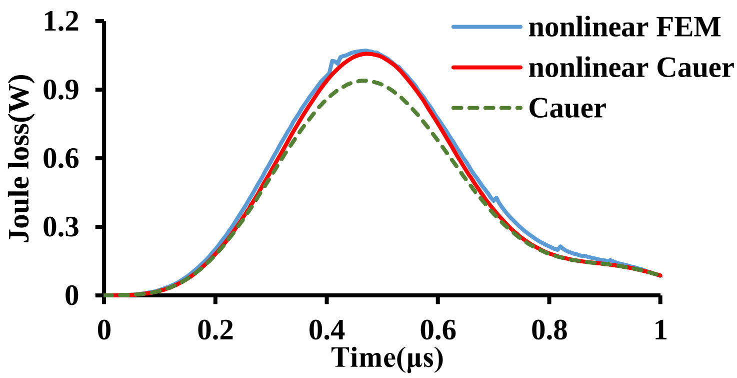

Fig. 2-13 Power loss of inductor

Subsequently, the proposed method was applied to an inductor to which PWM voltage was applied while considering two nonlinear Cauer circuits each comprising one and five stages, respectively. Besides the fundamental frequency, the PWM wave contains higher frequency harmonics that should also be considered. Cauer circuit can consider all the components of frequency at the same time. The results are shown in Fig. 2-14 and Fig. 2-15.

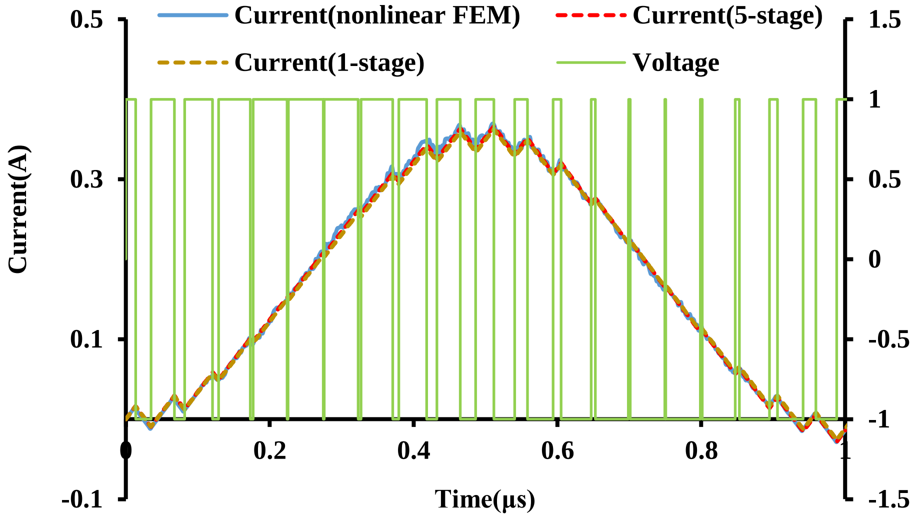

Fig. 2-14 Current response with PWM input

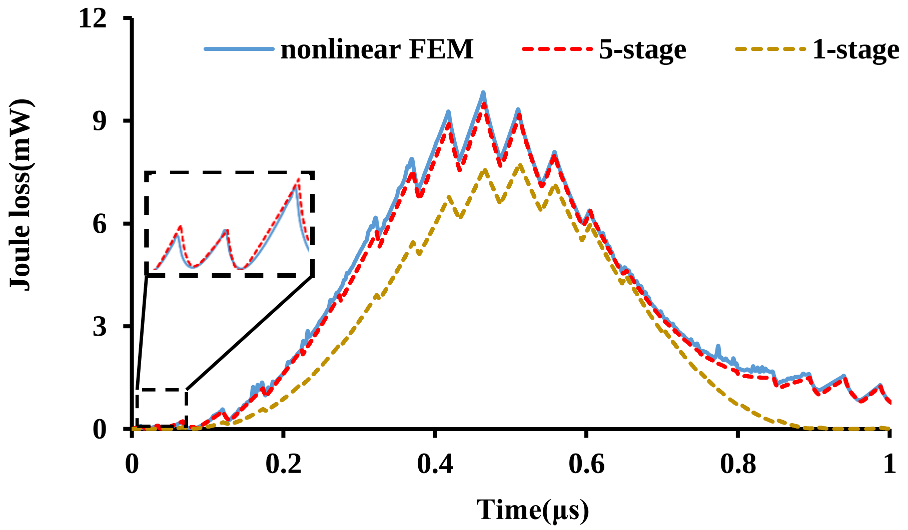

Fig. 2-15 Copper loss with PWM input

Because the reactance is much larger than the resistance at higher frequencies, the current characteristics of the 1-stage and 5-stage Cauer circuits exhibited minor variations only. While copper loss caused by eddy currents could not be determined in a 1-stage Cauer circuit, the copper loss of 5-stage Cauer circuit agreed well with that computed from the nonlinear transient FE analysis. It is worth noting that the computation time required when using the Cauer circuit was only 10 s, whereas the FEM analysis required approximately 50 h.

2.6 Wireless power transfer represented by Cauer circuit

2.6.1 Introduction of WPT

WPT is a revolutionary technology that enables the transfer of electrical energy from a power source to an electrical load without the need for physical connections like wires or cables. This technology has the potential to transform the way we access and use power in various applications [43]-[45].

One of the key methods employed in WPT is electromagnetic induction, which involves the transfer of energy between coils through a magnetic field. Resonant inductive coupling is a common technique used to enhance the efficiency of power transfer over longer distances. Other methods include radio frequency (RF) energy harvesting and microwaves. The schematic diagram is shown in Fig. 2-16.

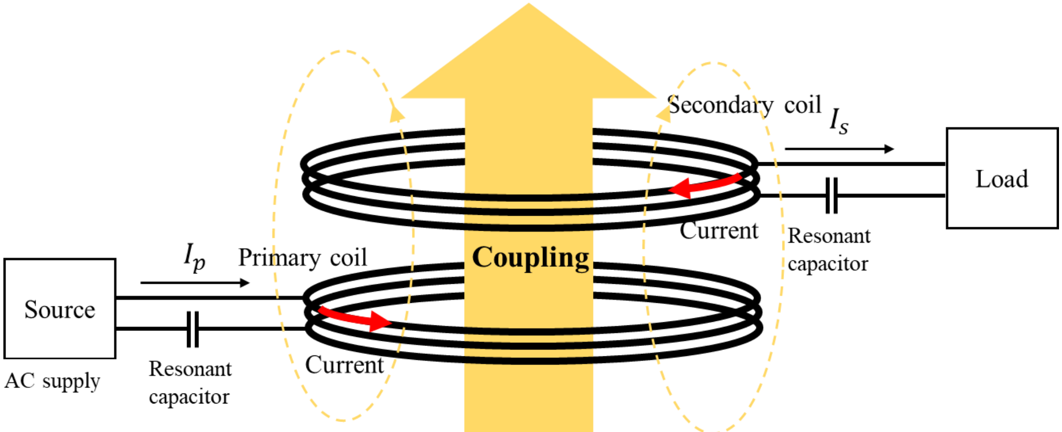

Fig. 2-16 Schematic diagram of WPT

While WPT holds great promise, challenges such as energy loss, safety concerns, and regulatory standards must be addressed to ensure widespread adoption. Ongoing research and development in this field aim to overcome these challenges and unlock the full potential of WPT for a more connected and efficient future.

Cauer circuit is a feasible method to represent the WPT device in both frequency and time domain. The transient process of current and copper loss can be simulated much more efficiently. Moreover, Cauer circuit can be combined into the electric power system to do some complex simulation.

2.6.2 Equivalent circuit of inductive coupling WPT

In Fig. 2-17, the equivalent circuits of a basic inductive coupling WPT system is shown, where I_1, R_1 and L_1 denote the input source, resistance, and self-inductance of primary coil, while R_2, L_2 and R_L denote the resistance and self-inductance of secondary coil, and the load resistance in the system respectively. And M is the mutual inductance between primary and secondary coil. For such system, the connection between two coils can also be represented by the coefficient *k.* It is defined as

$$k = \frac{\sqrt{L_1 L_2}}{M} \tag{2.41}$$

In electromagnetic simulation, the self-inductances of coils can be calculated by equation from the magnetic flux pass through (2.42), and mutual inductance can be obtained by equation (2.43).

$$\phi_i = L_i I_i \tag{2.42}$$

$$\phi_2 = \omega M I_1 \tag{2.43}$$

where ϕ_i and I_i represent, magnetic flux through the coils, and current in coils respectively. In equation (2.43), ϕ_2 and ω are the magnetic flux pass through secondary coil and angular frequency of the WPT system. All the equations are under the consumption that the opposite is open circuit.

To improve the efficiency of the WPT system, compensation capacitor is necessary to realize the resonance at specific frequency point. Two kinds of basic compensation are shown in Fig. 2-17.

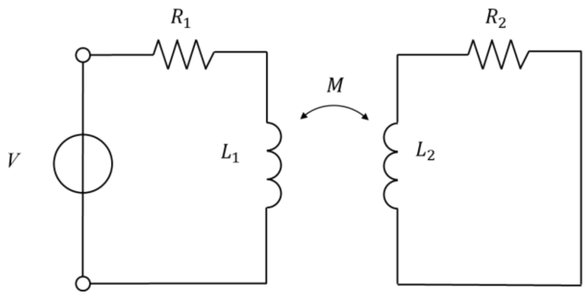

(a) Equivalent circuit of an inductive coupling WPT without compensation

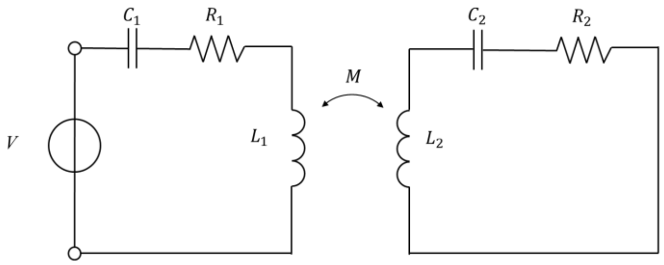

(b) Series compensation

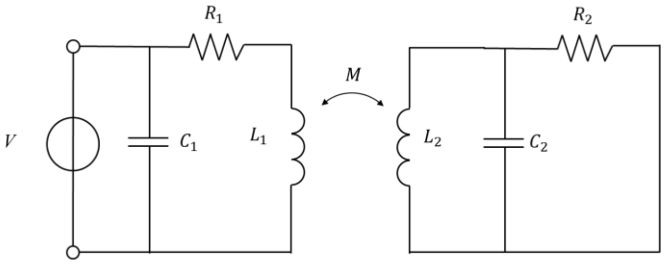

(c) Parallel compensation

Fig. 2-17 Equivalent circuit of an inductive coupling WPT

The resonant frequency of both series compensation and parallel compensation is calculated as (2.44). In general, the resonant frequency of both sides should be adjusted to the same value.

$$f = \frac{1}{2\pi}\sqrt{\frac{1}{LC}} \tag{2.44}$$

Thus, the WPT can work at the maximum efficiency at the frequency. To choose the compensation capacitor, it's crucial to calculate to it while considering the eddy current and displacement current effect. In this section we apply the Cauer circuit considering the eddy current only and apply equivalent circuit with displacement current to consider all the effect in Section.4.

2.6.3 Representation of WPT

As mentioned in this section, WPT has two or more parts that we have to use two or more Cauer circuits to represent the model.

Next, we considered a vehicle oriented WPT system, which contains a pair of ring coils as shown in Fig. 2-18, and used two Cauer circuits to represent them in both the frequency and time domains. Moreover, we also want to consider the misalignment WPT.

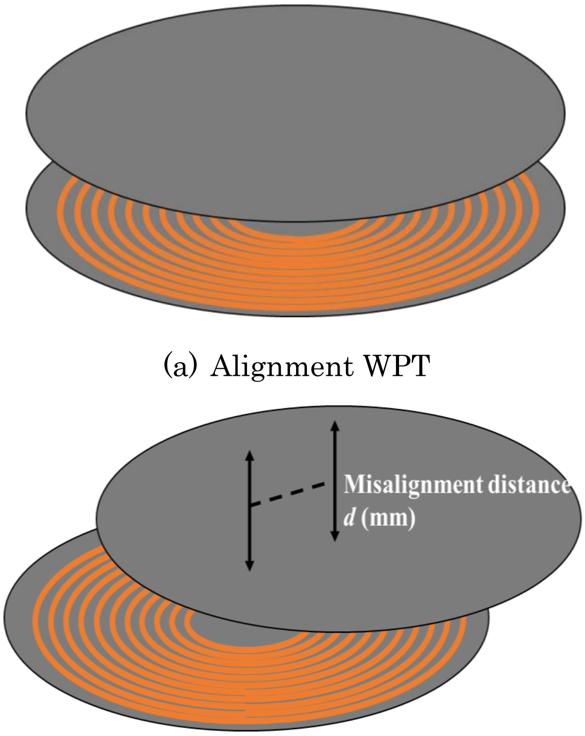

(a) Alignment WPT

(b) Misalignment WPT

Fig. 2-18 Schematic diagram of WPT

Tests were conducted to determine whether the Cauer circuits performed well for the WPT system with and without misalignment. Construction of the primary and secondary sides of the WPT system is identical, and the system parameters are shown in Table. 5.

Table. 5 Parameters of WPT

Turns	11	Pitch	10mm
Inner radius	100mm	Distance	100mm
μ_r of core	1000	Operation frequency	85kHz

For electric vehicle charging system, as noted in standards [46]-[47], the resonance frequency – the operating frequency of system as well – is specified between 79 to 90 kHz, of which 85 kHz is the most common frequency.

The equivalent circuit of WPT based on the Cauer circuit is shown in Fig. 2-19. Two parts of the WPT are connected by the current dependent voltage source.

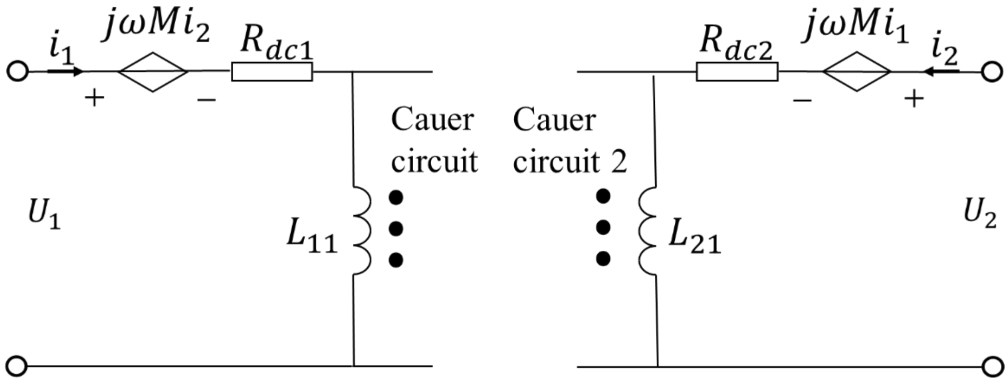

Fig. 2-19 Equivalent circuit of WPT based on Cauer circuit

The circuit equations of the equivalent circuit are shown as

$$Z_1(\omega)i_1 + j\omega M i_2 = V \tag{2.45}$$

$$Z_2(\omega)i_2 + j\omega M i_1 = 0 \tag{2.46}$$

The impedance of one part of WPT is frequency dependent that it is based on the input source. Cauer circuit is used to represent the model that the impedance fit well with result of FEM in all the frequency domain. Consequently, it is essential to get the input impedance for AVM to build the Cauer circuit.

For circuit identification, the input resistance was determined from the Joule loss of the primary coil for $\dot{U}_2 = 0$, to factor in the proximity effect on the resistance from the opposite side. The input reactance and mutual inductance M connecting the two parts were determined from $\dot{U}_1/\dot{I}_1$ and the magnetic flux through the secondary-side coil for $\dot{I}_2 = 0$. We adopted the same method to derive the input impedance of the secondary Cauer circuit as well. All the calculations are performed by FEM software JMAG.

Assuming that the operating frequency of the WPT is below MHz levels, a 4-stage Cauer circuit that is sufficient to demonstrate the eddy current effects was built. The resultant frequency-domain characteristics $\dot{Z}_1$ of the WPT ($\dot{U}_1/\dot{I}_1, \dot{U}_2 = 0$) are shown in Fig. 2-20.

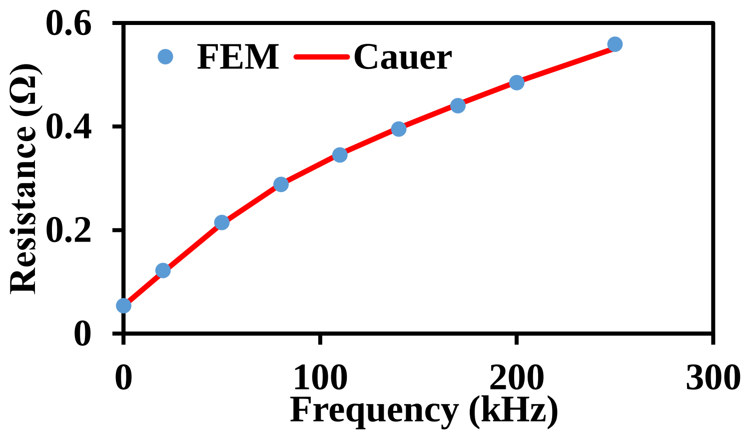

(a) Real part of Z_1

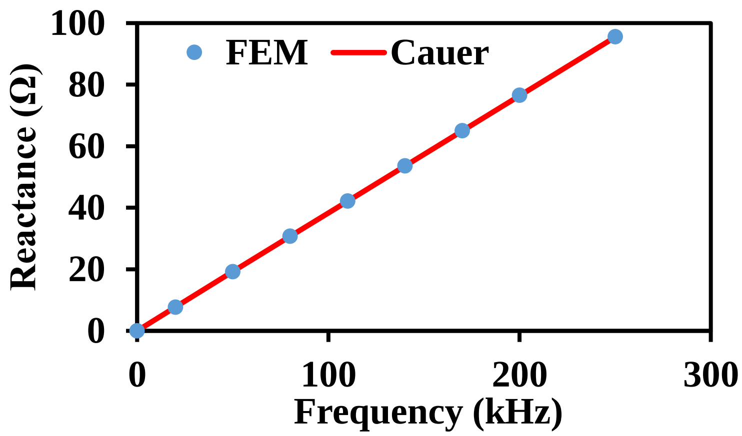

(b) Imaginary part of Z_1

Fig. 2-20 Frequency characteristics of WPT equivalent circuit

From the resultant frequency-domain characteristics, shown in Fig. 2-20, it is evident that the results obtained from the synthesized equivalent circuit and FEM analysis are in good agreement. Subsequently, the equivalent circuit was embedded into the WPT system, as shown in Fig. 2-21, to verify the performance of the equivalent circuit in the time domain. Series compensation is applied in the system to adjust the resonant frequency of both sides to 85kHz. The circuit parameters of the power transfer system are shown in Table. 6.

Table. 6 Parameters of WPT

Resonant capacitor	43.824 nF
Voltage stabilizing capacitor	1 μF
Voltage stabilizing resistor	0.0423 Ω
Load	20 Ω

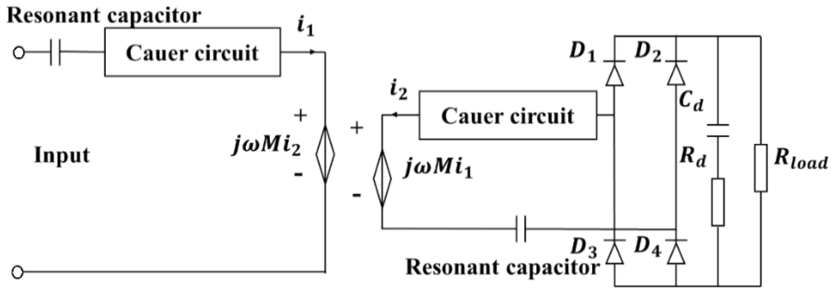

Fig. 2-21 WPT applied in power transfer system

The major advantage of the proposed equivalent circuit is the high-speed analysis in the time domain while accounting for the eddy current effects in the coil. The input was from a 110 V, 85 kHz voltage source. It took 25 min to build the Cauer circuit and perform the time-domain simulation, whereas 2 h was required for the time-domain FEM simulation. We find that the time evolutions for the current and loss obtained using the equivalent circuit agree well with those computed from the FEM analysis, as shown in Fig. 2-22 and Fig. 2-23.

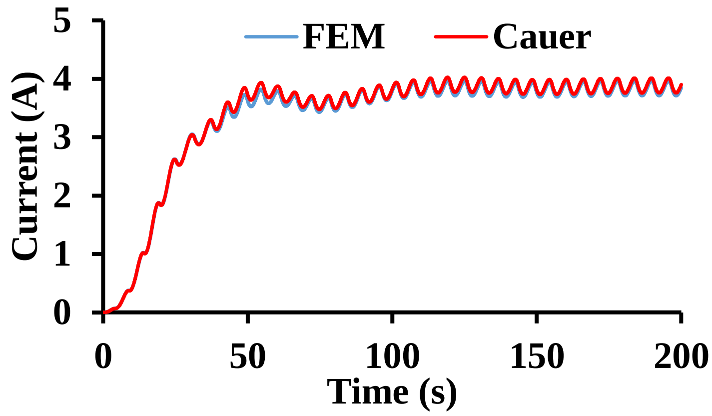

Fig. 2-22 Current response of load

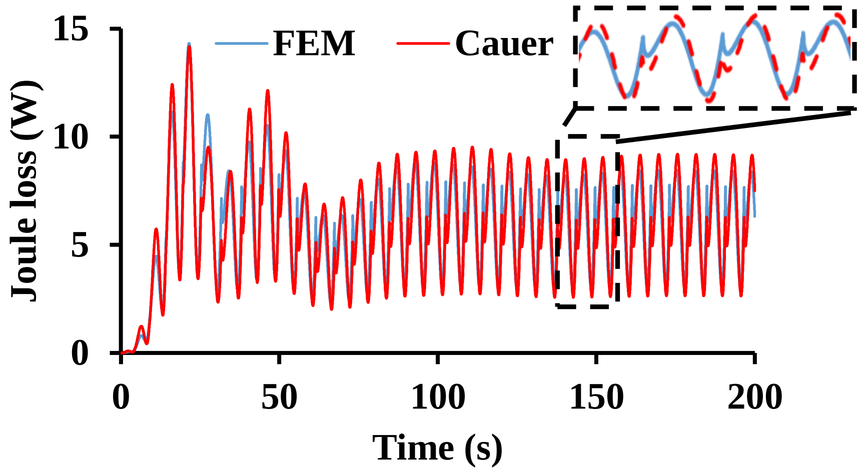

Fig. 2-23 Current response of secondary coil

2.6.4 Representation of misaligned WPT

Subsequently, the misaligned WPT that can only be analyzed using a three-dimensional model was considered. Impedance of WPT devices with misalignments of 20, 40, 60 and 80 mm were evaluated. The misalignment distance d of the WPT is shown in Fig. 2-18 (b), that is the horizontal distance between the center of two parts of WPT. Because of the existence of core and current in the opposite part, except for the DC resistance, which is constant, the other circuit parameters, viz., the inductance, mutual inductance and resistance, of each Cauer circuit are functions of d. Based on polynomial interpolation method, the Cauer circuit of a misaligned WPT with d of 0–80 mm can be predicted. The parameter L_1 in Fig. 2-2 and the mutual inductance versus displacement d are shown in Fig. 2-24, respectively. The Cauer circuits of the WPT with misalignment distances of 30 and 70 mm are predicted, and the frequency characteristics compared with results from the FEM analysis are shown in Fig. 2-25.

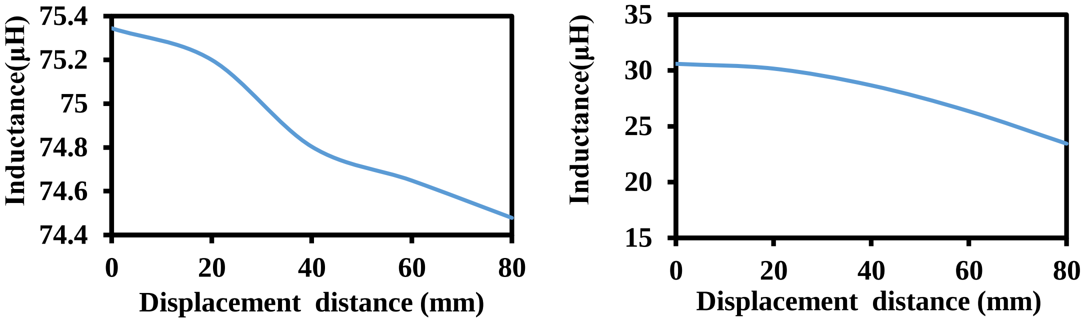

(a) L_1 in Cauer circuit (b) Mutual inductance M

Fig. 2-24 Parameter of Cauer circuit for different displacement distance

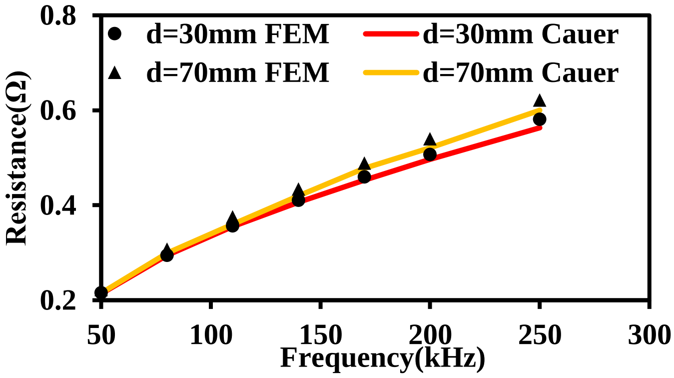

(a) Real part of $\dot{Z}_1$ with displacement distance

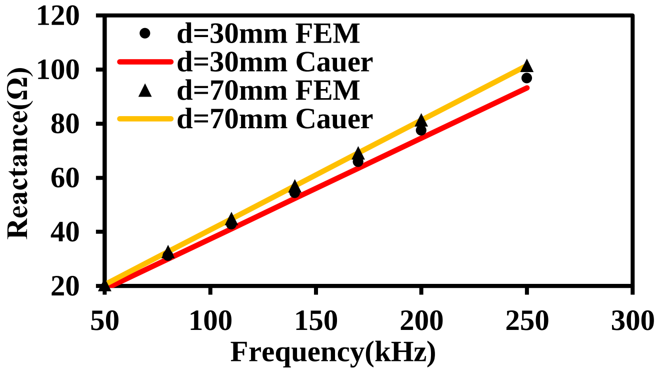

(b) Imaginary part of $\dot{Z}_1$ with displacement distance

Fig. 2-25 Frequency characteristics predicted by Cauer circuit

It can be observed from Fig. 2-25 that the Cauer circuit can predict the frequency characteristics of the impedance, which agrees well with those computed by FEM analysis. A time-domain analysis was also performed using the Cauer circuit embedded in the WPT system, as shown in Fig. 2-21, with 110 V, 85 kHz voltage source for $d = 30$ mm. A comparison of the current and copper losses of the primary coil with those computed using FEM analysis is presented in Fig. 2-26. In the results of the time-domain FEM analysis, the convergence did not perform very well, and it had an irregular shape in the current transient process.

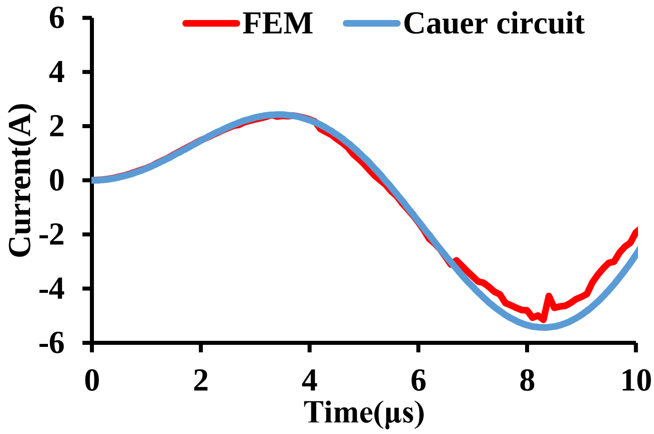

(a) Time evolution of current

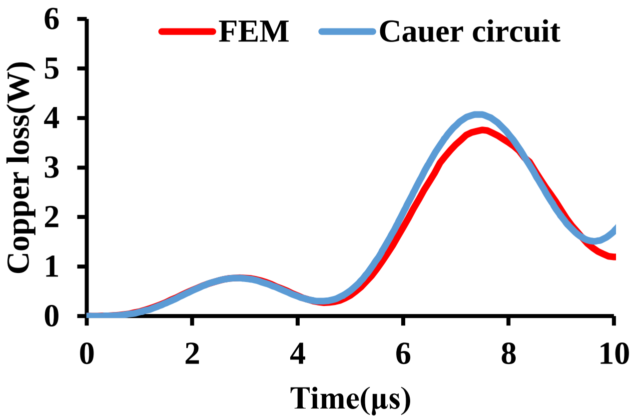

(b) Time evolution of copper loss

Fig. 2-26 Transient response of WPT device with misalignment (*d*=30mm)

It took two hours to build a Cauer circuit that could calculate the impedance of the misaligned model. However, it is much more effective than using FEM analysis to perform the time-domain analysis, which took 40 hours.

2.7 Conclusion

In this chapter, the backgrounds of Cauer circuit, moder order reduction method and identification method based on adjoint variable method introduced. Especially, the Maxwell equation for magneto-quasistatic FEM, formula to calculate the leakage inductance and AC resistance of transformer and procedure of the identification program are explained in detail. Based on these methods, several magnetic devices working at high frequency are represented by Cauer circuit based on the identification method to do the simulation efficiently while considering the eddy current.

As a result, based on the impedance calculated from the formula, the Cauer circuit can be constructed efficiently to represent the secondary short transformer and there is no need to build the complex model. The inductor with nonlinear material can also be represented by nonlinear Cauer circuit. The relationship between the input current and the inductance is introduced into the primal inductance of Cauer circuit. The result of nonlinear Cauer circuit in time domain fits well with nonlinear FEM even the input is PWM wave that contains high frequency harmonics. When the Cauer circuit is applied to represent WPT, it concludes that Cauer circuit can also be applied for magnetic devices which has more than two parts. The WPT represented by Cauer circuit can be embedded into electric power transmission system while considering the eddy current. Both the alignment and misalignment WPT can be represented by Cauer circuit and the parameters of Cauer circuit can be predicted by the interpolation method. The predicted Cauer circuit can also perform well in time domain simulation and much faster.

Chapter 3 Cauer circuit based on the homogenization method

In this chapter, the research background and basic theory of homogenized method will be introduced in detail firstly, following by that the Cauer circuit is built based on the input impedance and nonlinear relationship calculated from homogenized FEM. Then, Cauer circuit is built based on the complex permeability directly and applied to calculate the copper loss in motor windings.

3.1 Homogenized FEM method

As shown in Section.2, we find that to construct the Cauer circuit magneto-quasistatic FEM is necessary. Although FE analysis is applied only in frequency domain, it is still time-consuming in building the model or for large size device. Consequently, homogenized method is a method to accelerate the FEM simulation in frequency domain. Thus, it can accelerate the process of constructing the Cauer circuit without building complex model and discretizing the coil into very small elements [48].

3.1.1 Introduction of homogenized method

As mentioned in Section.2, when we analyze the devices operation at high frequency, eddy current has to be considered. Eddy current is caused by skin effect and proximity effect. Because currents in a wire tend to localize near its surface due to the skin effect that the cross-section area will reduce, the wire resistance increases with frequency. Proximity effect is due to the magnetic induction caused by external magnetic field surrounding the wire. In the coil, magnetic dipole will appear to prevent the change caused by the external magnetic field. Under this situation, the coil has the diamagnetic property, which has influence in the field analysis.

Some analytical approaches for calculation of power loss P in the coil have been proposed. In [49]-[50], infinitely long conducting foils are used to replace each column of round wires approximately. The P in coils can be computed under the assumption that the coil is immersed in a 1-D magnetic field. Another approach considers the coil is considered isolated that neglecting the magnetic field caused by the current flowing through the surrounding coils [51]. However, all these methods cannot compute the P exactly because the caused magnetic induction cannot be evaluated accurately [50].

It has been shown that P_{prox} can be effectively evaluated by subdividing the cross section of a multi-turn coil into elementary cells which spans one spatial period and performing FE analysis of quasi-static fields in the elementary cell under appropriate boundary conditions [52]. By this method, the homogenized complex permeability $< \dot{\mu}_r >$ evaluated from the quasi-static FE analysis can represent the diamagnetic effect in the coil caused by proximity effect. Then external magnetic field is determined from the magnetostatic FE analysis, in which the multi-turn coil is modeled as a homogeneous material whose permeability is $< \dot{\mu}_r >$. The defect of this method is FE analysis still has to be performed to get the complex permeability at different frequency and different volume fraction.

A semi-analytical approach for the eddy current analysis of multi-turn coils is proposed in [6]. The formula of complex permeability of a round wire is expressed in a closed form. The homogenized complex permeability $< \dot{\mu}_r >$ over the cross section of a multi-turn coil is analytically evaluated using the Ollendorff formula [53]. The homogenized complex permeability at any frequency and of any volume fraction can be computed directly. The power loss caused by proximity effect can be computed in static FE analysis and the power loss caused by skin effect is evaluated by introducing the AC resistance. We adopt this semi-analytical approach to construct the Cauer circuit using AVM.

3.1.2 Homogenized complex permeability of around wire

We consider a round wire immersed in a uniform time-harmonic magnetic field $Be^{j\omega t}$ which is vertical to the wire axis, and it is carrying a uniform current. The schematic diagram is shown in Fig. 3-1.

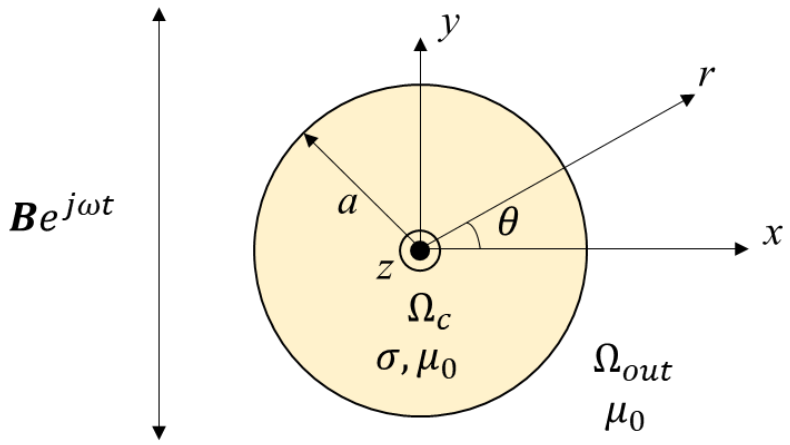

Fig. 3-1 Cross section of a round wire immersed in uniform, time-harmonic magnetic field

From the Maxwell's equation, the energy conservation law is expressed as

$$\int_{\Omega_C} (\sigma|\boldsymbol{E}|^2 + j\omega\mu|\boldsymbol{H}|^2)\, dv = -\int_{\partial\Omega_C} (\boldsymbol{E} \times \boldsymbol{H}^*)\, dS \tag{3.1}$$

Where $\boldsymbol{E}$, $\boldsymbol{H}$, σ, μ, ω and Ω_C denotes the electric field, magnetic field, conductivity of coil, permeability, operating frequency, and the region of coil. Additionally, the total power can be expressed by $P = \frac{1}{2}V * I^*$, which equals to the change in magnetic energy and the loss of eddy current in the wire. It's notable that the voltage and current is the maximum value that it's necessary to multiply 0.5. Hence, we get

$$P = \frac{j\omega}{2}\int_{\Omega_C+\Omega_{out}} \mu|\boldsymbol{H}|^2\, dv + \frac{1}{2}\int_{\Omega_C} \sigma|\boldsymbol{E}|^2\, dv \tag{3.2}$$

Based on the Maxwell's equation, the electric field and magnetic field in the coil region can be derived and the total power in coil region can finally be expressed as

$$P = \frac{j\omega}{2}\int_{\Omega_{out}} \mu|\boldsymbol{H}|^2\, dv + \frac{R_0 z J_0(z)}{4J_1(z)}|I|^2 + j2\pi\omega a^2 l B_0^2 \frac{\mu_r}{\mu_0}\frac{J_1(z)(zJ_0(z) - J_1(z))}{|zJ_0(z) + J_1(z)(\mu_r - 1)|^2} \tag{3.3}$$

$$z = \sqrt{-j\omega\sigma\mu} * a \tag{3.4}$$

where R_0, a, and l denote the DC resistance radius of wire and length of the coil. $J_n(z)$ is the n_{th} order Bessel function. The first, second and third terms in the right-hand represent the change of the energy stored in the external magnetic field, the power loss caused by DC resistance P_{skin} and the power loss caused by the external magnetic field P_{prox}.

When there is no eddy current from skin effect(static analysis) that the magnetic field can be represented by a dipole field. The magnetization can be expressed as

$$\boldsymbol{M} = 2\frac{\boldsymbol{B}}{\mu_0}\frac{\mu_r J_1(z) - zJ_1'(z)}{\mu_r J_1(z) + zJ_1'(z)} \tag{3.5}$$

In the static situation, ω limits to 0. M is reduced to the magnetization of a cylinder immersed in the magnetostatic field $\boldsymbol{B}$ [54]. It is expressed as

$$\boldsymbol{M} = 2\frac{\boldsymbol{B}}{\mu_0}\frac{\mu_r - 1}{\mu_r + 1} \tag{3.6}$$

A complex permeability is defined to make (3.6) consist with (3.5). Thus, we derive the complex permeability $\dot{\mu}_r$ from

$$\frac{\dot{\mu}_r - 1}{\dot{\mu}_r + 1} = \frac{\mu_r J_1(z) - zJ_1'(z)}{\mu_r J_1(z) + zJ_1'(z)} \tag{3.7}$$

It follows that

$$\dot{\mu}_r = \mu_r \frac{J_1(z)}{zJ_1'(z)} \tag{3.8}$$

The complex permeability leads to the complex power, which is consistent with result derived from the energy conservation law. It is of the fact that the dipole magnetic field generated by the eddy currents from the proximity effect is represented by (3.3) correctly. Under this assumption, it is concluded that the whole power can be computed from

$$P = \frac{j\omega}{2}\int_{\Omega_{in+out}} \dot{\mu}|\boldsymbol{H}|^2\, dv + \frac{R_0 z J_0(z)}{4J_1(z)}|I|^2 \tag{3.9}$$

The real part of the first term in right-hand is the power loss caused by proximity effect and the imaginary part means the variation in the stored energy in the magnetic field. The second term is the power loss caused by the skin effect. Consequently, we find that the power loss due to the proximity effect can be evaluated from the stored energy in magnetic field.

The complex permeability can be applied in the static FE analysis. However, the full model still needs to be constructed that is time-consuming. Homogenized method is effective to accelerate the simulate process. The homogenized permeability of magnetic composite $<\mu_r>$ can be evaluated using the Ollendorff formula [53].

$$<\mu_r>= 1 + \frac{\eta(\mu_r - 1)}{1 + N(1-\eta)(\mu_r - 1)} \tag{3.10}$$

η and N denotes the volume fraction and diamagnetic constant, where N is 1/2 for round wires. Subsequently, we extent the Ollendorff formula to complex permeability

$$<\dot{\mu}_r>= 1 + \frac{2\eta(\mu_r \frac{J_1(z)}{zJ_1'(z)} - 1)}{2+(1-\eta)(\mu_r \frac{J_1(z)}{zJ_1'(z)} - 1)} \tag{3.11}$$

The homogenized complex permeability is plotted versus the normalized wire radius a/δ in Fig. 3-2, where δ is the skin depth of the coil that is computed as $\delta = \sqrt{\frac{2}{\omega\sigma\mu}}$.

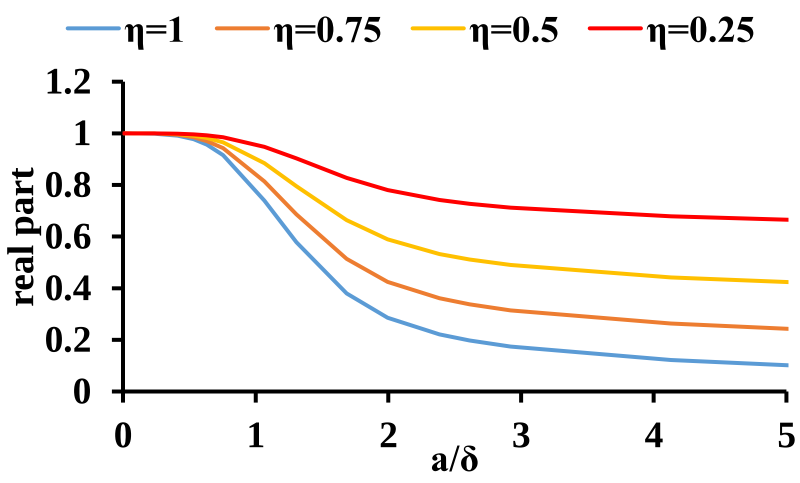

(a) Real part of homogenized complex permeability

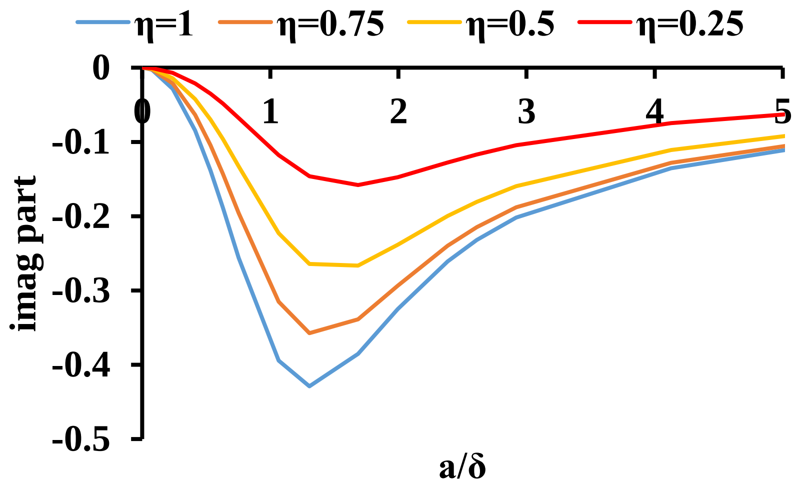

(b) Imaginary part of homogenized complex permeability

Fig. 3-2 Homogenized complex permeability versus normalized wire radius

3.1.3 Validation of homogenized FEM

An 81-turn inductor whose wire radius is 0.5 mm is constructed to validate the homogenized FEM and the original model in axis-symmetric coordination and the circuit set in FE analysis are shown as

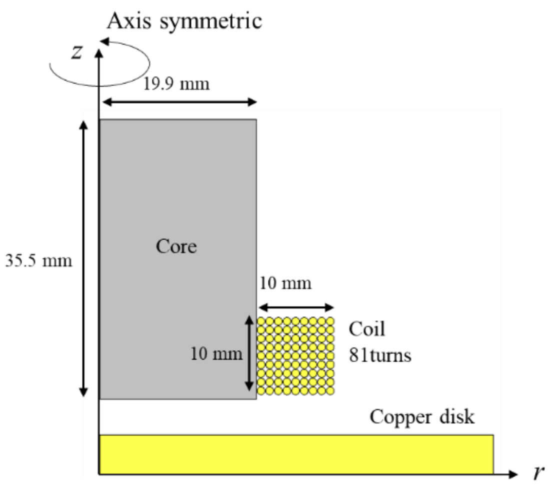

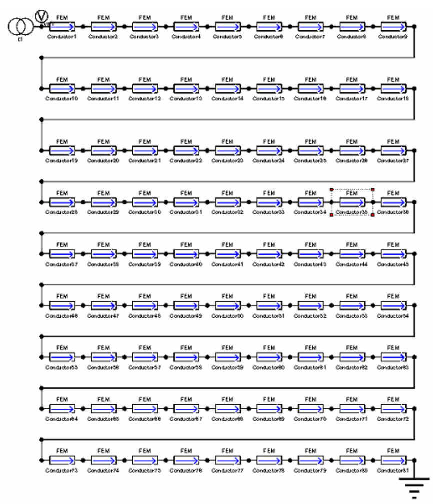

(a) Inductor model in JMAG (b) Circuit set in JMAG

Fig. 3-3 Original model and circuit in FE analysis

It's not convenient to set the analysis condition and the coil have to be discretized into sufficient fine that is smaller than 1/3 of skin depth. Subsequently, the homogenized inductor model is shown as

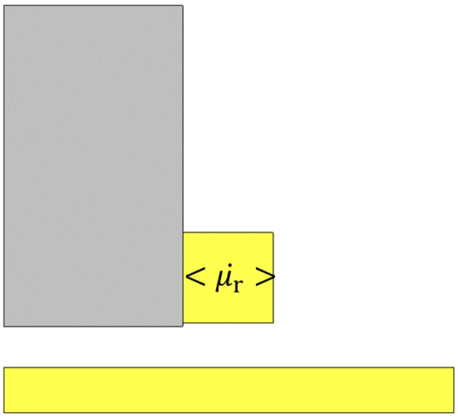

Fig. 3-4 Homogenized inductor model

Based on the homogenized inductor model, there is no need to build the complete model with so many turns of wires. Moreover, as the static FE analysis is applied rather than quasi-static FE analysis at high frequencies, the region of the coil does not have to be discretized into such tiny elements. The elements of the coil region from two models are plotted in Fig. 3-5. It is concluded that the element number in homogenized model is less than 1/10 of that in original model.

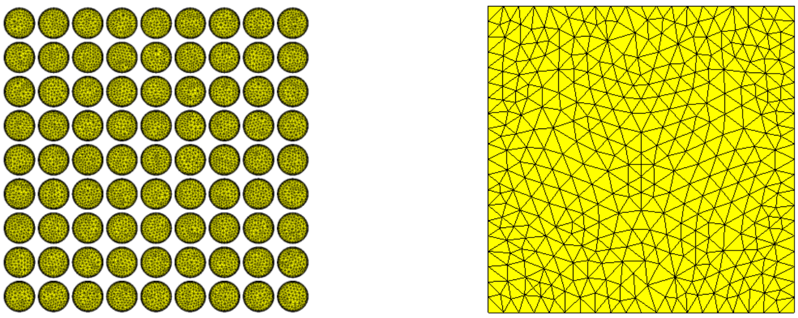

(a) Elements in original model (b) Elements in homogenized model

Fig. 3-5 Comparison of elements in coil region

Subsequently, we compare the impedance calculated from homogenized FEM based on the homogenized complex permeability in static study with that computed from conventional FEM. The result is shown as

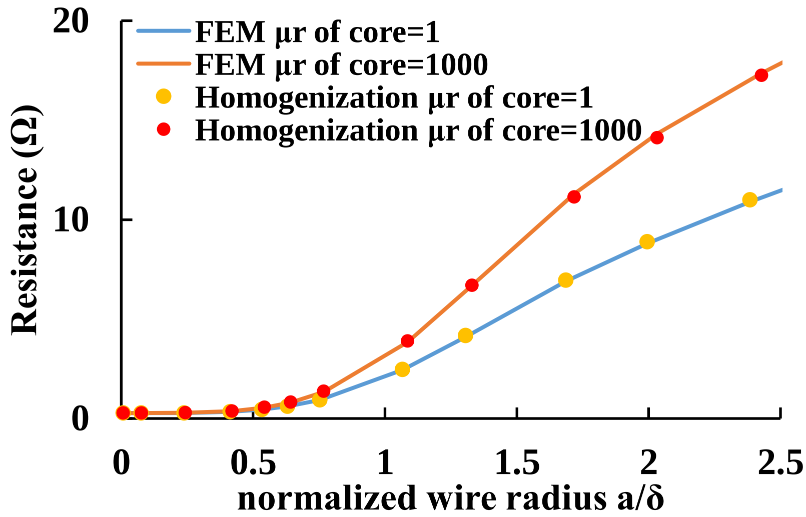

(a) Resistance versus normalized wire radius

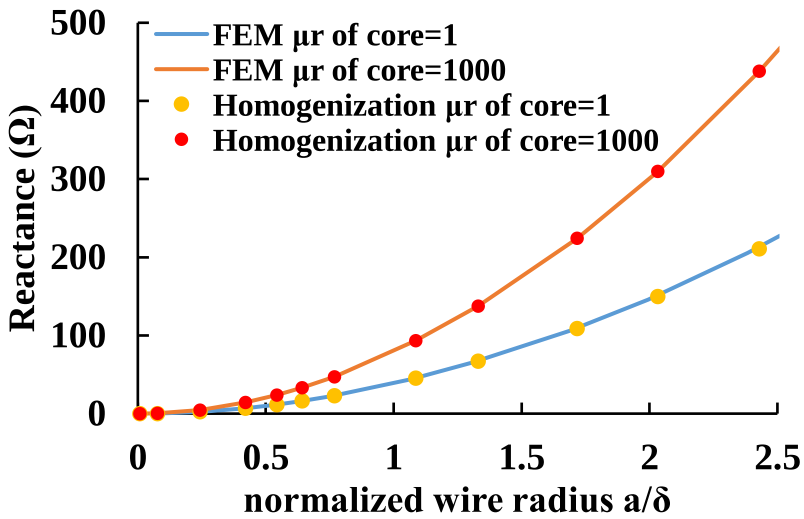

(b) Reactance versus normalized wire radius

Fig. 3-6 Impedance of multi-turn coils versus the normalized wire radius

It has shown that the impedance calculated from homogenized FEM agrees well with the impedance calculated from conventional FEM. Consequently, the Cauer circuit will be constructed based on the input impedance computed from homogenized FEM in next section.

3.2 Comparison of homogenization method and Dowell's method

In this section, the homogenization method is compared with the Dowell's method which is applied in some specific situations. Firstly, Dowell's method is introduced.

3.2.1 Introduction of Dowell's method

We consider conductors in the magnetic slot shown as Fig. 3-7 in 3-D rectangular coordinate system. The conductors are composed of several layers. The relative permeability of the core is set extreme high value that we assume the ***H*** in the core part is 0.

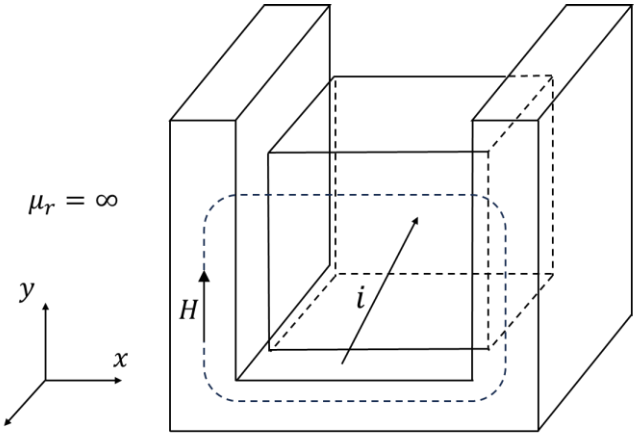

Fig. 3-7 Schematic diagram of conductors in a slot

Since the permeability of the core is assumed infinite, the leakage flux lines cross the slot rectilinearly. The vectors of the current density ***J*** and electric field strength ***E*** in the conductor have only a z-component. Moreover, the ***H*** and ***B*** have only an x-component across the conductor.

Under these conditions, the ***J*** in the conductor can be derived as a function of y. Consequently, the AC resistance R_{ac} of the conductors can be computed by integration of the power loss.

The schematic diagram of an inductor model is introduced to do the calculations.

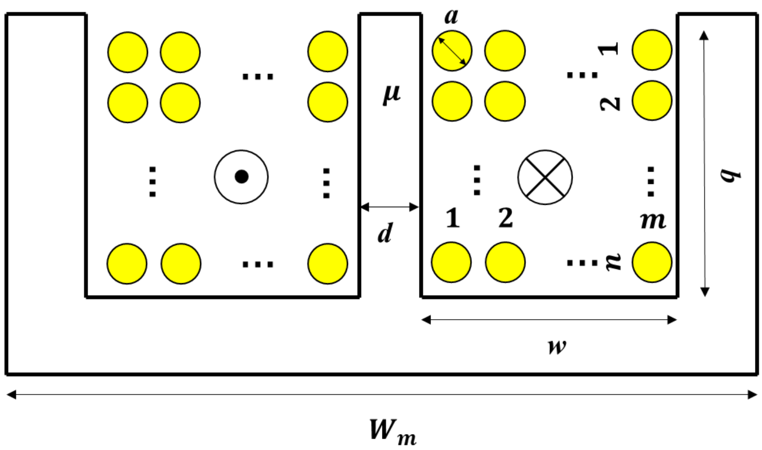

Fig. 3-8 Inductor model for Dowell’s method

As the coil in the inductor is round wire, we first transform it to the rectangular shape which has a same area. If the radius of the round wire is a, the side length of the rectangular is $d_c = \sqrt{\pi}a/2$.

The ratio of R_{ac} and R_{dc} is k_R and it is calculated as follows

$$k_R = \varphi(\xi) + \frac{n^2 - 1}{3}\psi(\xi) \tag{3.12}$$

$$\varphi(\xi) = \xi \frac{\sinh(2\xi) + \sin(2\xi)}{\cosh(2\xi) - \cos(2\xi)} \tag{3.13}$$

$$\psi(\xi) = 2\xi \frac{\sinh(\xi) - \sin(\xi)}{\cosh(\xi) + \cos(\xi)} \tag{3.14}$$

where n is the number of the layers of conductor and ξ is the reduced conductor height calculated as

$$\xi = d_c\sqrt{\frac{\mu_0\omega\sigma m d_c}{2w}} \tag{3.15}$$

where m denotes the number of conductors in one layer.

The R_{ac} of conductor whose length is l is calculated by Dowell's method shown as

$$R_{ac} = k_R \frac{mn}{\sigma d^2} l \tag{3.16}$$

3.2.2 Resistance comparison

We consider the inductor whose parameters are shown in Table. 7 and the resistance are computed by homogenization method, Dowell's method and FEM.

Table. 7 Parameters of inductor

w	10 mm	b	10 mm
d	10 mm	a	1 mm
m	8	n	8
W_m	50 mm	Length of model l	20 mm

The comparison of the resistance of the coils in right part computed by 3 methods from 1Hz to

100kHz is plotted in Fig. 3-9. The permeability of the core is set to different value.

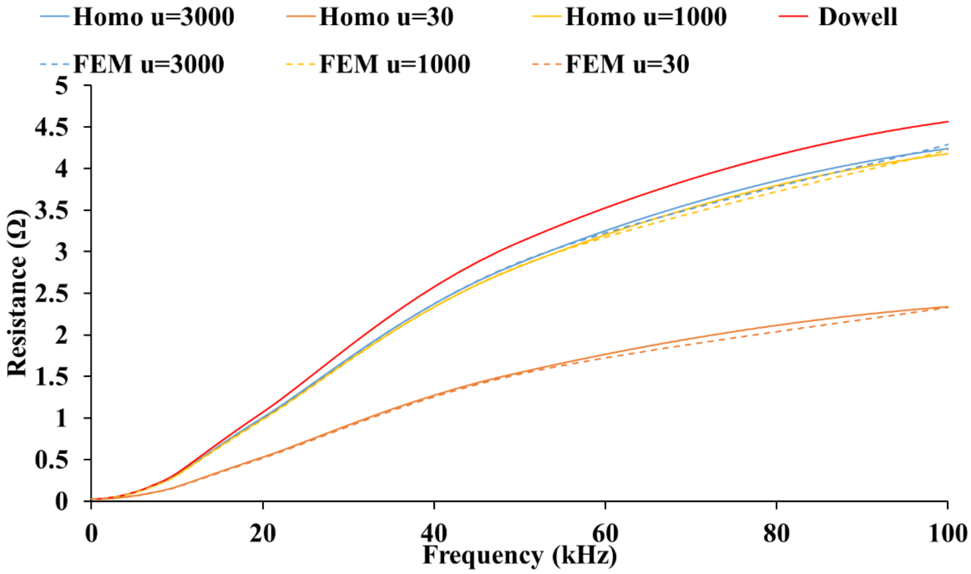

Fig. 3-9 Comparison of resistance of inductor

It is notable that when the permeability of the core is set as 3000 and 1000, at low frequencies, the resistance of three methods all agrees well. However, at frequencies higher than 20kHz, Dowell's method is larger than FEM obviously, while homogenization method still agrees well with FEM. Thus, although Dowell's method is easier than homogenization method, it can only be used of low frequency. When the frequency is higher, homogenization method is recommended.

Moreover, we find that when the permeability of the core is set as 30 that is the permeability of soft magnet material, Dowell's method cannot be applied as the magnetic flux cannot be confined in the core well. The distribution of $\boldsymbol{H}$ is shown in Fig. 3-10

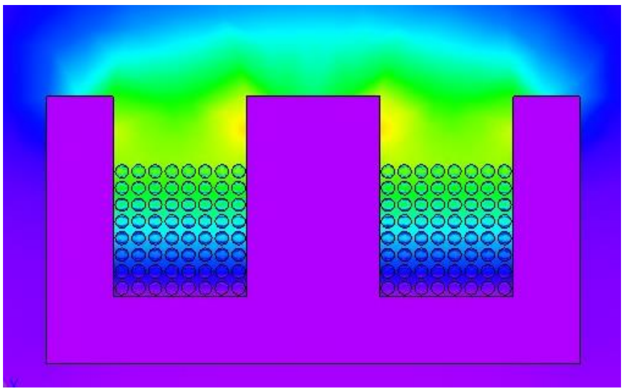

(a) Magnetic field strength ($\mu = 1000$)

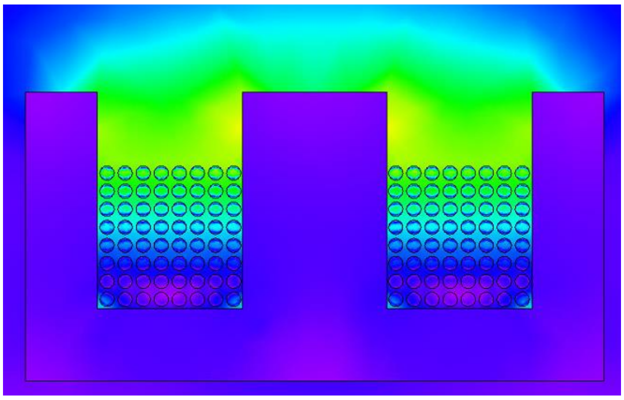

(b) Magnetic field strength ($\mu = 30$)

Fig. 3-10 Distribution of magnetic field strength

We find that when $\mu = 30$ the magnetic field strength is not same as the assumption that only changes in y direction. Homogenization method can still work because it is based on the computed stored energy.

Inductor that has a complete path of the magnetic flux shown in Fig. 3-11 is also simulated.

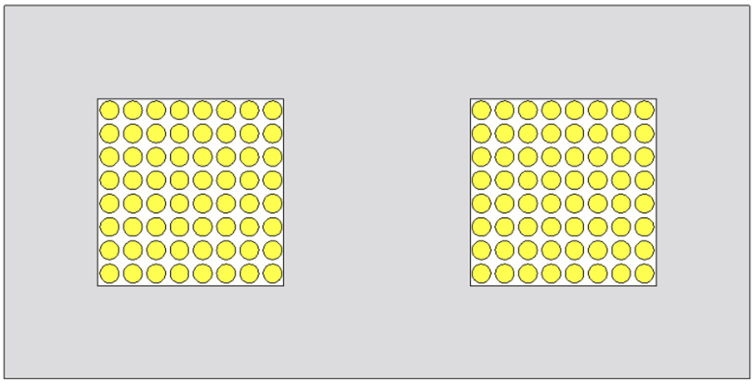

Fig. 3-11 Inductor with complete magnetic flux path

The impedance computed from homogenization method, Dowell's method and FEM are shown in Fig. 3-12. The distribution of $\boldsymbol{H}$ is shown in Fig. 3-13.

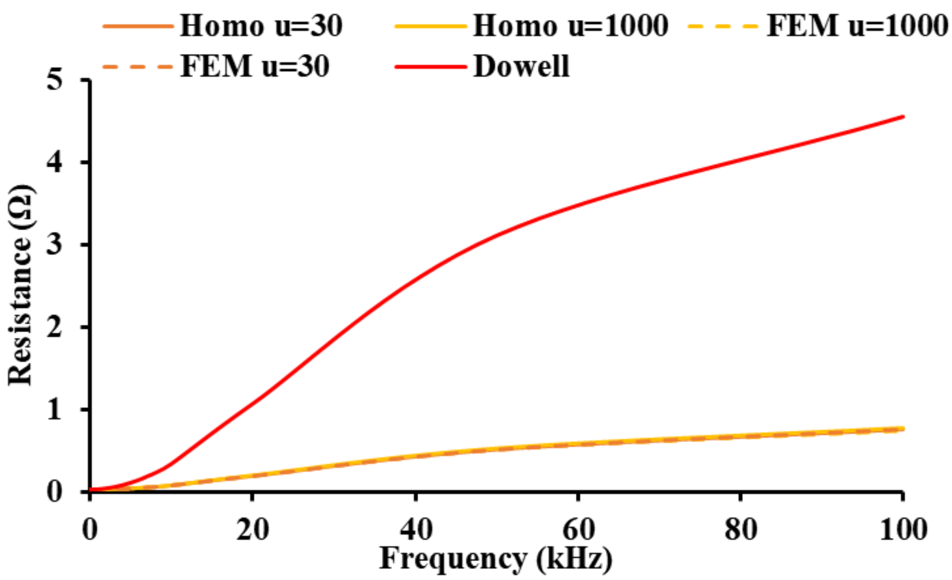

Fig. 3-12 Comparison of resistance of inductor with complete path

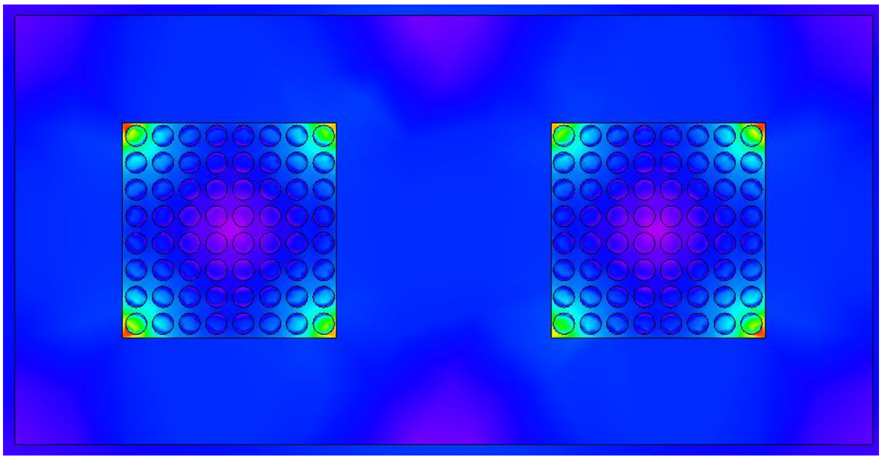

Fig. 3-13 Distribution of *H* of inductor with complete path

When there is a complete path in core for magnetic flux, the Dowell's method cannot work anymore for the sake that almost all the magnetic flux is confined in the core. Homogenization method, as observed, can fit well under all conditions.

3.3 Cauer circuit based on homogenized FEM method

Copper loss due to the skin and proximity effect can be prominent in high-speed electrical machines [55]. Moreover, the saturation of the core should also be considered. Conventional FEM modelling each turn of the winding can calculate the copper loss with an unacceptable time cost.

In this section, Cauer circuit will be built based on the homogenized FEM to represent the winding in the stator of the PMSM shown as

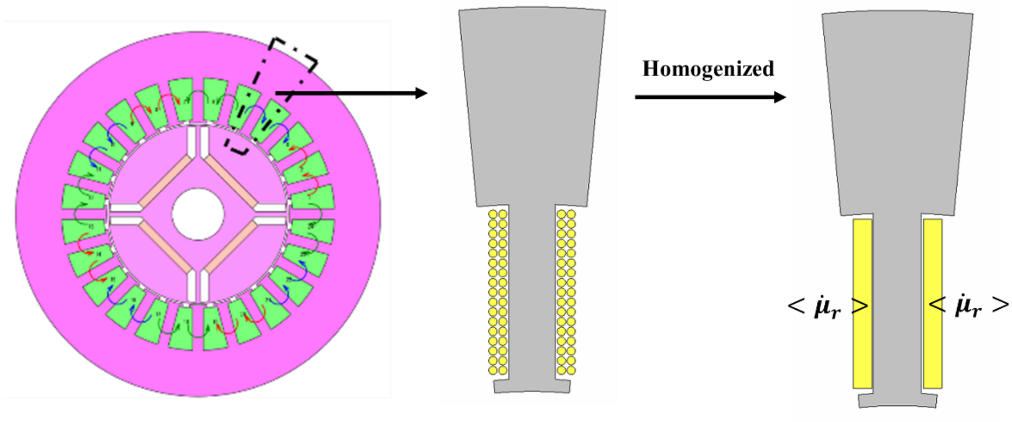

Fig. 3-14 Homogenized model of motor winding

The parameters of the PMSM and winding are shown in Table. 8.

Table. 8 Parameters of tooth model

Number of slots	24	Number of poles	4
Inner radius	56mm	Outer radius	112mm
Turns	34	Winding radius	0.3mm

The impedance of Cauer circuit, homogenized FEM and conventional FEM are shown in

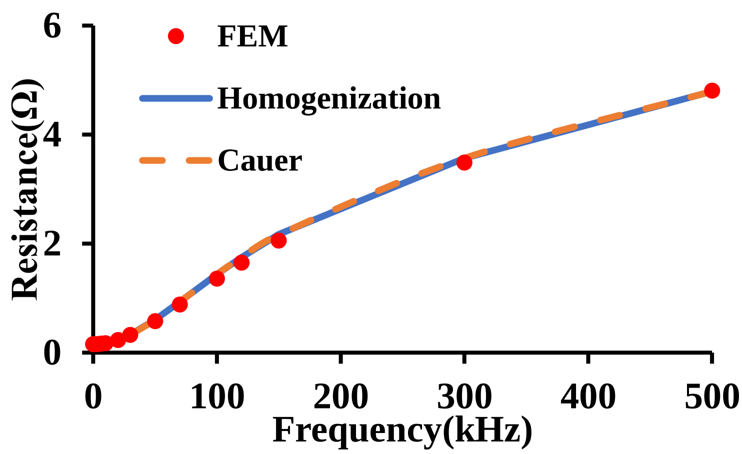

(a) Comparison of resistance

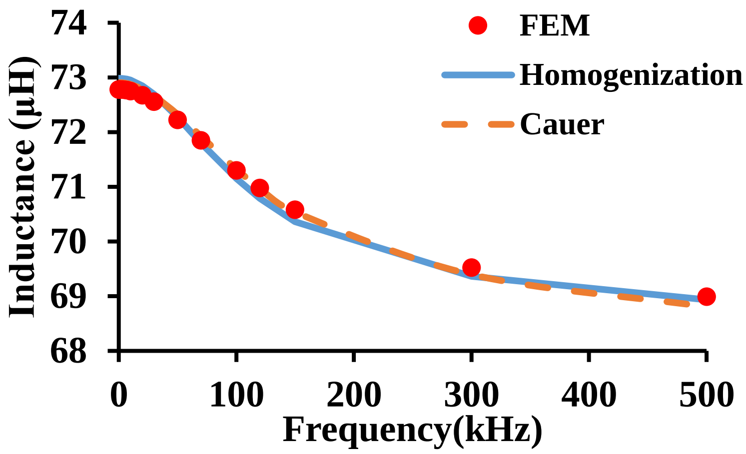

(b) Comparison of reactance

Fig. 3-15 Validation of Cauer circuit in frequency domain

It concludes that the identification method can also be applied based on the homogenized FEM, which is much faster than based on the conventional FEM. Subsequently, we consider the nonlinear relationship in the core based on the homogenized FEM. The nonlinear relationship is introduced to the primal inductance in the Cauer circuit and validated with conventional time domain FEM. The input is 1000Hz 150A current source. The voltage and copper loss of the winding in time domain are shown in Fig. 3-16.

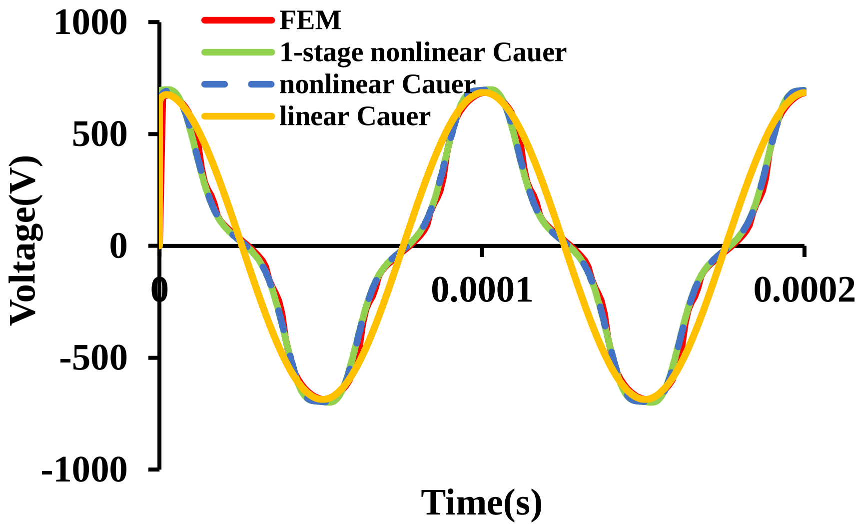

(a) Time revolution of voltage

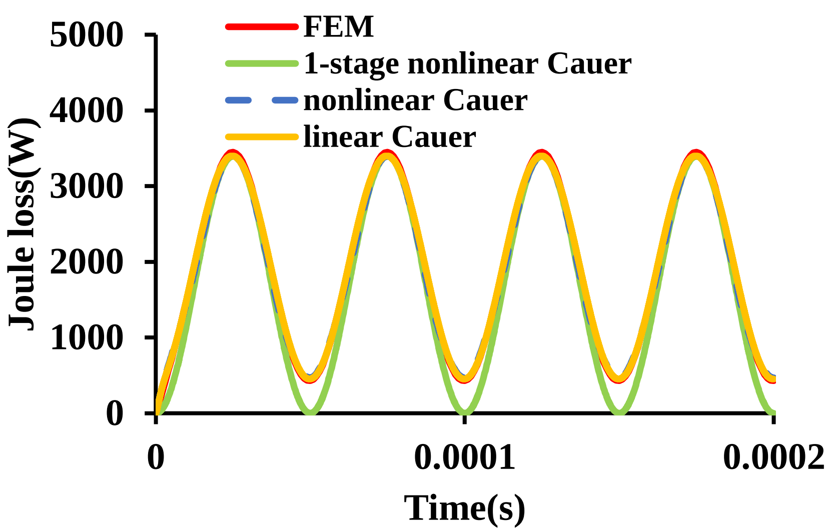

(b) Time revolution of voltage

Fig. 3-16 Validation of nonlinear Cauer circuit in time domain

The difference between the Cauer circuit and the 1-stage Cauer circuit is the power loss caused by the eddy current. Moreover, when the input current is large enough that nonlinear Cauer circuit is necessary to consider the saturation in the core.

It concludes that the nonlinear Cauer circuit performs well with conventional FEM and the construction process is faster than that based on conventional FEM.

3.4 Cauer circuit based on the homogenized complex permeability

It is concluded that the magnetic devices can be represented by nonlinear Cauer circuit based on the homogenized FEM in frequency domain. However, if there is an external magnetic field imposed on the device, the Cauer circuit cannot work unless the imposed magnetic field is decomposed into frequency components by discrete Fourier transform (DFT). In this section, Cauer circuit will be constructed based on the homogenized complex permeability directly to calculate the Joule loss in time domain and we name it as homogenized Cauer in the paper. The copper loss in the winding of PMSM is calculated by the homogenized Cauer circuit and compared with conventional FEM [56].

3.4.1 Construction of Cauer circuit based on complex permeability

The complex permeability of round wire is expressed by Bessel function shown as

$$\dot{\mu}_r = \frac{J_1(z)}{zJ_1'(z)} = \frac{J_1(z)}{zJ_0(z) - J_1(z)} = \frac{1}{\frac{zJ_0(z)}{J_1(z)} - 1} \tag{3.17}$$

The Bessel function can be expanded as

$$\frac{J_1(z)}{J_0(z)} = \frac{z}{2 - \frac{z^2}{4 - \frac{z^2}{6 - \frac{z^2}{8 - \cdots}}}} = \frac{z}{2-}\frac{z^2}{4-}\frac{z^2}{6-}\frac{z^2}{8-}\cdots \tag{3.18}$$

By substituting (3.18) into (3.19), we derived the fraction of $\dot{\mu}_r$ based on z as

$$\dot{\mu}_r = \frac{1}{1-}\frac{z^2}{4-}\frac{z^2}{6-}\frac{z^2}{8-}\cdots \tag{3.19}$$

As $z^2 = -ja^2\omega\sigma\mu_0$, the fraction of $\dot{\mu}_r$ can be expressed as

$$j\omega\dot{\mu} = j\omega\mu_0\dot{\mu}_r = \frac{1}{\frac{1}{j\omega\mu_0}+}\,\frac{1}{\frac{3}{a^2\sigma}+}\,\frac{1}{\frac{5}{j\omega\mu_0}+}\,\frac{1}{\frac{7}{a^2\sigma}+}\cdots \tag{3.20}$$

Another type of Cauer circuit is constructed as

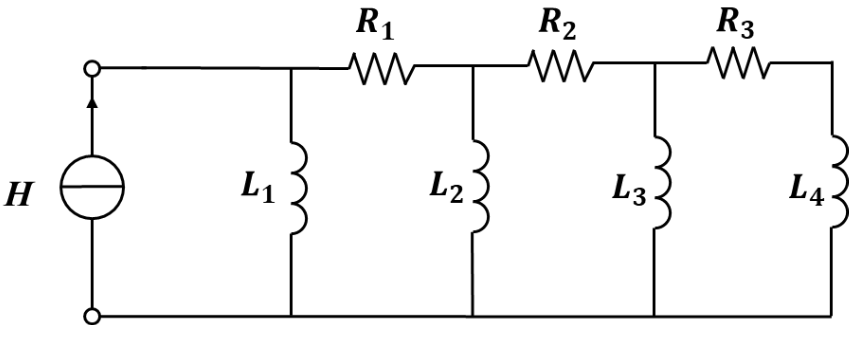

Fig.33 Construction of Cauer circuit based on complex permeability

The impedance of the Cauer circuit can derived as

$$Z(\omega) = \frac{1}{\frac{1}{j\omega L_1}+}\,\frac{1}{R_1+}\,\frac{1}{\frac{1}{j\omega L_2}+}\,\frac{1}{R_2+}\cdots \tag{3.21}$$

Match the impedance $Z(\omega)$ with the fraction of $j\omega\dot{\mu}$, the parameters of the Cauer circuit can be derived as following

$$R_k = \frac{4k-1}{a^2\sigma}, \quad L_k = \frac{4k-1}{a^2\sigma}, \quad k = 1,2,3 \ldots \tag{3.22}$$

As mentioned above, the Cauer circuit can represent the complex permeability of different volume fraction and radius of round wire. Because the impedance of the Cauer circuit equals to $j\omega\dot{\mu}$ at every frequency, we can do the simulation even the input contains high frequency harmonics in time domain.

The input of the Cauer circuit is set as current source whose value is H, and based on the physical meaning of the impedance of Cauer circuit $j\omega\dot{\mu}$ the voltage of the circuit is derived as

$$V = j\omega\dot{\mu}H = j\omega B \tag{3.23}$$

As shown, the voltage of the Cauer circuit is the derivative of B with respect to time. The real part of the power loss in the Cauer circuit is calculated as

$$P = Re(UI^*) = Re(j\omega BH^*) = Re(j\omega\dot{\mu}|H|^2) \tag{3.24}$$

We find the joule loss of the Cauer circuit multiply the volume of the homogenized model represents the copper loss of proximity effect caused by the external magnetic field. Thus, the eddy current loss of proximity effect can be computed for any magnetic field.

There is a physical explanation for the Cauer circuit. When the frequency is sufficient low, the flux almost only flow through L_1 that there is no eddy current loss caused. When the frequency becomes higher, the current will flow through R_1, and it represents the eddy current loss caused by the induced voltage from L_1. Subsequently, the eddy current will induce another voltage on L_2 and it will cause additional eddy current loss in R_2 and so on.

3.4.2 Construction of Cauer circuit based on homogenized complex permeability

In the previous section, the Cauer circuit is constructed based on the complex permeability and in this section, the Cauer circuit will be built based on the homogenized complex permeability that is much efficient. The homogenized complex permeability is expressed by Bessel function and shown as

$$< \dot{\mu}_r >= 1 + \frac{\eta(\dot{\mu}_r - 1)}{1 + \frac{1}{2}(1-\eta)(\dot{\mu}_r - 1)} = 1 + \frac{2\eta\left(\frac{J_1(z)}{zJ_0(z) - J_1(z)} - 1\right)}{2 + (1-\eta)\left(\frac{J_1(z)}{zJ_0(z) - J_1(z)} - 1\right)} \tag{3.26}$$

By transforming the formula, we can get

$$< \dot{\mu}_r >= 1 + \frac{2\eta(2J_1(z) - zJ_0(z)))}{(1+\eta)zJ_0(z) - 2\eta J_1(z)} \tag{3.27}$$

To transform the formula to the format that containing $\frac{zJ_0(z)}{J_1(z)}$, we divide both the numerator and denominator by $J_1(z)$.

$$< \dot{\mu}_r >= 1 + \frac{4\eta - 2\eta\frac{zJ_0(z)}{J_1(z)}}{(1+\eta)\frac{zJ_0(z)}{J_1(z)} - 2\eta} \tag{3.28}$$

By applying Euclidean algorithm to the formula, it comes to

$$= \frac{1-\eta}{1+\eta} + \frac{\frac{4\eta}{1+\eta}}{(1+\eta)\frac{zJ_0(z)}{J_1(z)} - 2\eta} \tag{3.29}$$

Until this step, we validate the real part and imaginary part of (3.29) with $< \dot{\mu}_r >$ and it shows there is no error until this step.

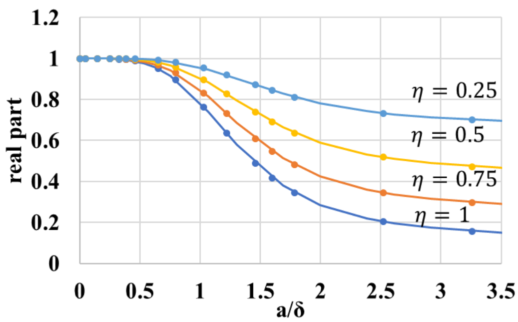

(a) Real part of $< \dot{\mu}_r >$

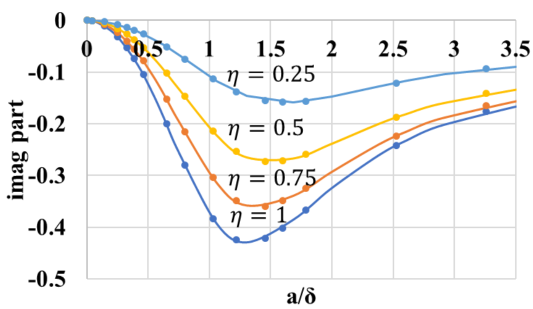

(b) Imaginary part of $< \dot{\mu}_r >$

Fig.34 Validation of the formula

Consequently, by substituting (3.18) into (3.29), the $j\omega < \dot{\mu}_r >$ is derived as

$$j\omega\mu_0 < \dot{\mu}_r >= j\omega\mu_0 \frac{1-\eta}{1+\eta} + j\omega\mu_0 \frac{\frac{4\eta}{1+\eta}}{2-(1+\eta)(\frac{z^2}{4-}\frac{z^2}{6-}\frac{z^2}{8-}\cdots)} \tag{3.30}$$

After substituting $z^2 = -ja^2\omega\sigma\mu_0$, we transform the formula to the format of Cauer circuit

$$j\omega\mu_0 < \dot{\mu}_r >= j\omega\mu_0 \frac{1-\eta}{1+\eta} + \cfrac{1}{\cfrac{1+\eta}{2\eta\cdot j\omega\mu_0} + \cfrac{(1+\eta)^2}{4\eta}\cdot\cfrac{1}{\cfrac{4}{a^2\sigma} + \cfrac{1}{\cfrac{6}{j\omega\mu_0} + \cfrac{1}{\cfrac{8}{a^2\sigma} + \cdots}}}} \tag{3.31}$$

The corresponding Cauer circuit is different with it based on the complex permeability, and the construction of it is shown as

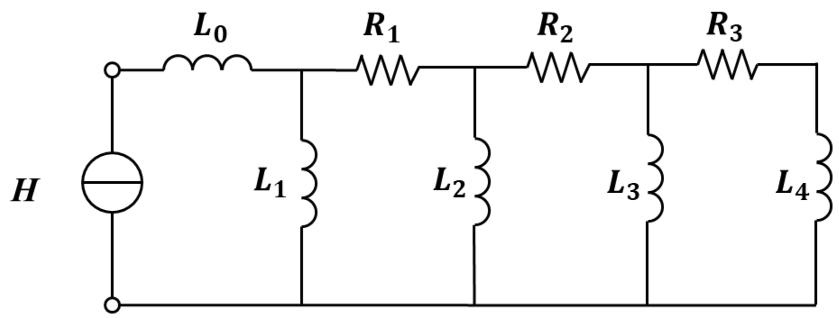

Fig. 3-17 Construction of Cauer circuit based on homogenized complex permeability

The impedance of the Cauer circuit is derived as

$$Z(\omega) = j\omega L_0 + \cfrac{1}{\cfrac{1}{j\omega L_1} + \cfrac{1}{R_1 + \cfrac{1}{\cfrac{1}{j\omega L_2} + \cfrac{1}{R_2 + \cdots}}}} \tag{3.32}$$

Match the impedance $Z(\omega)$ with the fraction of $j\omega\dot{\mu}$, the parameters of the Cauer circuit can be derived as following

$$L_0 = \mu_0 \frac{1-\eta}{1+\eta}$$

$$L_1 = \mu_0 \frac{2\eta}{1+\eta}$$

$$R_k = \frac{4k}{a^2\sigma}\frac{4\eta}{(1+\eta)^2} \quad \mathrm{k} = 1,2,3\ldots$$

$$L_k = \frac{2\eta\mu_0}{(2k-1)(1+\eta)^2} \quad \mathrm{k} = 2{,}3 \ldots \tag{3.33}$$

The homogenized Cauer circuit is built in LTSpice and the impedance of it is compared with $j\omega\mu_0$ for different volume fraction and wire radius.

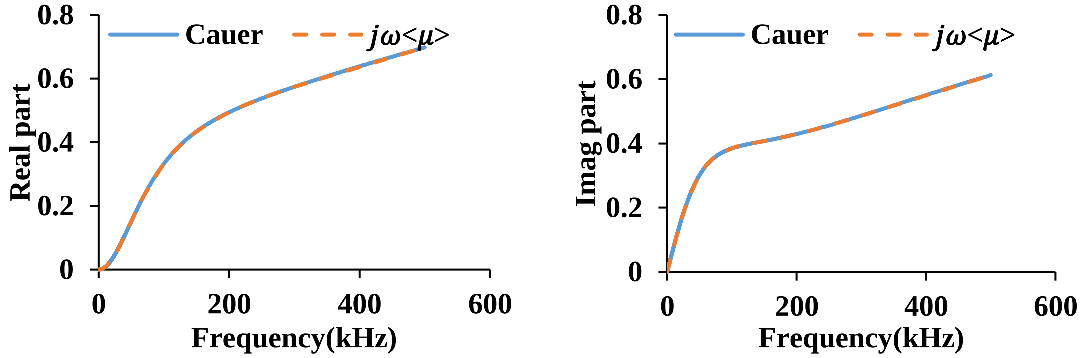

(a) Real part (b) Imaginary part

Fig. 3-18 Validation of homogenized Cauer circuit η=1 a=0.3mm

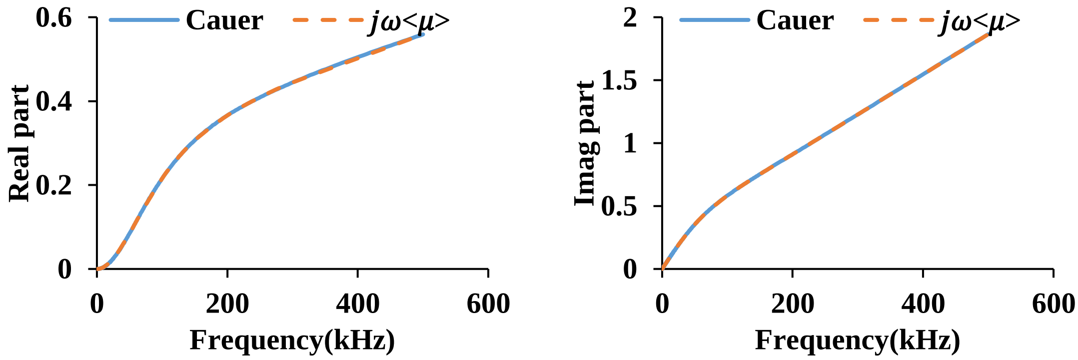

(a) Real part (b) Imaginary part

Fig. 3-19 Validation of homogenized Cauer circuit η=0.5 a=0.3mm

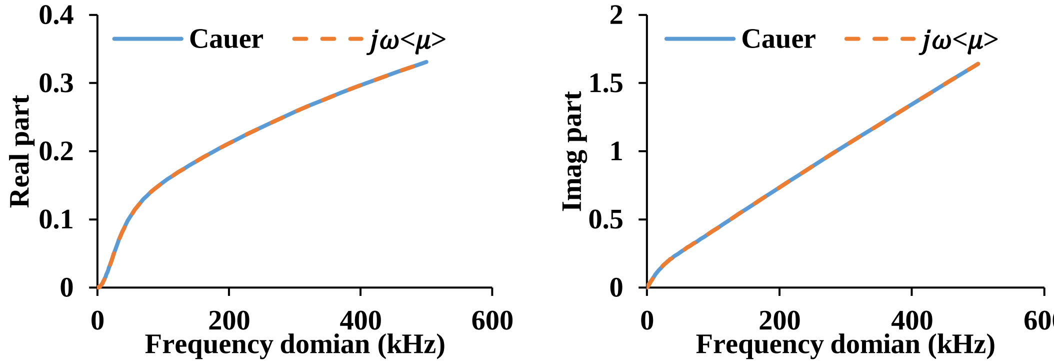

(a) Real part (b) Imaginary part

Fig. 3-20 Validation of homogenized Cauer circuit η=0.5 a=0.5mm

We find that the impedance of the homogenized Cauer circuit fit well with the formula that it can consider the input with any frequency.

3.5 Eddy current loss analysis based on homogenized Cauer

In this section, homogenized Cauer circuit is applied to analyze the eddy current loss caused by proximity effect. Firstly, the magnetic field strength H imposed on the homogenized model is computed by FEM without considering the eddy current. Subsequently, the H is set as the input for the homogenized Cauer circuit and the power loss of the Cauer circuit is exact the eddy current loss caused by proximity effect in the model. The eddy current loss caused by skin effect will be computed by formula additionally.

We consider the winding in the PMSM whose copper loss is induced from the magnet in the rotor and the saturation of the core should also be considered. The PMSM model and the homogenized model are shown in Fig. 3-21.

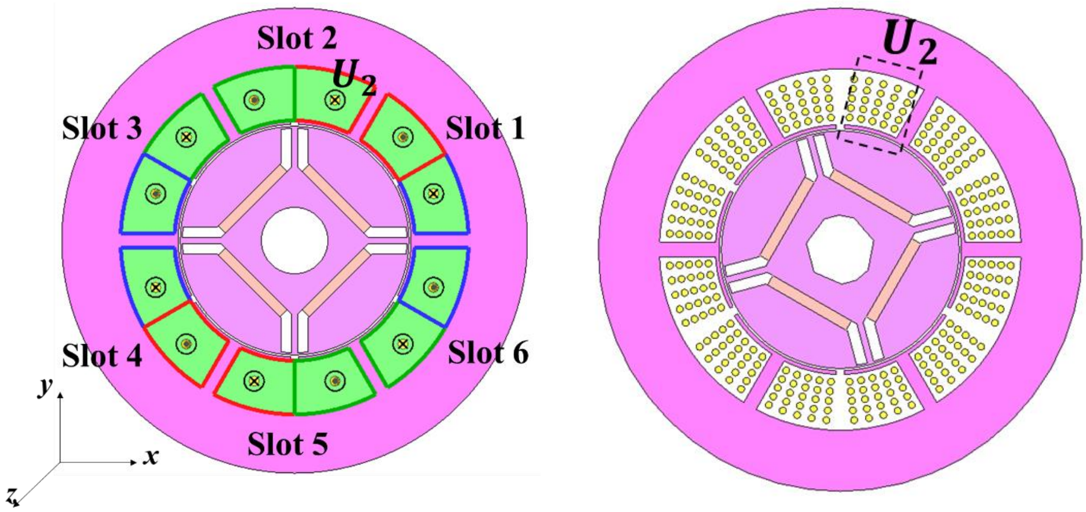

(a) Homogenized PMSM model (b) Original PMSM model

Fig. 3-21 Windings of PMSM

The parameters of the PMSM are shown in Table. 9.

Table. 9 Parameters of PMSM

Number of slots	6	Number of poles	4
Inner radius	56 mm	Outer radius	112 mm
Turns	25	Winding radius	0.8 mm
Material of core	50A1000	Material of magnet	NdFeB_Br=1.0T
Input source	1A 100Hz	Model length	37.5 mm

The slot view of the PMSM is shown in Fig. 3-22.

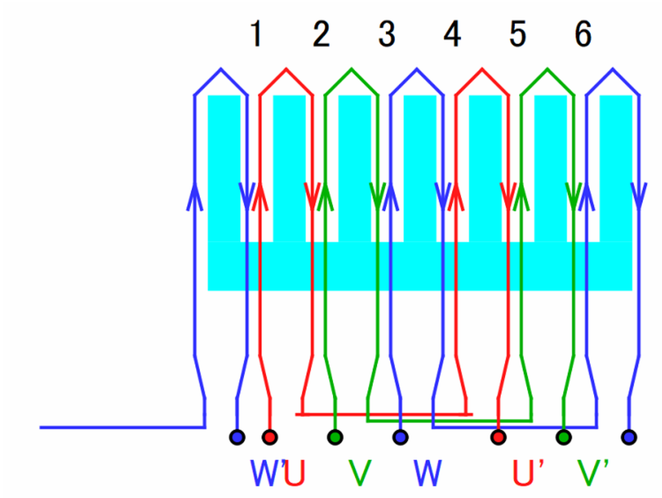

Fig. 3-22 Slot view of PMSM

3.5.1 Validation of homogenized Cauer circuit in frequency domain

The performance of the homogenized Cauer circuit is verified in frequency domain at first. Based on formula (3.24), the power loss caused by the external magnetic field in frequency domain can be evaluated. The *H* of one winding in time domain is computed by FEM and the DFT is applied to calculate the eddy current loss of each frequency. Subsequently, the result is compared with it computed by homogenized Cauer circuit.

We consider the *H* of the winding U_2 is composed of *x* and *y* components, and the average of the magnetic field in *x* direction H_x is calculated by

$$H_x = \sum_{i=0}^{N} H_{xi} S_i \,/ \sum_{i=0}^{N} S_i \tag{3.34}$$

where N, H_{xi}, and S_i denote the number of elements in U_2, the x direction magnetic field strength in i_{th} element and the area of i_{th} element. Because of the homogenized coil, the number of elements of one winding is only around 30. The averaged H_x is shown in Fig. 3-23. It is concluded that the H of the winding is of irregular waveform. Besides the basic frequency of 50Hz, there are some high harmonic frequencies that will induce eddy current loss in windings.

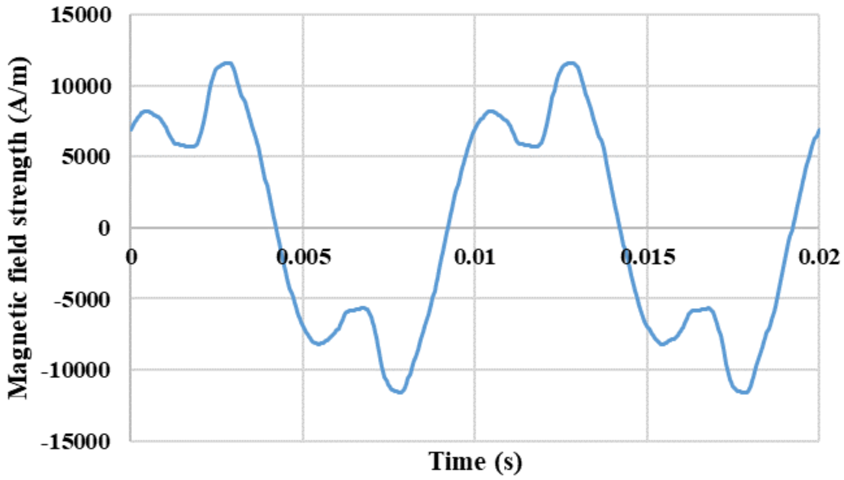

Fig. 3-23 Averaged H_x

Subsequently, we apply DFT to decompose the H_x. The basic theory of DFT is introduced first.

The DFT is a mathematical technique used in signal processing and digital signal analysis to convert a discrete signal from its time domain into a frequency domain. It decomposes a sequence of values into components of different frequencies, providing insights into the frequency content of the signal. The DFT essentially represents a signal as a sum of sinusoidal components of varying frequencies, phases, and amplitudes. It is represented mathematically as

$$H(k) = \sum_{n=0}^{N-1} h(n) \cdot e^{-j\frac{2\pi}{N}kn} \tag{3.35}$$

where $H(k)$, $h(n)$, N and k denotes the output of the DFT at frequency index k, the input signal at discrete time index n, the total number of samples in the input signal and the frequency index ranging from 0 to N-1. By applying DFT to H_x, we derive the stem graph shown as follows.

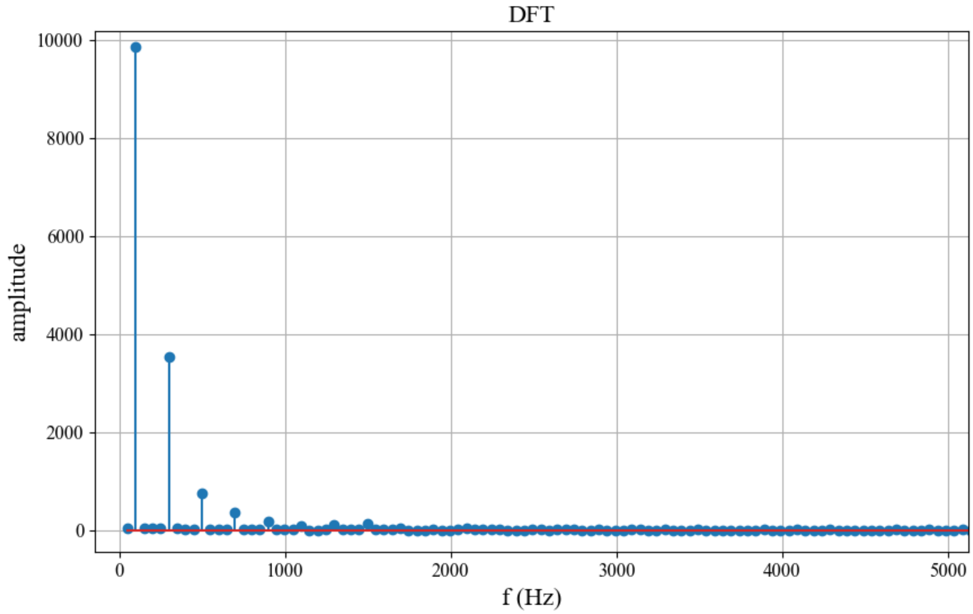

Fig. 3-24 Result of DFT

The components of H_x whose amplitude is larger than 100 is shown in Table. 10.

Table. 10 Components of H_x

Frequency $\omega_i/2\pi$	Amplitude $\|H_{xi}\|$	Phase
100	9861.2335	-1.16145
300	3526.6518	0.280466
500	750.16014	-2.06879
700	356.64624	1.304334
900	167.29261	-1.98595
1300	103.80672	0.045217
1500	128.62345	-2.88124

The contribution of H_x to the eddy current power in winding is expressed as

$$P = \frac{1}{2}\sum_{i=0}^{N} Re(j\omega_i < \dot{\mu}_i > |H_{xi}|^2) * V \tag{3.36}$$

where i denotes the ith components of H_x and the $< \dot{\mu}_i >$ is the corresponding homogenized complex permeability. V is the volume of the homogenized model. The calculation result is 2.05mW.

Subsequently, to validate the result we set the input of homogenized Cauer circuit as H_x, then we get the power loss of Cauer circuit in time domain. By integrating the power loss in 1 second, the eddy current power is computed. The joule loss of Cauer circuit in time domain is plotted in Fig. 3-25.

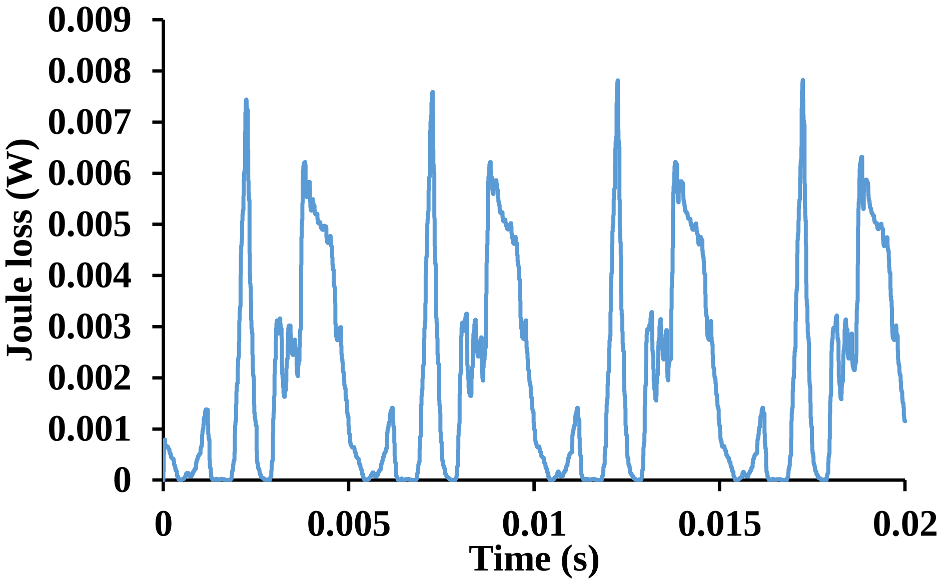

Fig. 3-25 Joule loss of Cauer circuit

The result computed from homogenized Cauer circuit agrees well with it calculated from the formula (3.36). It concludes that the homogenized Cauer circuit can be applied to compute the copper loss induced by the external magnetic field in frequency domain.

3.5.2 Validation of homogenized Cauer circuit in time domain

After we have confirmed the homogenized Cauer circuit in frequency domain, in this section we validate its performance in time domain. For the reason that we have to derive the H of the winding to calculate the eddy current loss in the winding, we first consider the method to derive the waveform of the H.

The first method to derive the H of the winding is calculating the H in x and y directions from all elements in the winding based on the area of the element.

$$H_x = \sum_{i=0}^{N} H_{xi} S_i \,/ \sum_{i=0}^{N} S_i$$

$$H_y = \sum_{i=0}^{N} H_{yi} S_i \,/ \sum_{i=0}^{N} S_i \tag{3.37}$$

The eddy current loss caused by H_x and H_y are calculated separately based on the homogenized Cauer circuit and added together. The eddy current loss $P_{prox\,H_x}(t)$ and $P_{prox\,H_y}(t)$ are shown in Fig. 3-26.

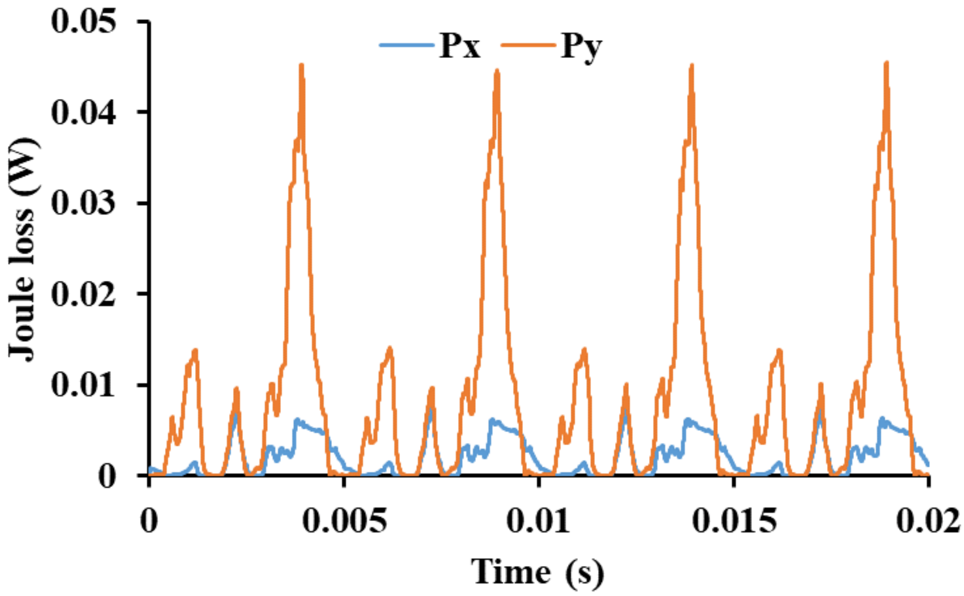

Fig. 3-26 Power loss of *x* and *y* direction

Besides the eddy current loss caused by proximity effect, the eddy current loss caused by skin effect and DC resistance is calculated by the formula shown as

$$P_{skin}(t) = \frac{R_0 z J_0(z)}{2J_1(z)} |I(t)|^2 \tag{3.38}$$

The total power loss of winding is calculated as

$$P(t) = P_{prox\,H_x}(t) + P_{prox\,H_y}(t) + P_{skin}(t) \tag{3.39}$$

To do the validation, the power loss of winding is computed from the conventional FEM. The comparison of power loss of winding U_2 is plotted in the Fig. 3-27.

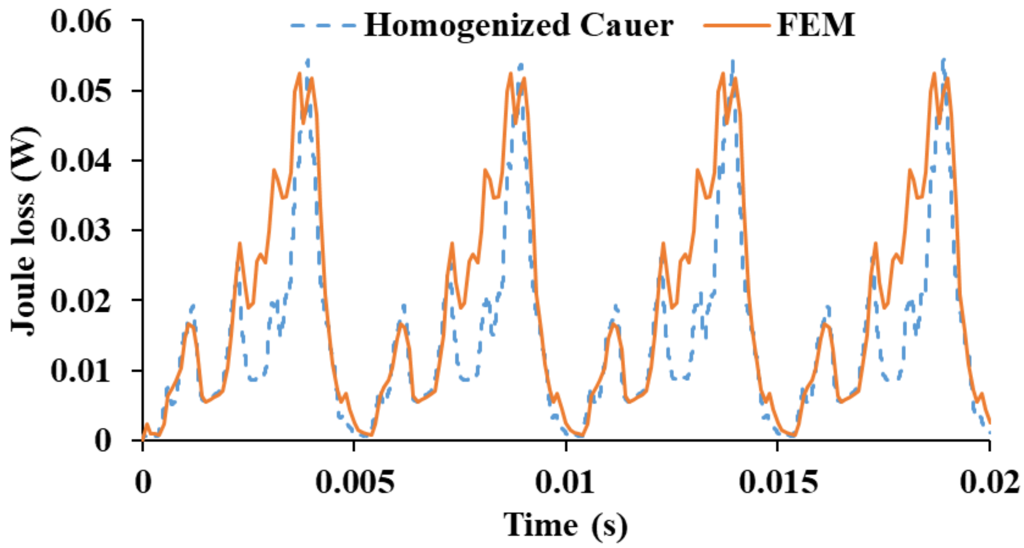

Fig. 3-27 Comparison of power loss in winding U_2 with method 1

For the reason that the ***H*** of the winding is calculated from average value of all elements, there could be some error in the calculation. Thus, we try to verify the amplitude of the ***H*** based on the stored energy which is calculated from

$$E_{stored}(t) = \frac{\mu_0}{2}\left(H_x(t)^2 + H_y(t)^2\right) * V_w \tag{3.40}$$

Where E_{stored} and V_w denote the stored energy in the winding and the volume of the winding. The stored energy of the winding calculated by the ***H*** is compared with the result of FEM shown in Fig. 3-28 and we find that the stored energy calculated from the ***H*** cannot fit with result of FEM that could cause the difference.

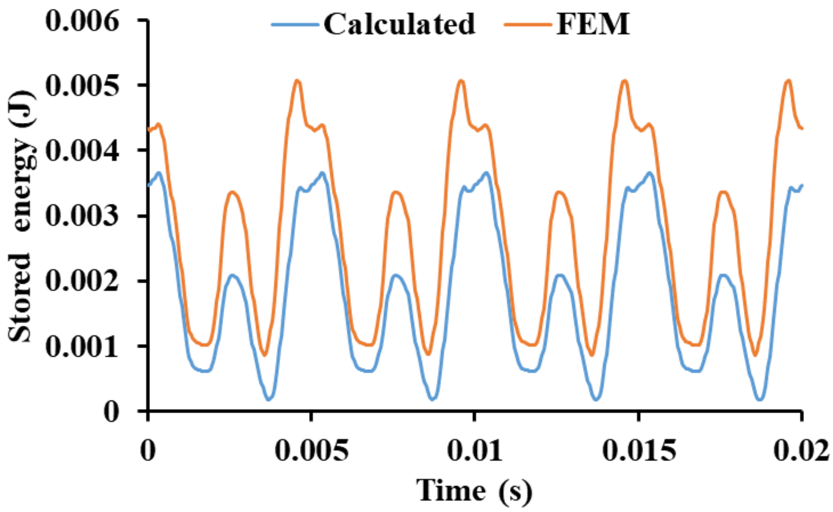

Fig. 3-28 Comparison of stored energy in winding U_2

The second method is calculating all the eddy current loss in each element. The eddy current loss in each element is calculated by H_x and H_y of it and all the eddy current losses are added together while considering the area of elements. The calculation method is shown as

$$P(t) = \sum_{i=0}^{N} P_{prox\,i}(t) + P_{skin}(t) \tag{3.41}$$

where $P_{prox\,i}(t)$ is the eddy current loss in i_{th} element. The comparison of power loss of winding U_2 is plotted in the Fig. 3-29 [56].

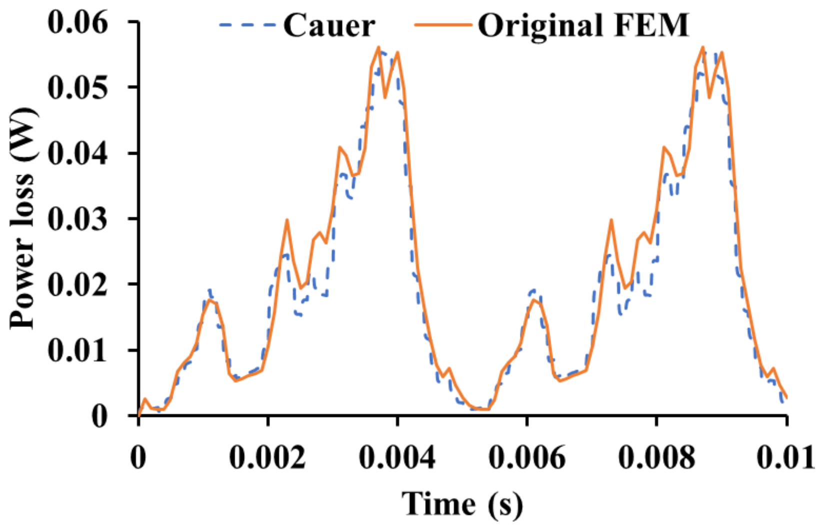

Fig. 3-29 Comparison of power loss in winding U_2 with method 2

As shown in the comparison figure, it concludes the power loss calculated from method 2 fits well with it from FEM. Even the shape of the copper loss is irregular, the homogenized Cauer circuit can still work well to calculate it. Then we calculate the copper loss of all the windings in the PMSM and the result is shown in the Fig. 3-30 [56].

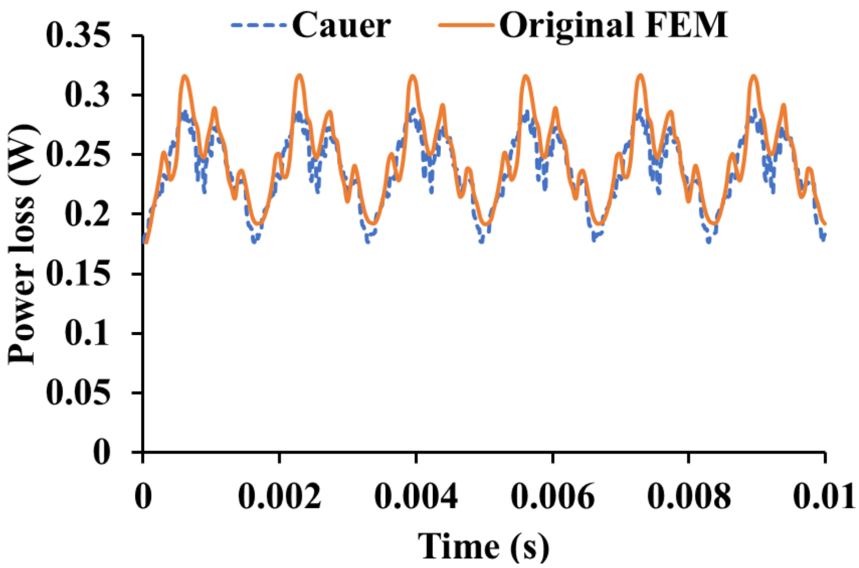

Fig. 3-30 Comparison of stored energy per cubic meter

The total copper loss of PMSM windings calculated from homogenized Cauer circuit still fits well with FEM. If we want to decrease the error further, we can make a better homogenized model to fit the coil region better.

3.6 Conclusion

In this chapter, the homogenization method is introduced, and the impedance of the multi-turn round wire inductor can be computed based on the static FE analysis. Based on homogenization method, we do not have to build the complex model and perform the FE analysis in high frequency with small elements. Moreover, the comparison of results from FE analysis, homogenization method and Dowell's method is shown, and we find that although in some specific situations Dowell's method is more convenient, homogenization method has a wider range of applications.

Subsequently, Cauer circuit is constructed based on the input impedance computed from homogenized FE analysis. The Cauer circuit performs well both in frequency and time domain considering the saturation of the core.

To consider the influence from the magnet in the rotor, we construct the homogenized Cauer circuit from the formula of $< \dot{\mu}_r >$ directly. The Bessel function is decomposed into fractions which has the same form with the impedance of Cauer circuit. The impedance of homogenized Cauer circuit fits well with $j\omega < \dot{\mu}_r >$ in frequency domain for different volume fraction and radius of round wire.

The copper loss of motor winding can be computed from the homogenized Cauer circuit and fits well with the result computed from formula based on DFT in frequency domain. Complex calculations are eliminated, and we only need to calculate the power loss in the resistance of homogenized Cauer circuit.

The copper loss of winding is also computed in time domain with two methods, one based on the average of H_x and H_y, and the other based on the loss of every element. We find that method 2 performs better with FEM. It should be noted that the stored energy per unit volume in the homogenized model has some differences in the peak value region and it may cause the error in the power loss calculation. Thus, if we want to decrease the error further, a better homogenized model is necessary to minimize the error of the stored energy per unit volume in homogenized model and original model.

Chapter 4 Equivalent circuit for magnetic device considering displacement current and eddy current

In chapter 2 and 3, Cauer circuit is introduced to represent the electric device while considering the eddy current at high frequency. However, when the frequency is so high that changes in the electric field cannot be ignored, we have to consider the displacement current between each part of the device shown as Fig. 4-1. In this chapter, the equivalent circuit with displacement current is applied to represent the magnetic device based on the complex mutual inductance to consider the eddy current and displacement current at same time without repeating FE analysis.

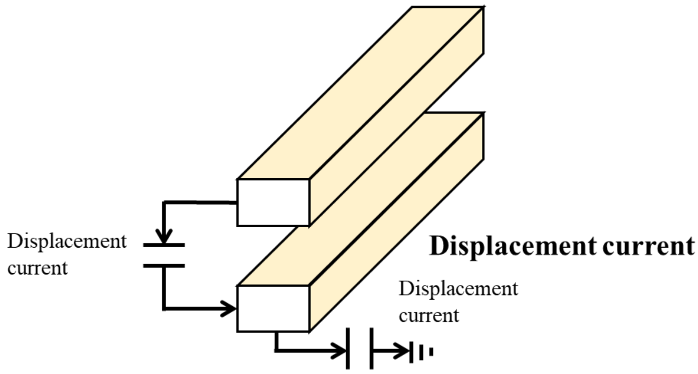

Fig. 4-1 Displacement current

4.1 Construction of equivalent circuit with displacement current

4.1.1 Introduction of equivalent circuit with displacement current

The equivalent circuit with displacement current is a robust computational technique utilized extensively in the analysis and design of complex electromagnetic systems. It serves as an effective approach to model and simulate various electrical and electronic components, particularly in high-frequency applications.

At its core, the equivalent circuit with displacement current dissects intricate electromagnetic structures into smaller, manageable parts. These parts encompass conductors, dielectrics, magnetic materials, and other components integral to the system under study. Each individual part is characterized by its electrical properties, including resistance, capacitance, and inductance, and its interaction with adjacent parts within the system.

The fundamental concept behind equivalent circuit with displacement current lies in the consideration of both the self-impedance of each element and its mutual interactions with neighboring elements. By comprehensively analyzing these interactions through the formulation of partial circuit equivalents for each component, equivalent circuit with displacement current enables the accurate prediction of the system's behavior [57]-[58].

The eddy currents are considered by introducing AC resistance in [16], for which several times of calculation using FEM are necessary that might be time-consuming. The eddy current loss is not taken into consideration in [5] that R_{DC} is applied in each branch and it will occur error as R_{AC} resistance is much larger than R_{DC} resistance. In our research, we propose an equivalent circuit model based on [42] in which the complex inductance is introduced to consider the eddy current effect without iterative computations. The construction of equivalent circuit with displacement current is shown in Fig. 4-2.

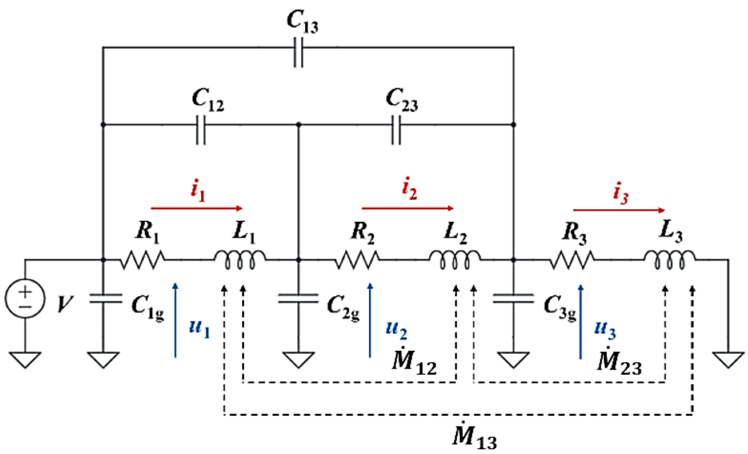

Fig. 4-2 Equivalent circuit with displacement current for a 3-turn model

The spiral coil is here assumed to be divided into three separated closed coils for simplicity. Each branch contains DC resistor and complex self-inductance $\dot{L}$ and complex mutual inductance $\dot{M}$ among the other coils. Moreover, we consider the stray capacitance among the separated coils.

The parameters of equivalent circuit with displacement current are derived from static electric field FE analysis and magneto-quasistatic FE analysis based on self-made code .

4.1.2 Static electric field analysis

To calculate the capacitance in the equivalent circuit with displacement current, static electric field FE analysis is necessary. The difference of the capacitance in high frequency is ignored. In this section the basic formula of static electric field FE analysis will be introduced.

The Poisson's equation in the static electric field analysis is shown as

$$\nabla^2 \varphi = -\frac{\rho}{\varepsilon_0} \tag{4.1}$$

Where φ, ρ and ε_0 denote the scalar potential, charge density and the vacuum dielectric constant.

In 2-D FEM, the equation can be written as

$$\frac{\partial}{\partial x}\left(\varepsilon_0 \frac{\partial \varphi}{\partial x}\right) + \frac{\partial}{\partial y}\left(\varepsilon_0 \frac{\partial \varphi}{\partial y}\right) = -\rho \tag{4.2}$$

By applying the Galerkin method with the weighted residue method, we obtain the weak form of the equation as

$$\int N(x,y)\left(\frac{\partial}{\partial x}\left(\varepsilon_0 \frac{\partial \varphi}{\partial x}\right) + \frac{\partial}{\partial y}\left(\varepsilon_0 \frac{\partial \varphi}{\partial y}\right)\right) dS = -\int N(x,y)\rho dS \tag{4.3}$$

Where N is the basic function of Galerkin method.

Using partial integration and Gauss's divergence theorem, we can transform it as follows

$$\oint N(x,y)\varepsilon_0(\nabla\varphi \cdot \boldsymbol{n})dl - \int (\frac{\partial N}{\partial x}\varepsilon_0 \frac{\partial \varphi}{\partial x} + \frac{\partial N}{\partial y}\varepsilon_0 \frac{\partial \varphi}{\partial y})dS = -\int N(x,y)\rho dS \tag{4.4}$$

The first term on the left side is the unit normal vector taken outward to this boundary line in the circuit integral around the boundary of the analysis area. If the normal component of the electric field is zero on the boundary, this integral vanishes. Also, if the potential value is fixed on the boundary, there is no need to consider this integral. This section will be ignored as these conditions will be met in the future. Subsequently, the final form of the equation is shown as

$$\int (\frac{\partial N}{\partial x}\varepsilon_0\frac{\partial \varphi}{\partial x}+\frac{\partial N}{\partial y}\varepsilon_0\frac{\partial \varphi}{\partial y})dS=\int N(x,y)\rho dS \tag{4.5}$$

Based on the ICCG method, φ at every element can be calculated. Moreover, the electric field strength $\boldsymbol{E}$ is calculated from the derivation of the φ.

4.1.3 Derivation of the circuit parameters

All the parameters of equivalent circuit with displacement current are computed from the FE analysis introduced in chapter 2 and 4.

We consider a 3-turn air core inductor as example.

To calculate the capacitance in the equivalent circuit with displacement current, static electric field FE analysis is applied. By using single turn approximation, the object model is divided into several parts firstly, and based on the static electric field FE analysis the electric charge and potential difference in each part can be calculated. Thus, we set the boundary condition of one part is 1V while others are 0 and the ρ is 0 in all the mesh. The electric charge is calculated by the integration of the electric displacement $\boldsymbol{D}$. The distribution of $\boldsymbol{E}$ calculated by self-made program in 2-D rotation coordination is shown in Fig. 4-3.

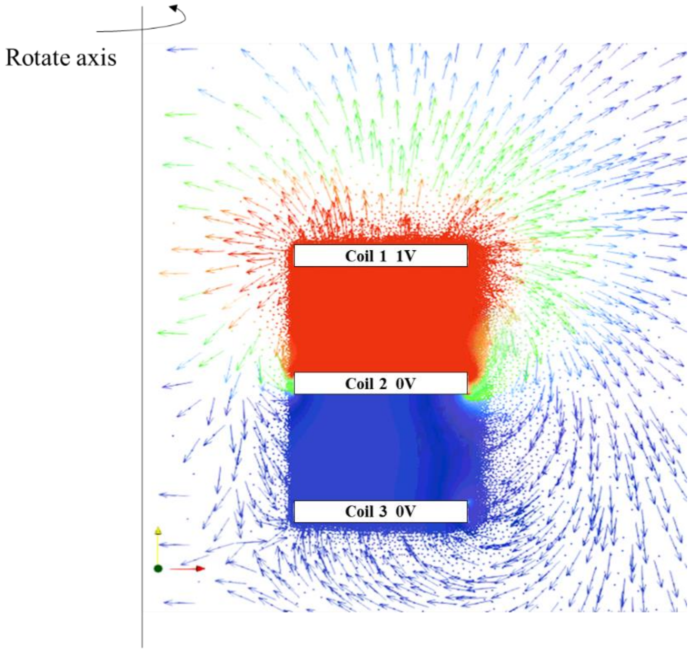

Fig. 4-3 Distribution of *E* of a 3-turn air core inductor

As shown the ***E*** is calculated and the capacitance between part 1 and j C_{1j} is calculated by

$$C_{1j} = \frac{Q_j}{V_{1j}} \tag{4.6}$$

where Q_j is the induced electric charge in part j, V_{1j} is the potential difference which is 1 in this case. The calculation method of Q_j is shown as below

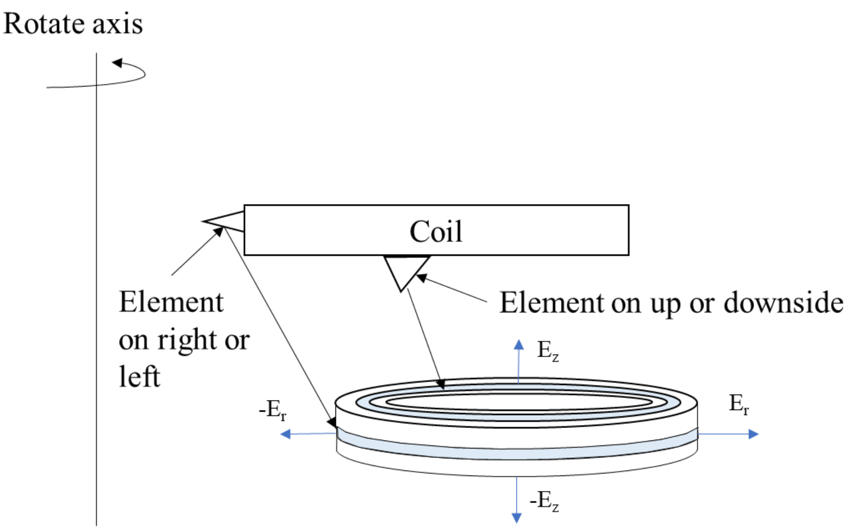

Fig. 4-4 Calculation of the electric charge in the coil

The area integration is applied on all faces of the coil and the reference direction is as shown in

Fig. 4-4. The Q_j is calculated by the formula as follows

$$Q_j = \oiint_{S_i} \varepsilon_0 E \, dS \tag{4.7}$$

To calculate the resistance, inductance of each branch and complex mutual inductance between each branch, magneto-quasistatic FE analysis is applied. As introduced in chapter.2, the eddy current loss can be considered by the analysis. The power loss relevant to the inductor is expressed as follows

$$P_{inductive} = \frac{1}{2} j\omega \dot{L}_{11} I_1^2 + \frac{1}{2} j\omega \dot{L}_{22} I_2^2 + \cdots + j\omega \dot{M}_{12} I_1 I_2 + j\omega \dot{M}_{13} I_1 I_3 + \cdots \tag{4.8}$$

The real part in formula represents the stored power whereas the imaginary part represents the eddy current loss. The complex mutual inductance $\dot{M}$ included in formula which is computed by magneto-quasistatic FEM only once represents the proximity effect. The complex self-inductance $\dot{L}$, which is relevant to the skin and proximity effects, is computed in the following way; we set the amplitude of the time-harmonic current flowing *j*-th coil to 1A, and other coils to 0, which are assumed parallel to z axis. Then, we compute from

$$\dot{L}_{ij} = \int_{\Omega_i} \dot{A}_z^j \, dS \tag{4.9}$$

where $\dot{A}_z^j$ denotes the vector potential generated by the unit current in *j*-th coil. It is remarked that $\dot{L}_{ij}$ is a function of frequency.

The distribution of magnetic flux in the FE analysis is shown as

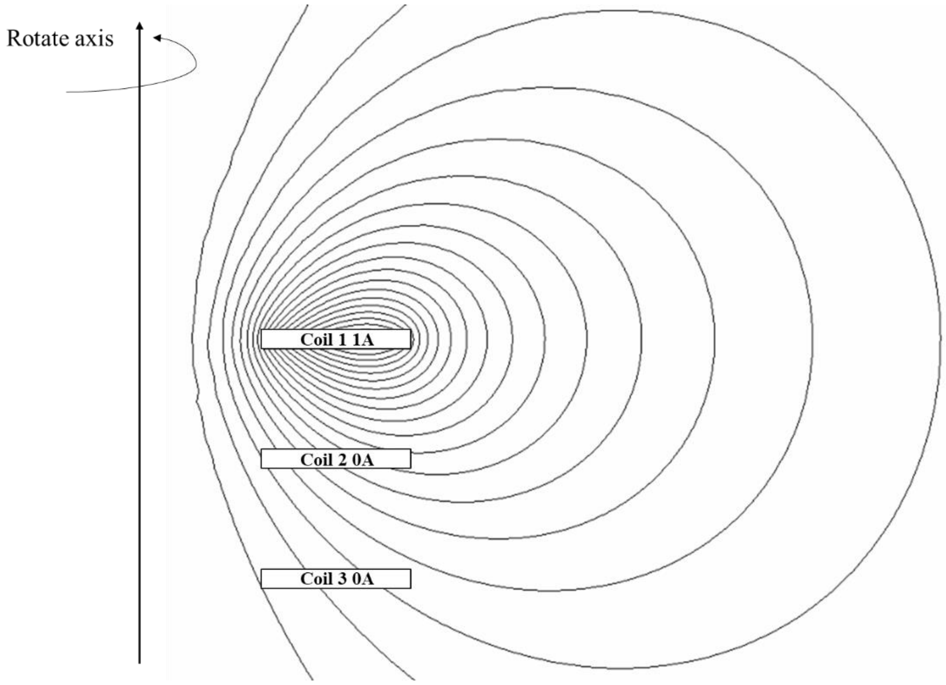

Fig. 4-5 Distribution of *B* of a 3-turn air core inductor

4.1.4 Solution of equivalent circuit with displacement current

Consequently, we will introduce how to solve the equivalent circuit. For the calculation of current and voltage in equivalent circuit with displacement current in frequency domain, we choose Python to solve the circuit as the complex inductance is dependent on frequency. Based on Kirchhoff's current law and Kirchhoff's voltage law, the circuit equation matrix is derived as

$$\left\{jw\begin{bmatrix}[\dot{L}] & 0\\ 0 & [C]\end{bmatrix}+\begin{bmatrix}[R] & [K]\\ [K]^t & 0\end{bmatrix}\right\}\begin{bmatrix}\{I\}\\ \{U\}\end{bmatrix}=\begin{bmatrix}\{\alpha\}\\ \{\beta\}\end{bmatrix} \tag{4.10}$$

$\dot{L}$, C, R, K, I and U denote matrix of self-inductance and complex mutual inductance, stray capacitance between coils, resistance of each branch, coefficient matrix, current and voltage of each branch or node. α and β are source terms. For the equivalent circuit with displacement current of a 3-turn air core inductor, the full circuit equation matrix is shown as

$$\begin{bmatrix} j\omega\dot{L}_1 & j\omega\dot{M}_{12} & j\omega\dot{M}_{13} & 0 & 0\\ j\omega\dot{M}_{12} & j\omega\dot{L}_2 & j\omega\dot{M}_{23} & 0 & 0\\ j\omega\dot{M}_{13} & j\omega\dot{M}_{23} & j\omega\dot{L}_3 & 0 & 0\\ 0 & 0 & 0 & -j\omega(C_{12}+C_{2g}+C_{23}) & j\omega C_{23}\\ 0 & 0 & 0 & j\omega C_{23} & -j\omega(C_{13}+C_{23}+C_{3g}) \end{bmatrix}+$$

$$\begin{bmatrix} R_1 & 0 & 0 & 1 & 0 \\ 0 & R_2 & 0 & -1 & 1 \\ 0 & 0 & R_3 & 0 & -1 \\ 1 & -1 & 0 & 0 & 0 \\ 0 & 1 & -1 & 0 & 0 \end{bmatrix}) \begin{bmatrix} I_1 \\ I_2 \\ I_3 \\ U_2 \\ U_3 \end{bmatrix} = \begin{bmatrix} V \\ 0 \\ 0 \\ -j\omega C_{12}V \\ -j\omega C_{13}V \end{bmatrix} \tag{4.11}$$

$\dot{L}_i$, $\dot{M}_{ij}$, C_{ij}, R_i, I_i, U_2, V and ω denote the complex self-inductance of branch i, complex mutual inductance between branch i and j, the stray capacitance between branch i and j, resistance of branch i, current in branch i, voltage of node i, input voltage and the operating frequency of the model.

4.2 Representation of WPT based on equivalent circuit with displacement current

4.2.1 Self-resonant coil in strong coupled WPT

The self-resonant coil plays a crucial role in Strongly Coupled WPT systems, especially in applications where high efficiency and power transfer over relatively large distances are essential.

In the realm of WPT, self-resonance refers to the condition where the inductive reactance (X_L) and the capacitive reactance (X_C) of the coil cancel each other out, resulting in a purely resistive impedance. This state is characterized by a resonance frequency (f_r) at which the coil naturally tends to oscillate. The schematic diagram of self-resonant coil in strong coupled WPT is shown in Fig. 4-6.

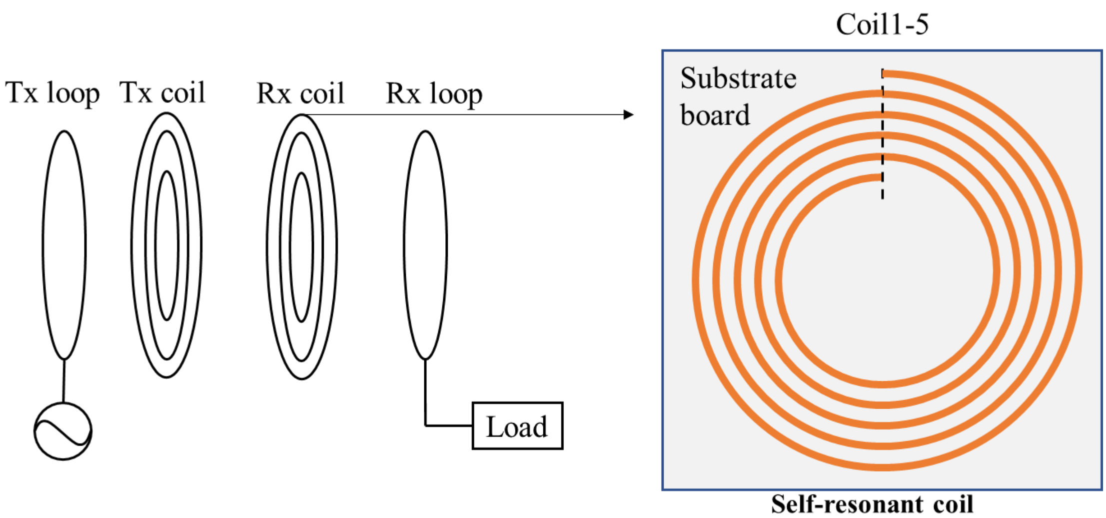

Fig. 4-6 Schematic diagram of self-resonant coil in strong coupled WPT

The self-resonant coil is designed to operate at or near this resonant frequency. At resonance, the coil exhibits minimal losses, optimizing the efficiency of power transfer. When the transmitter and receiver coils are both tuned to this frequency, the mutual coupling between them is maximized, enabling efficient power transfer over greater distances [59].

The design of a self-resonant coil involves careful consideration of its physical parameters, such as the number of turns, coil geometry, material properties, and the addition of tuning capacitors to achieve the desired resonant frequency. The aim is to achieve a high-quality factor Q at resonance, maximizing the power transfer efficiency and enabling practical applications like wireless charging for electric vehicles.

In this section, equivalent circuit with displacement current containing complex inductance is applied to represent the self-resonant coil in WPT and the parameters of one self-resonant coil is shown in Table. 11. All the parameters of equivalent circuit with displacement current are computed as introduced in previous section.

Table. 11 Parameters of self-resonant coil

Number of turns	5
Clearance between turns	7 mm
Substrate thickness	0.105mm
Wire width	2.54 mm
Inner radius	200 mm
Wire thickness	0.105mm

The impedance of the self-resonant coil is plotted versus operating frequency in Fig. 4-7. The impedance is calculated by quasi-static FEM, full wave FEM software Femtet^{TM}, and equivalent circuit with displacement current.

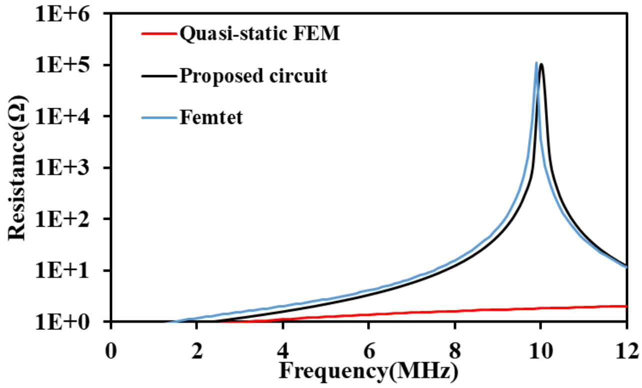

(a) Resistance of self-resonant coil

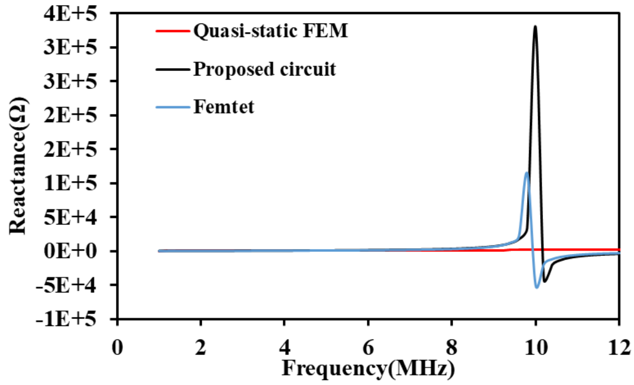

(b) Reactance of self-resonant coil

Fig. 4-7 Impedance of the self-resonant coil

The resistance of the self-resonant coil calculated by Femtet and equivalent circuit with displacement current reach a peak value at around 10Mhz which is the self-resonant frequency. The result calculated from quasi-static FE analysis cannot show this phenomenon. Moreover, the reactance of the self-resonant coil changes from positive value to negative value and it notes the coil's attribute changes from inductive to capacitive. It concludes that equivalent circuit with displacement current performs well in frequency domain and can be applied in electric system to do the time domain analysis.

4.2.2 Spiral coil of WPT printed on a substrate board

The planar spiral coils printed on a substrate board, called printed spiral coil (PSC), has been studied for possible uses for small or medium electric devices [60]. A fast numerical model of

PSC used in coupled magnetic resonance system has been required for its design [5], [61]. For such a model, eddy currents in the coils and displacement currents flowing between the coils have to be adequately considered. In this section we consider the coupled magnetic WPT which applies PSC as its transmitting and receiving coil based on the equivalent circuit with displacement current. Different with strong coupled WPT, it contains only two parts both connecting with a resonant capacitor.

The PSC composes of rectangular coils on one side, whose feasibility is demonstrated by [60]. The operating frequency of the WPT system of our interest is 6.78MHz (one of the ISM band) which is suitable for consumer electronics applications. A 6 turns PSC model is shown as Fig. 4-8. The parameter is shown in Table. 12.

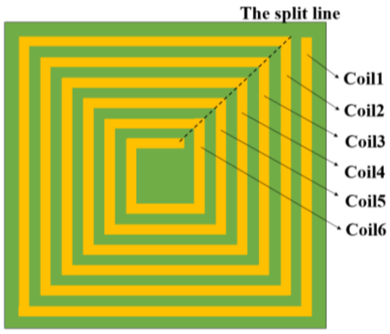

(a) Simplified structure of PSC

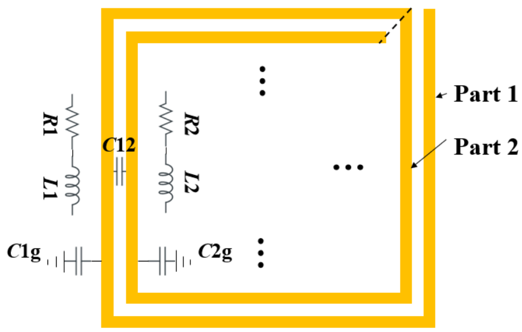

(b) Schematic diagram of partition for part 1,2

Fig. 4-8 Simplified 6 turns PSC

Resistors R_{kg} that represents the dielectric loss of the substrate board which are series connected to the ground and evaluated from

$$R_{kg} = \frac{\tan \delta}{\omega C_{kg}} \qquad k = 1,2 \cdots 6 \tag{4.12}$$

Table. 12 Parameters of PSC

Side length of outer turn	70mm
Number of turns	6
Wire width	3mm
Wire thickness	0.105mm
Clearance between turns	2mm
Substrate thickness	0.33mm

Both sides of WPT are represented using proposed equivalent circuit to consider the eddy current and displacement current at same time. The mutual inductance $\dot{M}$ between coils in two side only take the real part into consideration. Moreover, external capacitance is added to tune the resonant frequency (6.78MHz) at both sides.

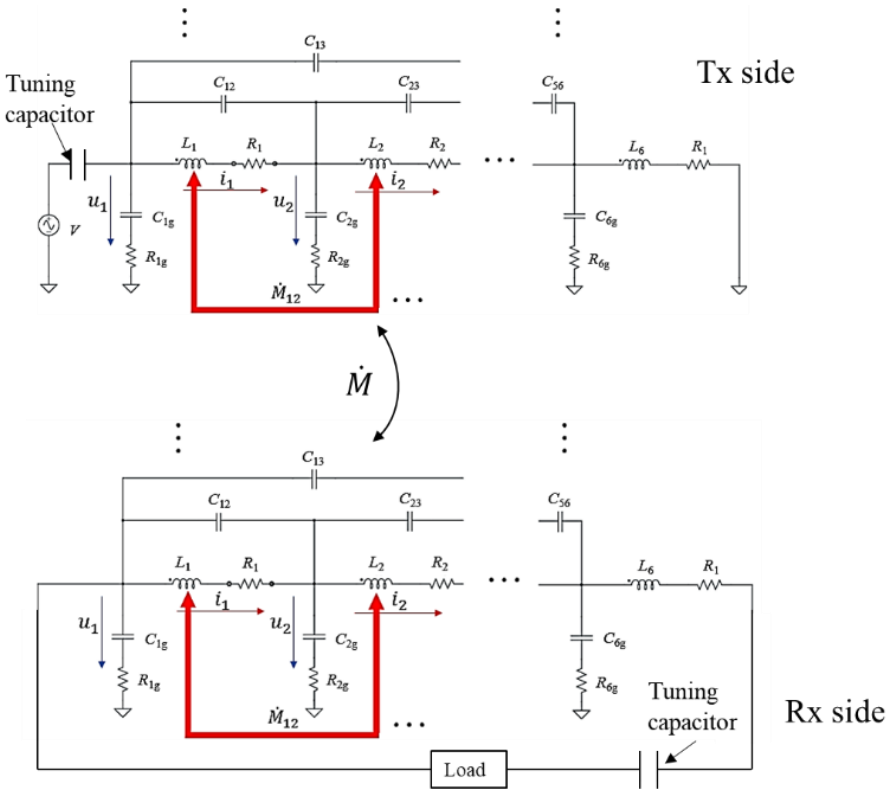

Fig. 4-9 Proposed equivalent circuit for power transmission analysis

Firstly, we do not connect the resonant capacitance into the circuit to see the self-resonant point of the Tx coil. The result compared with that computed from Femtet is plotted in Fig. 4-10.

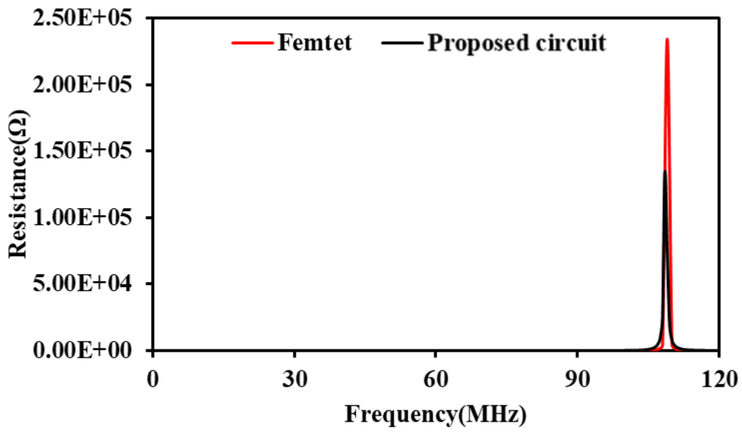

(a) Resistance of Tx coil

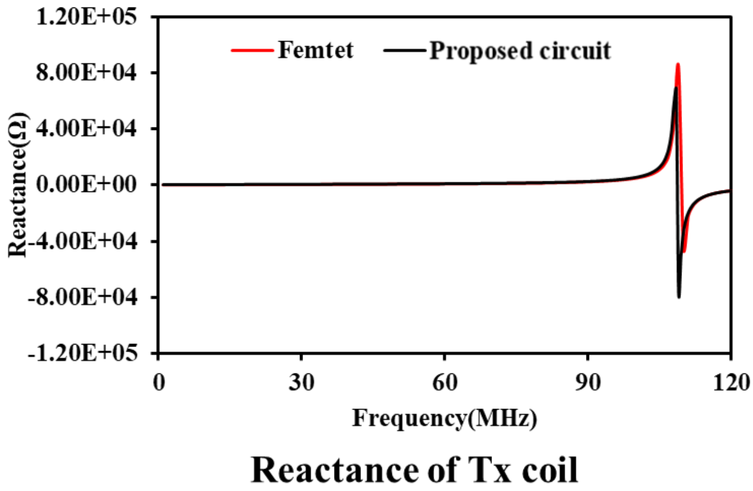

(b) Reactance of Tx coil

Fig. 4-10 Self-resonant of Tx coil

At 6.78MHz, the frequency is low that there is no influence from displacement current. The power transmission of conventional equivalent circuit for series resonant WPT should be same with proposed equivalent circuit. Moreover, the impedance of the conventional equivalent also changes to consider the eddy current.

We set the transmitting distance of WPT as 15mm, the input voltage is 1V and load is 10Ω. The active power of transmitting coil and load are shown in Fig. 4-11.

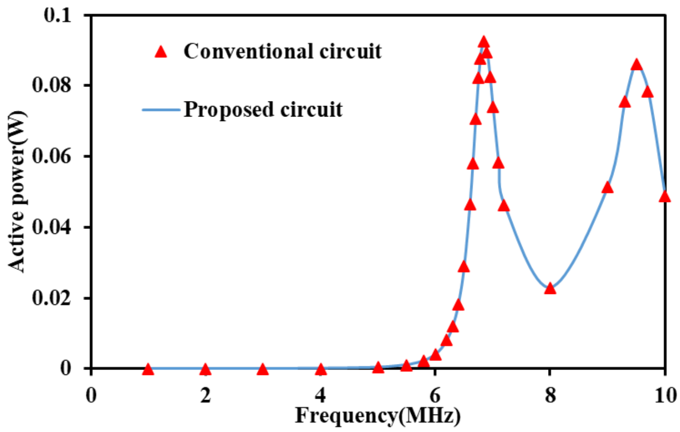

(a) Active power of transmitting side

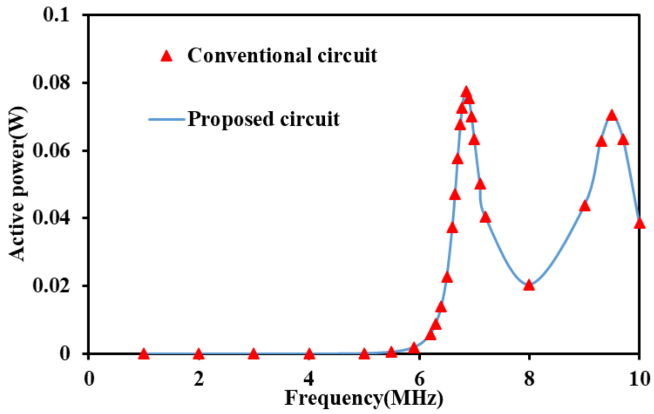

(b) Active power of load

Fig. 4-11 Comparison of active power

Both active powers fit well with conventional equivalent circuit. When displacement current has no effect on WPT, conventional equivalent circuit is sufficient to analyze the model. If the WPT has a larger size or operating at a higher frequency, the equivalent circuit with displacement current should be applied.

4.3 Representation of inductor based on equivalent circuit with displacement current

Inductors, vital components in electronic circuits, possess inherent properties that facilitate their interaction with other elements. However, one common challenge they face is the influence of parasitic capacitance, which can lead to resonant behavior [62], [63].

In practical terms, this resonance can have significant implications for circuit performance. At the resonant frequency, the resistance of the inductor and capacitor combination becomes maximized, potentially leading to decreased current flow in the circuit. Engineers must account for and mitigate the impact of parasitic capacitance in inductor design to avoid unintended resonance effects that could disrupt circuit functionality or lead to undesired outcomes [64], [65].

4.3.1 The simulation result in frequency and time domain

We consider an 6-turn air-core inductor model with separated six-coils, shown in **Fig. 4-12**, to verify the proposed equivalent circuit. The values of the capacitance and inductance in the matrices are visualized in **Fig. 4-13**.

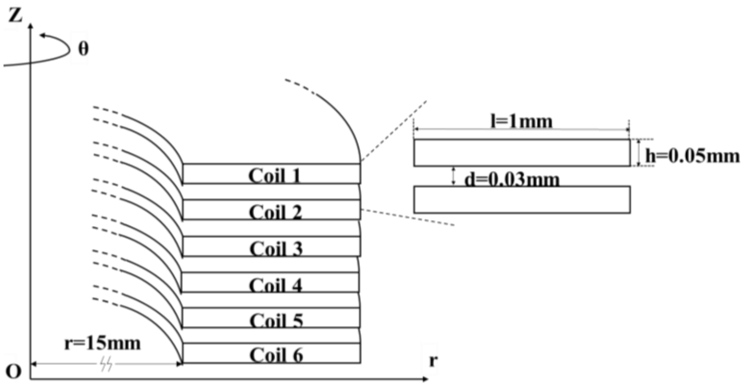

Fig. 4-12 Air-core six-coils inductor

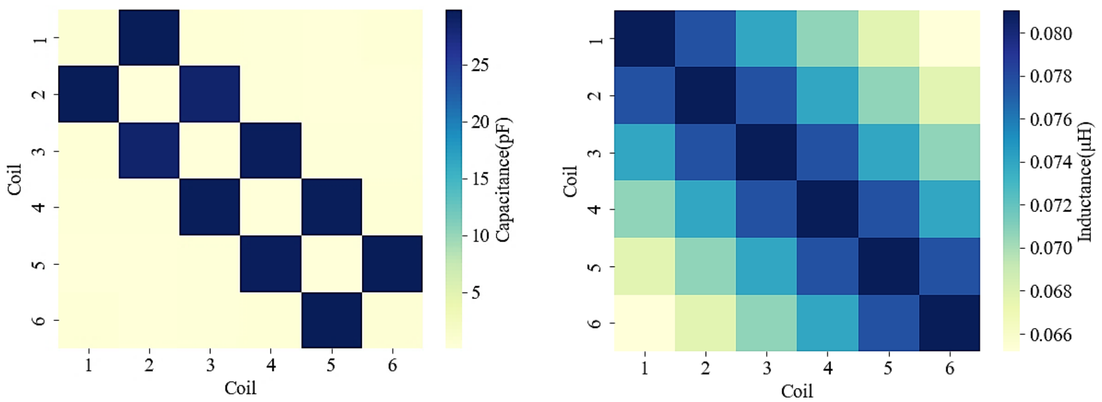

(a) Capacitance matrix $[C]$ (b) Inductance matrix $[\dot{L}]$ (magnitude)

Fig. 4-13 Visualization of entities in capacitance and inductance matrices

First the stray capacitance is neglected in the equivalent circuit, and the result is compared with the magneto-quasistatic FE analysis by which the displacement current is neglected too. The impedance of the inductor is plotted in **Fig. 4-14**.

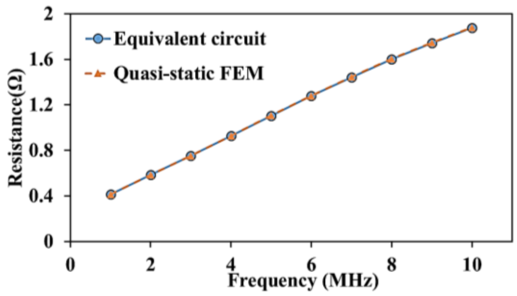

(a) Resistance

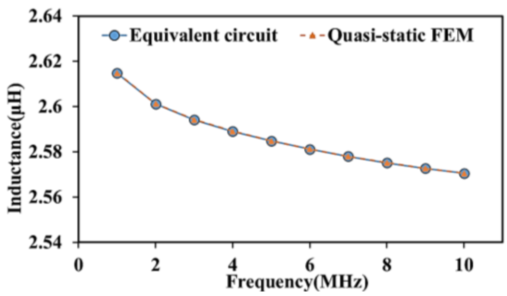

(b) Inductance

Fig. 4-14 Comparison of resistance and inductance for cases without stray capacitance

We next consider the equivalent circuit that includes the capacitance. The resistance, reactance and quality factor obtained by the equivalent circuit with and without considering eddy currents, as well as those computed by the magneto-quasi-static FEM are plotted versus frequency in Fig. 4-15. From Fig. 4-15 we can find the effect of eddy current and displacement current clearly.

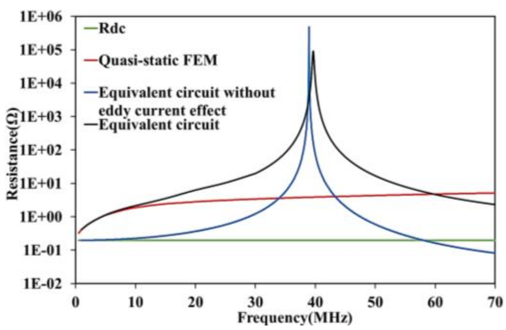

(a) Resistance

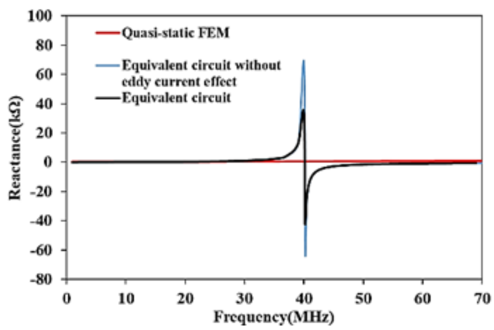

(b) Reactance

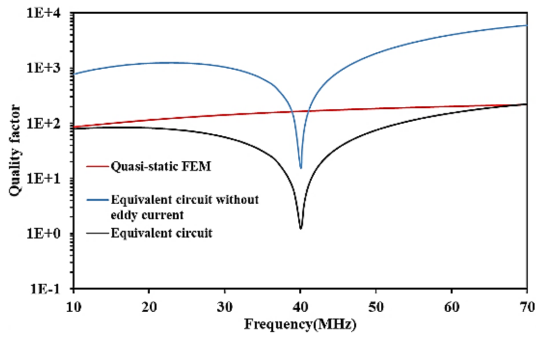

(c) Quality factor

Fig. 4-15 Frequency response of equivalent circuit

At low frequencies, the result computed from the equivalent circuit considering the eddy current is consistent with that computed by FEM under magneto-quasi-static approximation. At the frequencies over 10MHz, we observe the effect from the stray capacitance. In this region, both eddy and displacement currents contribute to the input impedance. There exists an LCR parallel resonance at round 40MHz.

For the design of inductors, the quality factor Q is another important characteristic. As we can see in Fig. 4-15 (c), Q becomes very small near the resonant frequency. The value of Q computed by the proposed equivalent circuit is 10 times larger than that computed by the conventional equivalent circuit neglecting the eddy currents.

We also perform the time-domain analysis using the proposed equivalent circuit. For such an analysis using FEM, the time step would be estimated as $\Delta t = \Delta x / c \sim 10^{-11}$s from the Courant condition where Δx is assumed to be 1mm and $c = 3 \times 10^8$ m/s. This means that we need ten thousand steps for a period $T \sim 10^{-7}$s which would be prohibitive for FEM that has a large computing cost. In Fig. 4-16 (a) and (b), input voltage is assumed to be triangular wave whose fundamental frequency is 5MHz and 30MHz and the time step is set to 10^{-11}s. The triangular wave contains higher harmonics ω_n that can be dealt separately. The triangular wave is decomposed into Fourier components to which the time responses are computed using the corresponding equivalent circuit that contains $\dot{L}(\omega_n)$. We use the LTSpice simulator in which the proposed equivalent circuit is modeled to compute the time response.

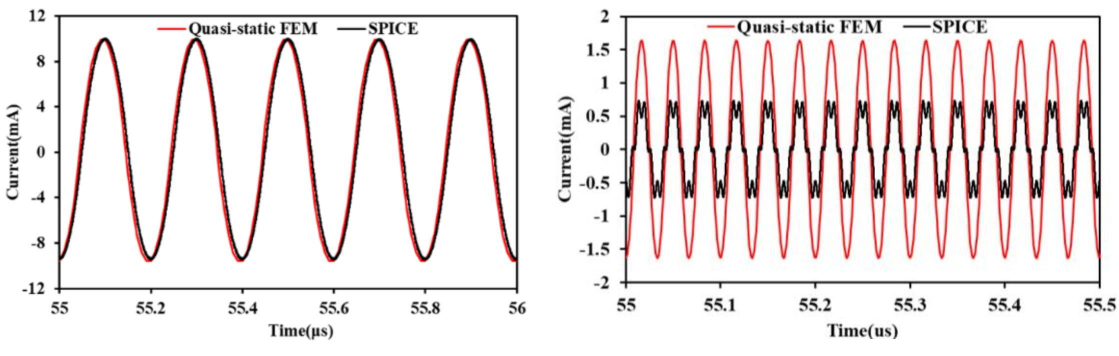

(a) Current response at 5MHz (b) Current response at 30MHz

Fig. 4-16. Comparison of current waveforms in time domain

4.3.2 The measurement result in frequency domain

For verification of the prosed method, we measured the resistance of an air-core inductor with a flat wire shown in Fig. 4-17, whose parameters are summarized in Table. 13.

(a) Main view (b) Top view

Fig. 4-17. Air-core inductor with flat wire for measurement

Table. 13 Parameters of measured inductor

Number of turns	20	Thickness of one turn	1 mm
Space between each turn	0.25 mm	Width of one turn	5.5 mm
Inner radius	7 mm	Length of end side	10 mm

Fig. 4-18. Photograph of LCR meter and inductor

The *LCR* meter IM3536 shown in Fig. 4-18 can measure impedance from 4 Hz to 8 MHz. The measured resistance and that computed from the equivalent circuit and quasi- magnetostatic FE analysis are plotted versus frequency in Fig. 4-19. There are fluctuations in the resistance measured over 6 MHz, the maximum, minimum and averaged values are plotted in Fig. 4-19 (a). The resistance at frequencies lower than 4 MHz can be represented well both by FE analysis and the equivalent circuit. When frequency is higher than 4 MHz, effect of stray capacitance becomes predominant so that the result computed from the equivalent circuit fit better to the measured result. In this frequency range, FEM underestimates the resistance. The maximum operation frequency of the *LCR* meter, 8 MHz, does not reach the resonant frequency of inductor. However, the effect owing to the stray capacitance can be clearly observed in the measured frequency range. The result computed from the equivalent circuit suggests that the resonance would be around 25 MHz for this coil as shown in Fig. 4-19 (c).

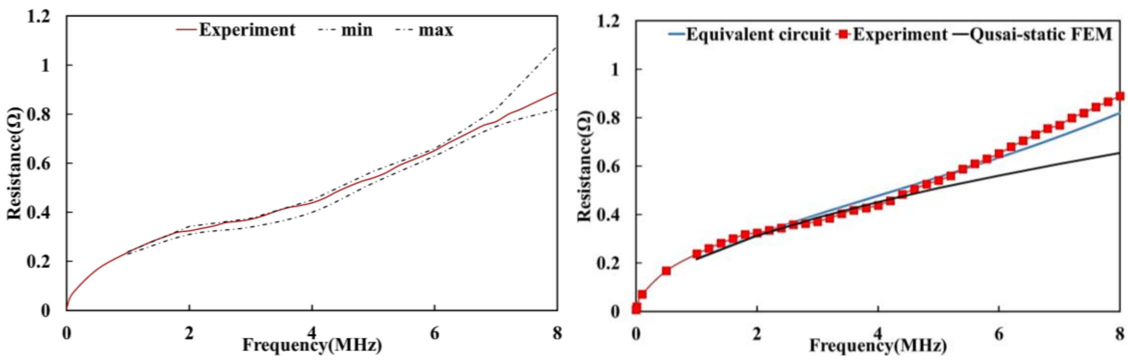

Fig. 4-19. Comparison with computed and measured results

4.4 Conclusion

In this chapter, we have proposed an equivalent circuit for coils considering both eddy currents and displacement currents. The present equivalent circuit includes the complex inductance computed by magneto-quasistatic FE analysis considering the skin and proximity effects. Moreover, it also includes the capacitance computed by the electrostatic FE analysis. Using the proposed equivalent circuit, we can perform the frequency and time-domain analysis over the resonance for air-core inductor and coils of WPT. At low frequencies where the displacement currents are negligible, the impedance computed by the proposed circuit agrees well with that computed by magneto-quasistatic FEM.

Moreover, the measured resistance of an air-core coil is consistent with that computed by the proposed equivalent circuit whereas the magneto-quasi-static FEM underestimate the resistance.

It would be possible to extend the proposed method to the analysis of the coils with magnetic cores. To obtain the impulse response, we have to compute the complex inductance for all the frequencies. However, such computation needs large number of finite elements. These remain for our future task.

Chapter 5 Conclusion

In this thesis, to represent the magnetic device operation at high frequency, several works have been proposed, focusing on different situations, using different methods. In general, the development of equivalent circuit and homogenization method focus on the two following issues.

1. When there is only eddy current to be considered, how to build a Cauer circuit more precisely and efficiently to accelerate the analysis of device.
2. When the frequency is high enough that the displacement current cannot be ignored, how to represent the device efficiently considering all the current effects.

Aiming to solve these problems, the Cauer circuit based on the identification method, Cauer circuit combined with homogenization method and equivalent circuit with displacement current with complex permeability are applied in this paper.

5.1 Cauer equivalent circuit based on the input data

In this chapter, several magnetic devices working at high frequency are represented by Cauer circuit based on the identification method to do the simulation efficiently while considering the eddy current.

As a result, based on the impedance calculated from the formula, the Cauer circuit can be constructed efficiently to represent the secondary short transformer and there is no need to build the complex model. The inductor with nonlinear material can also be represented by nonlinear Cauer circuit which introduce the relationship between the input current and the inductance into the primal inductance of Cauer circuit. The result of nonlinear Cauer circuit in time domain fits well with nonlinear FEM even the input is PWM wave that contains high frequency harmonics. When the Cauer circuit is applied to represent WPT, it concludes that Cauer circuit can also be applied for magnetic devices which has more than two parts and can be embedded into electric power transmission system while considering the eddy current. Both the alignment and misalignment WPT can be represented by Cauer circuit.

5.2 Cauer circuit based on the homogenization method

In this chapter, the comparison of results from FE analysis, homogenization method and Dowell's method is shown, and we find that although in some specific situations Dowell's method is more convenient, homogenization method has a wider range of applications. Moreover, based on homogenization method, we build the Cauer circuit without complex model and perform the FE analysis in high frequency with small elements.

To consider the influence from the magnet in the rotor, we construct the homogenized Cauer circuit from the formula of $<\dot{\mu}_r>$ directly. The impedance of homogenized Cauer circuit fits well with $j\omega<\dot{\mu}_r>$ in frequency domain for different volume fraction and radius of round wire.

The copper loss of motor winding can be computed from the homogenized Cauer circuit and fits well with the result computed from formula based on DFT in frequency domain.

The copper loss of winding is also computed in time domain. However, some error at the peak value region still exists. It should be noted that the stored energy per unit volume in the homogenized model has some differences in the peak value region and it may cause the error in the power loss calculation.

5.3 Equivalent circuit for magnetic device considering displacement current and eddy current

In this chapter, we have proposed an equivalent circuit for coils considering both eddy currents and displacement currents based on the complex mutual inductance. It doesn't need repeatable computation . Using the proposed equivalent circuit, we can perform the frequency and time-domain analysis over the resonance for air-core inductor and coils of WPT. At low frequencies where the displacement currents are negligible, the impedance computed by the proposed circuit agrees well with that computed by magneto-quasistatic FEM.

Moreover, the measured resistance of an air-core coil is consistent with that computed by the proposed equivalent circuit whereas the magneto-quasi-static FEM underestimate the resistance.

5.4 Future work

The research of Cauer circuit shows that it performs well in the calculation of copper loss and current response in time domain. How to calculate the iron loss based on the Cauer circuit remains to be solved. Moreover, further optimization should be done based on the Cauer circuit.

As to the homogenized Cauer circuit, the future work is to find a more exact method to minimize the error of the stored energy per unit volume in homogenized model and original model.

For equivalent circuit with displacement current, a validation in time domain analysis should be completed in future.

References

[1] R. S. Yang, A. J. Hanson, B. A. Reese, C. R. Sullivan and D. J. Perreault, "A Low-Loss Inductor Structure and Design Guidelines for High-Frequency Applications," in IEEE Transactions on Power Electronics, vol. 34, no. 10, pp. 9993-10005, Oct. 2019, doi: 10.1109/TPEL.2019.2892397.

[2] G. Grandi, M. K. Kazimierczuk, A. Massarini and U. Reggiani, "Stray capacitances of single-layer solenoid air-core inductors," in IEEE Transactions on Industry Applications, vol. 35, no. 5, pp. 1162-1168, Sept.-Oct. 1999, doi: 10.1109/28.793378.

[3] Y. Otomo and H. Igarashi, "Synthesis of a Cauer Equivalent Circuit for Electric Devices From Computed and Measured Data," in IEEE Transactions on Power Electronics, vol. 36, no. 4, pp. 4513-4521, April 2021, doi: 10.1109/TPEL.2020.3022167.

[4] D. Voltolina, R. Torchio, P. Bettini, R. Cavazzana and M. Moresco, "equivalent circuit with displacement current Modeling of Planar Spiral Resonators," in IEEE Transactions on Magnetics, vol. 56, no. 1, pp. 1-4, Jan. 2020, Art no. 6700404, doi: 10.1109/TMAG.2019.2949481.

[5] K. Chen and Z. Zhao, "Analysis of the Double-Layer Printed Spiral Coil for Wireless Power Transfer," in IEEE Journal of Emerging and Selected Topics in Power Electronics, vol. 1, no. 2, pp. 114-121, June 2013, doi: 10.1109/JESTPE.2013.2272696.

[6] H. Igarashi, "Semi-Analytical Approach for Finite-Element Analysis of Multi-Turn Coil Considering Skin and Proximity Effects," in IEEE Transactions on Magnetics, vol. 53, no. 1, pp. 1-7, Jan. 2017, Art no. 7400107, doi: 10.1109/TMAG.2016.2601066.

[7] Y. Sato and H. Igarashi, "Generation of Equivalent Circuit From Finite-Element Model Using Model Order Reduction," in IEEE Transactions on Magnetics, vol. 52, no. 3, pp. 1-4, March 2016, Art no. 1100304, doi: 10.1109/TMAG.2015.2476370.

[8] A. Kameari, H. Ebrahimi, K. Sugahara, Y. Shindo and T. Matsuo, "Cauer Ladder Network Representation of Eddy-Current Fields for Model Order Reduction Using Finite-Element Method," in IEEE Transactions on Magnetics, vol. 54, no. 3, pp. 1-4, March 2018, Art no. 7201804, doi: 10.1109/TMAG.2017.2743224.

[9] Y. Otomo, Y. Sato, S. Fujita and H. Igarashi, "Synthesis of Equivalent Circuit of Wireless Power Transfer Device Using Homogenization-Based FEM," in IEEE Transactions on Magnetics, vol. 54, no. 3, pp. 1-5, March 2018, Art no. 7401005, doi: 10.1109/TMAG.2017.2749968.

[10] A. Ayachit and M. K. Kazimierczuk, "Self-Capacitance of Single-Layer Inductors With Separation Between Conductor Turns," in IEEE Transactions on Electromagnetic Compatibility, vol. 59, no. 5, pp. 1642-1645, Oct. 2017, doi: 10.1109/TEMC.2017.2681578.

[11] P. A. Kyaw, A. L. F. Stein and C. R. Sullivan, "High-Q resonator with integrated capacitance for resonant power conversion," 2017 IEEE Applied Power Electronics Conference and Exposition (APEC), 2017, pp. 2519-2526, doi: 10.1109/APEC.2017.7931052.

[12] B. Rejaei, "Mixed-potential volume integral-equation approach for circular spiral inductors," in IEEE Transactions on Microwave Theory and Techniques, vol. 52, no. 8, pp. 1820-1829, Aug. 2004, doi: 10.1109/TMTT.2004.831567.

[13] A. Massarini, "Analytical Approach to the Calculation of Parasitic Capacitance Between Winding Turns," 2018 IEEE 4th International Forum on Research and Technology for Society and Industry (RTSI), 2018, pp. 1-4, doi: 10.1109/RTSI.2018.8548511.

[14] Jasmin Smajic, Thorsten Steinmetz, Martin Rüegg, Zeljko Tanasic, Roman Obrist, Jens Tepper, Benjamin Weber and Martin Carlen., "Simulation and Measurement of Lightning-Impulse Voltage Distributions Over Transformer Windings," in IEEE Transactions on Magnetics, vol. 50, no. 2, pp. 553-556, Feb. 2014, Art no. 7013604, doi: 10.1109/TMAG.2013.2283061.

[15] T. Župan, B. Trkulja, R. Obrist, T. Franz, B. Cranganu-Cretu and J. Smajic, "Transformer Windings' RLC Parameters Calculation and Lightning Impulse Voltage Distribution Simulation," in IEEE Transactions on Magnetics, vol. 52, no. 3, pp. 1-4, March 2016, Art no. 8400204, doi: 10.1109/TMAG.2015.2481004.

[16] K. Preis, W. Renhart, A. Rabel and O. Bíró, "Transient Behavior of Large Transformer Windings Taking Capacitances and Eddy Currents Into Account," in IEEE Transactions on Magnetics, vol. 54, no. 3, pp. 1-4, March 2018, Art no. 7203904, doi: 10.1109/TMAG.2017.2766761.

[17] Q. Liu et al., "Loss Evaluation of Magnetic Devices using Cauer Equivalent Circuit Identified from Input Impedance," in IEEE Transactions on Magnetics, doi: 10.1109/TMAG.2023.3303880.

[18] Liu, Qiao et al. 'Equivalent Circuit of High Frequency Inductor to Consider Eddy Currents and Resonance'. International Journal of Applied Electromagnetics and Mechanics, vol. 71, no. S1, pp. S275-S282, 2023.

[19] T. Miyazaki, T. Mifune, T. Matsuo, Y. Shindo, Y. Takahashi, and K. Fujiwara, "Equivalent circuit modeling of dynamic hysteretic property of silicon steel under pulse width modulation excitation," J. Appl. Phys., vol. 117, 2015, Art. no. 17D110.

[20] E. J. Tarasiewicz, A. S. Morched, A. Narang, and E. P. Dick, "Frequency dependent eddy current models for nonlinear iron cores," IEEE Trans. Power Syst., vol. 8, no. 2, pp. 588–597, May 1993.

[21] Y. Shindo and O. Noro, "Simple circuit simulation models for eddy current in magnetic sheets and wires," IEE J. Trans. Fundam. Mater., vol. 134, no. 4, pp. 173–181, 2014.

[22] S. Hiruma and H. Igarashi, "Model Order Reduction for Linear Time-Invariant System With Symmetric Positive-Definite Matrices: Synthesis of Cauer-Equivalent Circuit," in IEEE Transactions on Magnetics, vol. 56, no. 3, pp. 1-8, March 2020, Art no. 7400608, doi: 10.1109/TMAG.2019.2962665.

[23] A. Kameari, H. Ebrahimi, K. Sugahara, Y. Shindo and T. Matsuo, "Cauer Ladder Network Representation of Eddy-Current Fields for Model Order Reduction Using Finite-Element Method," in IEEE Transactions on Magnetics, vol. 54, no. 3, pp. 1-4, March 2018, Art no. 7201804, doi: 10.1109/TMAG.2017.2743224.

[24] P. Mukherjee and L. Satish, "Construction of equivalent circuit of a single and isolated transformer winding from FRA data using the ABC algorithm," IEEE Trans. Power Del., vol. 27, no. 2, pp. 963–970, Apr. 2012.

[25] N. V. Korovkin, V. L. Chechurin, and M. Hayakawa, Inverse Problems in Electric Circuits and Electromagnetics. New York, NY, USA: Springer, 2007, ch. 5, pp. 275–285.

[26] M. M. Shabestary, A. J. Ghanizadeh, G. B. Gharehpetian, and M. AghaMirsalim, "Ladder network parameters determination considering nondominant resonances of the transformer winding," IEEE Trans. Power Del., vol. 29, no. 1, pp. 108–117, Feb. 2014.

[27] A. Shintemirov, W. H. Tang, and Q. H. Wu, "Transformer core parameter identification using frequency response analysis," IEEE Trans. Magn., vol. 46, no. 1, pp. 141–149, Jan. 2010.

[28] V. Rashtchi, E. Rahimpour, and E. M. Rezapour, "Using a genetic algorithm for parameter identification of transformer R-L-C-M model," Elect. Eng., vol. 88, no. 5, pp. 417–422, 2006.

[29] T. Shimotani, H. Igarashi, E. Hashimoto and H. Imanari, "Equivalent Circuit Allowing Loss Separation Synthesized From Field Computations: Application to Induction Heating," in IEEE Transactions on Magnetics, vol. 56, no. 2, pp. 1-5, Feb. 2020, Art no. 7505405, doi: 10.1109/TMAG.2019.2948570.

[30] S. W. Director and R. A. Rohrer, "The generalized adjoint network and network sensitivities," IEEE Trans. Circuit Theory, vol. CT-16, no. 3, pp. 318–323, Aug. 1969.

[31] S. W. Director and R. A. Rohrer, "Automated network design–the frequency–domain case," IEEE Trans. Circuit Theory, vol. CT-16, no. 3, pp. 330–337, Aug. 1969.

[32] P. Penfield, R. Spence, and S. Duinker, "A generalized form of Tellegen's theorem," IEEE Trans. Circuit Theory, vol. CT-17, no. 3, pp. 302–305, Aug. 1970.

[33] V. A. Monaco and P. Tiberio, "Computer-aided analysis of microwave circuits," IEEE Trans. Microw. Theory Techn., vol. MTT-22, no. 3, pp. 249–263, Mar. 1974.

[34] Z. Ren, H. Qu, and X. Xu, "Computation of second order capacitance sensitivity using adjoint method in finite element modeling," IEEE Trans. Magn., vol. 48, no. 2, pp. 231–234, Feb. 2012.

[35] S.Barmada, A. Musolino,R.Rizzo, and M. Tucci, "Multi-resolution based sensitivity analysis of complex non-linear circuits," IET Circuits Devices Syst., vol. 6, no. 3, pp. 176–186, 2012.

[36] N. K. Nikolova, J. W. Bandler, and M. H. Bakr, "Adjoint techniques for sensitivity analysis in high-frequency structure CAD," IEEE Trans. Microw. Theory Techn., vol. 52, no. 1, pp. 403–419, Jan. 2004.

[37] H. Igarashi and K. Watanabe, “Complex adjoint variable method for finite element analysis of eddy current problems,” IEEE Trans. Magn., vol. 46, no. 8, pp. 2739–2742, Aug. 2010.

[38] Y. Sato, T. Shimotani and H. Igarashi, "Synthesis of Cauer-Equivalent Circuit Based on Model Order Reduction Considering Nonlinear Magnetic Property," *IEEE Trans. on Magnetics*, vol. 53, no. 6, pp. 1–4, 2017, 1100204.

[39] J. Nocedal and S.J.Wright,Numerical Optimization. New York, NY, USA: Springer, 2006, ch. 17, pp. 497–528.

[40] M. K. Kazimierczuk, High-Frequency Magnetic Components, 2nd ed. Chichester, U.K.: Wiley, 2009.

[41] Z. Ouyang, J. Zhang and W. G. Hurley, "Calculation of Leakage Inductance for High-Frequency Transformers," in IEEE Transactions on Power Electronics, vol. 30, no. 10, pp. 5769-5775, Oct. 2015, doi: 10.1109/TPEL.2014.2382175.

[42] Qiao Liu, Yoshitsugu Otomo, Hajime Igarashi, “On Equivalent Circuit Representation of Transformer Considering Eddy Currents,” The 40th JSST Annual International Conference on Simulation Technology (JSST2021), pp.261-264, Sep., 2021.

[43] Y. Nagatsuka, N. Ehara, Y. Kaneko, S. Abe, and T. Yasuda, “Compact contactless power transfer system for electric vehicles,” in Proc. Int. Power Electron. Conf., Jun. 2010, pp. 807–813.

[44] Z. Yang, W. Liu, and E. Basham, “Inductor modeling in wireless links for implantable electronics,” IEEE Trans. Magn., vol. 43, no. 10, pp. 3851–3860, Oct. 2007.

[45] S. Hasanzadeh, S. Vaez-Zadeh, and A. H. Isfahani, “Optimization of a contactless power transfer system for electric vehicles,” IEEE Trans. Veh. Technol., vol. 61, no. 8, pp. 3566–3573, Oct. 2012.

[46] International Standard SAE J2954, “Wireless Power Transfer for Light-Duty Plug-In/Electric Vehicles and Alignment Methodology,” 2020.

[47] IEC TS 61980-3, “Electric vehicle wireless power transfer (WPT) systems - Part 3: Specific requirements for the magnetic field wireless power transfer systems,” 2019.

[48] Qiao Liu, Hajime Igarashi, Homogenized Finite Element Analysis of Motor Windings Based on Cauer circuit, OIPE2023, Poster Session-Part2:13, Graz, Austria, September, 2023

[49] P. L. Dowell, “Effects of eddy currents in transformer windings,” Proc. IEEE, vol. 113, no. 8, pp. 1387–1394, Aug. 1966.

[50] X. Nan and C. R. Sullivan, “An improved calculation of proximity effect loss in high-frequency windings of round conductors,” in Proc. IEEE 34th Annu. Power Electron. Specialist Conf., vol. 2. Jun. 2003, pp. 853–860.

[51] J. A. Ferreira, “Improved analytical modeling of conductive losses in magnetic components,” IEEE Trans. Power Electron., vol. 9, no. 1, pp. 127–131, Jan. 1994.

[52] A. D. Podoltsev, I. N. Kucheryavaya, and B. B. Lebedev, “Analysis of effective resistance and eddy-current losses in multiturn winding of high frequency magnetic components,” IEEE Trans. Magn., vol. 39, no. 1, pp. 539–548, Jan. 2003

[53] F. Ollendorff, "Magnetostatik der Massekerne," Arch. Elektrotechnik, vol. 25, pp. 436–447, Jun. 1931.

[54] J. A. Stratton, Electromagnetic Theory. New York, NY, USA: MacGrawHill, 1941, sec. 4.20.

[55] M. U. Hassan, H. Carlier, J. Gyselinck and Y. Mollet, "Homogenization of Multi-turn Windings in Electrical Machines with Fewer Number of Conductors," 2019 Electric Vehicles International Conference (EV), Bucharest, Romania, 2019, pp. 1-4, doi: 10.1109/EV.2019.8892952.

[56] Q. Liu, H. Igarashi, "Time-domain analysis of motor winding copper losses based on the homogenization method and Cauer circuit" Reiwa 6th National Conference of the Institute of Electrical Engineers of Japan. (submitted)

[57] A. E. Ruehli, "Equivalent circuit models for three-dimensional multiconductor systems," IEEE Trans. Microw. Theory Tech., vol. 22, no. 3, pp. 216–221, Mar. 1974.

[58] X. Zhang, S. L. Ho, and W. N. Fu, "Quantitative analysis of a wireless power transfer cell with planar spiral structures," IEEE Trans. Magn., vol. 47, no. 10, pp. 3200–3203, Oct. 2011.

[59] M. Koohestani, M. Zhadobov and M. Ettorre, "Design Methodology of a Printed WPT System for HF-Band Mid-Range Applications Considering Human Safety Regulations," in IEEE Transactions on Microwave Theory and Techniques, vol. 65, no. 1, pp. 270-279, Jan. 2017, doi: 10.1109/TMTT.2016.2609931.

[60] W. -S. Lee, W. -I. Son, K. -S. Oh and J. -W. Yu, "Contactless Energy Transfer Systems Using Antiparallel Resonant Loops," in IEEE Transactions on Industrial Electronics, vol. 60, no. 1, pp. 350-359, Jan. 2013

[61] N. Van T. "Magnetic resonance wireless power transfer using three-coil system with single planar receiver for laptop applications" in IEEE Transactions on Consumer Electronics,vol.61, no.2, pp.160-166, May 2015

[62] W. Chen, J. L. Dawson, "Inductor parasitic capacitance modeling and optimization for high-frequency dc-dc converters," IEEE Transactions on Power Electronics, vol. 20, no. 5, pp. 1057-1065, Sep. 2005.

[63] R. Yang, J. W. Kim, "Analysis and reduction of winding capacitance in high frequency inductors for voltage regulator modules (VRMs)," IEEE Transactions on Components and Packaging Technologies, vol. 28, no. 4, pp. 716-723, Dec. 2005.

[64] H. Wang, D. Boroyevich, F. C. Lee, "Design methodology to minimize the effects of winding capacitance in high-frequency power transformers," IEEE Transactions on Power Electronics, vol. 16, no. 2, pp. 233-241, Mar. 2001.

[65] C. Qian, D. C. Hamill, "Modeling and reduction of winding capacitance in power magnetic components," IEEE Transactions on Power Electronics, vol. 27, no. 6, pp. 3013-3022, Jun. 2012

Research Achievements

Journal

[1] Liu, Qiao et al. 'Equivalent Circuit of High Frequency Inductor to Consider Eddy Currents and Resonance'. International Journal of Applied Electromagnetics and Mechanics, vol. 71, no. S1, pp. S275-S282, 2023.
[2] Q. Liu et al., "Loss Evaluation of Magnetic Devices using Cauer Equivalent Circuit Identified from Input Impedance," in IEEE Transactions on Magnetics, doi: 10.1109/TMAG.2023.3303880.

International conference

[1] Qiao Liu, Yoshitsugu Otomo, Hajime Igarashi, "On Equivalent Circuit Representation of Transformer Considering Eddy Currents," The 40th JSST Annual International Conference on Simulation Technology (JSST2021), pp.261-264, Sep. 2021.
[2] Qiao Liu, Yoshitsugu Otomo, Yunyi Gong, Hajime Igarashi, "Equivalent Circuit of High Frequency Inductor to Consider Eddy Currents and Resonance," The 20th International Symposium on Applied Electromagnetics and Mechanics (ISEM2022), pp.101-102, Jun. 2022.
[3] Qiao Liu, Hajime Igarashi, "Equivalent Circuit for Wireless Power Transfer Considering Eddy and Displacement Currents," The 41st JSST Annual International Conference on Simulation Technology (JSST2022), Sep., 2022. (Student presentation award)
[4] Qiao Liu, Hajime Igarashi, "Loss Evaluation of Magnetic Devices using Cauer Equivalent Circuit Identified from Input Impedance" Compumag 2023, May 2023. Kyoto, PB-A1
[5] Qiao Liu, Hajime Igarashi, "Analysis of Magnetic Device Using Homogenized Finite Element Method and Cauer Circuit" The 42nd JSST Annual International Conference on Simulation Technology (JSST2023), Agu., 2023.
[6] Qiao Liu, Hajime Igarashi, Homogenized Finite Element Analysis of Motor Windings Based on Cauer circuit, OIPE2023, Poster Session-Part2:13, Graz, Austria, September 2023

Domestic conference

[1] Qiao Liu, Yunyi Gong, Hajime Igarashi, "Simulation of Wireless Power Transfer using Cauer Equivalent Circuit Identified from Input Impedance" 令和5年電気全国大会, Mar., 2023. Nagoya

Acknowledgement

Sincere thanks to all everyone who helped me during my whole student period from junior high school to doctor course.

First and foremost, I want to express my gratitude to my advisor Professor. Hajime Igarashi. He is best professor I have ever met. When graduate from my master course, it’s him that gave the chance to go on chase my doctor course. He is always very passionate in guiding me in researching and rarely being impatient for my ignorance, negligence, and laziness. For three years researching life in Sapporo, I can feel my growth clearly in studying and dealing with things under the nurture from professor.

Next, I want to thank for Professor. Noguchi, Mr. Imai, and Ms. Saito. During the 3 years in research room, I received a lot of help from them. Anytime I met trouble in my daily life, they are always being there and reliable.

I’d like to say that I’m very grateful for all the help from Mr. Y. Otomo. Although we had only one year together in research room, Mr. Y. Otomo never hesitated to help me whenever I got stuck in some research problems. The first year was the most difficult period for me, but with the assistance from Mr. Y. Otomo I overcame a lot of setbacks.

All other Chinese students in the research room are also my precious companionship during my doctor course. Mr. Y. Gong always gives me some advice in doing research and daily life. By having dinner with him, I know many delicious restaurants and a lot of tips about eating Ramen. I wish he can enjoy his life in Tokyo and one day fine a girlfriend. Mr. C. Deng took me to deal with a lot of formalities in extreme weather like blizzard just after I arrived in Sapporo that indeed helped me a lot. Ms. X. Kong and I stayed in the same research room in the last two years. I can always talk with her during daily life, and she is a nice and positive person that also influence me a lot. I wish she everything goes well in her post-doctor stage. Finally, Ms. S. Yin gave me a lot of help in my job hunting. She is always optimistic and diligent that always imparts energy to people around her. I wish she can finally find a nice job of teaching position in Xi An.

Basketball has been a part of my life for a long time. All of my friends playing basketball together with me is treasure. Especially, I want to show my thanks to Mr. X. Pan, Mr. Y. Mu, Mr. C. Zhang, and Mr. Y. Jin that they companied me for all the 3 years. I wish all of them can complete their studies successfully.

I'd also like to thank for Mr. Y. Wang, Mr. H. Gao, and Mr. Y. Zhang. They participated in a lot of my daily leisure life. Hope they can have a bright future.

Here I extend my deepest gratitude to Ms. Y. Liu that she is the most important one for me in Japan. She companied with me for a lot of time that I will never forget. Thank for her endless patience, for standing by me during my busiest times, and for being the source of my strength. Love and support have made all the difference.

Finally, I am profoundly grateful to express my heartfelt appreciation to my parents Mr. Y. Liu and Ms. D. Zhang. They are always my final stand-by. Whatever I choose to do they will support me unconditionally. I will do my best to repay them after I get into work.

All in all, there are still many people in my life that is important to me. All things happen to me led to who I am now.